Studies on the Dynamics and Stability of Bicycles

A Thesis
Submitted for the Degree of
Doctor of Philosophy
in the Faculty of Engineering

By
Pradipta Basu-Mandal

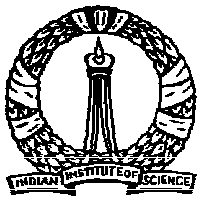

Department of Mechanical Engineering
Indian Institute of Science
Bangalore - 560 012
India

September 2007

Dedicated to

my late maternal aunt

Abstract

This thesis studies the dynamics and stability of some bicycles. The dynamics of idealized bicycles is of interest due to complexities associated with the behaviour of this seemingly simple machine. It is also useful as it can be a starting point for analysis of more complicated systems, such as motorcycles with suspensions, frame flexibility and thick tyres. Finally, accurate and reliable analyses of bicycles can provide benchmarks for checking the correctness of general multibody dynamics codes.

The first part of the thesis deals with the derivation of fully nonlinear differential equations of motion for a bicycle. Lagrange's equations are derived along with the constraint equations in an algorithmic way using computer algebra. Then equivalent equations are obtained numerically using a Newton-Euler formulation. The Newton-Euler formulation is less straightforward than the Lagrangian one and it requires the solution of a bigger system of linear equations in the unknowns. However, it is computationally faster because it has been implemented numerically, unlike Lagrange's equations which involve long analytical expressions that need to be transferred to a numerical computing environment before being integrated. The two sets of equations are validated against each other using consistent initial conditions. The match obtained is, expectedly, very accurate.

The second part of the thesis discusses the linearization of the full nonlinear equations of motion. Lagrange's equations have been used. The equations are linearized and the

corresponding eigenvalue problem studied. The eigenvalues are plotted as functions of the forward speed v of the bicycle. Several eigenmodes, like weave, capsize, and a stable mode called caster, have been identified along with the speed intervals where they are dominant. The results obtained, for certain parameter values, are in complete numerical agreement with those obtained by other independent researchers, and further validate the equations of motion. The bicycle with these parameters is called the benchmark bicycle.

The third part of the thesis makes a detailed and comprehensive study of hands-free circular motions of the benchmark bicycle. Various one-parameter families of circular motions have been identified. Three distinct families exist: (1) A handlebar-forward family, starting from capsize bifurcation off straight-line motion, and ending in an unstable static equilibrium with the frame perfectly upright, and the front wheel almost perpendicular. (2) A handlebar-reversed family, starting again from capsize bifurcation, but ending with the front wheel again steered straight, the bicycle spinning infinitely fast in small circles while lying flat in the ground plane. (3) Lastly, a family joining a similar flat spinning motion (with handlebar forward), to a handlebar-reversed limit, circling in dynamic balance at infinite speed, with the frame near upright and the front wheel almost perpendicular; the transition between handlebar forward and reversed is through moderate-speed circular pivoting with the rear wheel not rotating, and the bicycle virtually upright.

In the fourth part of this thesis, some of the parameters (both geometrical and inertial) for the benchmark bicycle have been changed and the resulting different bicycles and their circular motions studied showing other families of circular motions.

Finally, some of the circular motions have been examined, numerically and analytically, for stability.

Acknowledgements

I thank my advisor Dr. Anindya Chatterjee who guided me throughout this work. His direct involvement in the research topic and knowledge of rigid-body dynamics have helped me in completing this work. I also thank Dr. James Papadopoulos for his avid interest in this work and also for making many constructive suggestions towards its improvement. I also mention here that some of my numerical results were verified to high accuracy by Dr. Arend Schwab; the match obtained by him increased my confidence in the accuracy of my own results.

I am deeply indebted to my parents, my late maternal aunt, uncle, brother-in-law, sister and my two cousins who have encouraged me to join IISc to pursue my Ph.D. I also thank my young nephew who has always been telling me to finish this work and come back home.

Next I would like to thank all the members of my lab. Healthy discussions both technical as well as non-technical, held during innumerable visits to Tea Board have resulted in conceptual clarity, development of new ideas and fun as well. I thank my colleagues Satwinder, Pankaj, Amol, Pradeep, Nandakumar, Manga Raju, Jitpal, Sandeep, Vamshi, Umesh, Arjun and Navendu. I also thank Venkatesh, Rahul, Dhananjay, Vidyadhar, Vinay, Vivek and Prateek.

Apart from the lab members, I enjoyed the company of my good friends Kamalesh,

Ghatak, Debmalya, Saikat, Subho, Abhijit, Prabir, Soumen and my school mates Arnab, Arindam and Amitava. I take the opportunity to specially thank Pijush in whose room I have watched numerous gripping football and tennis matches and F1 races on the TV.

There are many whose names I can not list here, but who have helped me in various ways. I express my sincere thanks to all of them.

Contents

List of Figures

List of Tables

Chapter 1

Introduction and Literature Review

This thesis presents a study of the dynamics and stability of bicycles. It presents, for the first time, multiply cross-verified (benchmark) numerical results for certain bicycle parameter values that can be used with confidence by future researchers in bicycle dynamics as well as people interested in examining the accuracy of general purpose multibody dynamics codes. It also presents, in addition to numerical results, detailed discussions of hands-free circular motions of some bicycles. Although the full set of hands-free circular motions is complicated and varies from bicycle to bicycle, some significant new insights are obtained into these motions, including some insights into the role played by handlebar asymmetry (turning the handlebar by 180 degrees changes the dynamics; but in some cases not by much). Finally, analytical and numerical stability analyses of these circular motions have been carried out for the first time.

Bicycle dynamics has a long and scattered history. Since their inception, bicycles have attracted attention from many scientists and engineers. The literature on bicycle dynamics gradually started swelling towards the latter half of the twentieth century as computers made integration of the governing differential equations possible. Apart from attempts to write equations of motion, other bicycle analyses were aimed at understanding rider control, based on qualitative dynamics discussions that are too simplified to capture, say, the ability of a moving bicycle to balance itself.

This thesis consists of four parts. In the first part, we derive Lagrange's equations of motion for the bicycle. Then we write an equivalent set of equations using Newton-Euler

equations. The derivation of Lagrange's equations is more algorithmic and tedious. The derivation has been done using Maple. The implementation of the Newton-Euler equations is fully numerical and less routine than Lagrange's equations.

In the second part of the thesis, the equations are linearized about straight motion and the corresponding eigenvalue problem is studied.

The third and fourth parts of the thesis present a complete description of the hands-free circular motions of different bicycles. Different families of circular motions have been found. The effect of handlebar asymmetry has been studied in some detail. The equations governing circular motions have been explicitly linearized and the corresponding eigenvalue problem has been studied. Numerical evaluation of stability has also been carried out. Stable circular motions have been found to exist.

A major portion of the work contained in this thesis has been published in [2]. The work contained in chapter 8 has not yet been published elsewhere.

1.1 Brief Literature Review

Since their inception more than a century ago, bicycles have attracted attention from many scientists and engineers including Rankine [20] and Whipple [23] from the nineteenth century. The literature started growing towards the latter half of the twentieth century with the advent of computers which made numerical integration of differential equations relatively easy. During this time notable contributions to bicycle mechanics were made by [18] and [11]. Research on the dynamics of bicycles modelled as linked rigid bodies was reviewed in [9]. Models with compliance were reviewed in [22]. Many bicycle analyses aimed at understanding rider control are based on qualitative dynamics discussions that are too simplified to capture the ability of a moving bicycle to balance itself. Such discussions can be found in Jones [10] and [13]. Others, appropriately for basic studies of rider control, use models with geometry and/or mass distribution that are too simplified to allow self-stability. Still others, even if using a bicycle model that is as general as the one studied here, use rules for the control of the steer and thus skip the equation for self-steer dynamics. Such simple and/or steer-controlled approaches are found in, e.g., [8] and [1]. Issues pertaining

to self-steer dynamics of bicycles are discussed in Meijaard *et al.* [17]. A highly detailed discussion of the linear literature on bicycles with many cross-references is also given in [17]. Hence, we will not discuss the linear literature on bicycles in any more detail here.

Now we discuss the literature concerning nonlinear motions of bicycles. For circular motions, the analytical literature is smaller and less verifiably correct. The fully nonlinear equations for bicycles are long, and their explicit form varies with the approach used in deriving them. For example, the two independent (and numerically cross-verified) sets of equations presented in the thesis differ greatly in length and defy full manual comparison. We advocate the view, therefore, that numerical agreement to many digits (say, 10 or more) between outputs (accelerations) from two sets of equations for several sets of *randomly* generated inputs may be taken as a reliable demonstration of equivalence of the same. In this light, we note that full nonlinear equations and/or simulations are presented, among others, by [3], [21], [19], [7] and [14]; but we are unable to comment on their correctness here beyond a qualitative comparison between their results and ours. We also acknowledge the significant amount of work done on motorcycles, using more complex and therefore less easily verifiable models: see, e.g., [16] and [5], as well as references therein.

The topic of hands-free circular motions might be initially misunderstood because human riders can easily follow a wide range of circles at quite arbitrary speeds. But in general this is possible only by imposing handlebar torques, or upper-body displacement from the symmetry plane. With zero handle torque (i.e., hands-free) and a centred rider, only a few discrete lean angles are possible at each speed.

We mention for motivation that straight-line motions of most standard bicycles, including the benchmark bicycle with its handlebars forward (HF) or reversed (HR), have a finite range of stable speeds. A bifurcation known as *capsize* occurs at the upper limit, where (by linear analysis) steady turns at all large radii can be sustained with zero steering torque. These HF and HR bifurcations are the origins of two distinct circular-motion families. Moreover, as we will show, there are other families as well.

Prior work on hands-free circular motions of bicycles and motorcycles is limited, incomplete, and occasionally arguable in terms of conclusions presented.

The paper by [11] on steady turns of a motorcycle with front and rear point masses, linearized in the steer angle but not the lean, contains plots of steer angle (to 12 degrees)

versus steer torque (which we take as zero), parameterized by lean, steer, and turn radius. The zero-torque axis seems difficult to relate to our results below. Later, a fully nonlinear treatment is given in [15] where the effects of distributed masses, tyre slip relations, and the possibility of rider lean relative to the frame were explored. The results in figures 5 and 6 of that paper (and associated text) seem to imply that any desired turn radius can be achieved at a given speed, without altering steer angle; and indeed that turn radius at a given speed is independent of steer angle. This result, arguably lying outside normal bicycling experience, may be due to details of tyre slip modelling. No evidence of bifurcation from straight motion or other hands-free turning is apparent.

Psiaki [19] found one solution family (off point B in our figure 6.1, which we will discuss in detail later), calculated eigenvalues, and reported stability up to a lean of about 18°. The mechanical parameters of the bicycle were different, and speeds studied ranged from the capsize speed to about 2% below it. Our corresponding solutions below are unstable.

Franke *et al.* [7] studied the nonlinear motions of a bicycle, modelled using some point mass simplifications; without providing full details of mechanical parameters; and allowing for lateral displacement of the rider. Their results (for zero rider displacement) show only one solution family (corresponding to our curve BA in our figure 6.1), which like ours is unstable.

Cossalter *et al.* [4] evaluated steady turns of a motorcycle with toroidal wheels, and various tyre parameters. In the upper left plot of their figure 5 (rigid tyres), a line of zero steer torque is plotted on axes of curvature and speed. It seems equivalent to most of our curve BA in our figure 6.1, with a bifurcation around 5 m/s; and with turn radius decreasing to about 5m at a speed of 4 m/s. No other circular motion families are apparent.

Lennartsson [14] presented a thoroughgoing analysis of circular motions of a bicycle, with different parameters, where he finds all but one of the solution families we will display later (curve CDE in our figure 6.1 even though he separately determines the HR bifurcation that gives rise to it). For yet other parameter values, Aström [1] again overlooked the same family.

In this light, a careful, complete, and cross-verified study of circular motions of some bicycles seems missing in the literature, and constitutes the primary contribution of this

thesis.

1.2 Organization of the Thesis

Chapter 2 presents the derivation of Lagrange's equations of motion. It starts with the assumptions made for deriving the equations of motion. Then it discusses the generalized coordinates that describe the bicycle. It also includes a discussion on the notation that has been used to describe Euler angle rotations. Then the procedure for obtaining the Lagrangian is discussed in detail along with the method for obtaining the constraint equations for the wheels.

Chapter 3 deals with the derivation of the equations of motion by the Newton-Euler method. It starts with the momentum balance equations for the rear wheel, front wheel and the rear frame and the rear wheel combined. Then momentum balance equations for the entire bicycle are written. The constraint equations (in vector form) are then written for the two wheels. Then further kinematic relations connecting the linear and angular accelerations of the four rigid bodies constituting the bicycle are written down. A system of linear equations is obtained which can be solved numerically.

Chapter 4 deals with the numerical solution of the differential equations of motion of the bicycle. It contains a table showing the second derivatives of the coordinates describing a bicycle as obtained using Lagrange's equations and Newton-Euler equations. The values of these derivatives match to 16 decimal places showing that the two sets of equations derived in chapter 2 and chapter 3 are exactly equivalent. It also includes a numerical simulation of the full nonlinear equations of motion using a set of initial conditions which are consistent with the imposed constraints. It concludes with a discussion of the method of coordinate partitioning on velocities which has been implemented in the Matlab code to eliminate the problem of drift in the velocity and acceleration constraints.

Chapter 5 deals with linearized equations of motion and the accompanying eigenvalue problem for studying the straight line motion of the bicycle and its stability. The stability results are presented for both handlebar-forward (HF) and handlebar-reversed (HR) configurations. A speed range has been identified in which the uncontrolled bicycle

can balance itself for both HF and HR cases.

Chapter 6 studies circular motions of the bicycle in detail. The chapter starts with a discussion of the strategy that has been employed to find the various circular motion families. Then follows a detailed discussion of each. Various special motions and limiting configurations which are attained by the bicycle are discussed. Some precise values (initial conditions leading to circular motions), which serve a benchmarking purpose, are listed. In addition, some special and precise numerical values related to limiting configurations are listed. A full numerical simulation of one circular motion is included. Finally, a detailed discussion of a somewhat unexpected static equilibrium solution for the bicycle is presented.

Chapter 7 studies the stability of circular motions. A procedure to obtain linearized equations for circular motions has been developed. A table showing the four non-trivial eigenvalues governing the stability of circular motions, for several motions, has been shown. A discussion on which equations to include for linearization (because the equations are not independent and they admit a one-parameter family of solutions) is provided. Relevant numerical issues pertaining to the multiplicity of the zero eigenvalues are discussed. Finally a numerical scheme involving finite differences to find the stability eigenvalues of circular motions quickly, with low computational effort, has been provided.

Chapter 8 makes a study of circular motions of various bicycles obtained by changing some of the parameter values of the benchmark bicycle. Effects of handlebar asymmetry and removal of the same are discussed in detail. In the course of this study, qualitatively new families of circular motions have been found. They have been studied and plotted in the same manner as in chapter 6. Stability analysis of these families has been conducted. Many circular motions have been found to be stable for certain choices of parameter values.

Chapter 9 makes a limited comparison of some of the results obtained in this thesis with prior experiments.

Finally some concluding discussion is presented in chapter 10.

Chapter 2

Lagrange's Equations of Motion

2.1 Introduction

There are several ways of writing equations of motion for a bicycle. These equations are a set of differential equations. One can assemble them using the Newton-Euler rigid-body equations, or using Lagrange's equations with Lagrange multipliers for the in-ground-plane rolling-contact forces, or one can use methods based on the principle of virtual velocities (e.g., Kane's method [12]), etc. In this chapter, we use a Lagrangian formulation for deriving the same.

2.2 Preliminaries

2.2.1 Mechanical model

The mechanical model of the bicycle used here has four rigid bodies: the rear frame with the rider rigidly attached; the front frame consisting of the front fork and the handlebar assembly; and two wheels. These bodies are interconnected by frictionless hinges at the steering head (between rear frame and front frame) and at the two wheel hubs. The

wheels make knife-edged contact with the ground; their centers of mass coincide with their geometrical centers; and they roll on horizontal ground without slip or dissipation. There is no propulsive thrust. The parameter values used here are based on the further assumption of lateral symmetry, though such symmetry is not assumed in our derivation (unlike [17]).

2.2.2 Generalized coordinates and constraints

We begin with nine generalized coordinates, not all independent. Three coordinates x, y and z specify the position of the centre of mass of the rear wheel in the global reference frame XYZ (see figure 2.1). Note that the same point is attached to the rear frame as well. Three angles θ, ψ and ϕ (in (3,1,3) Euler angle sequence) specify the configuration of the rear frame. The rotation of the rear wheel relative to the rear frame is β_r. The rotation of the front fork (steering angle) relative to the rear frame is ψ_f. Finally, the rotation of the front wheel relative to the front fork is β_f.

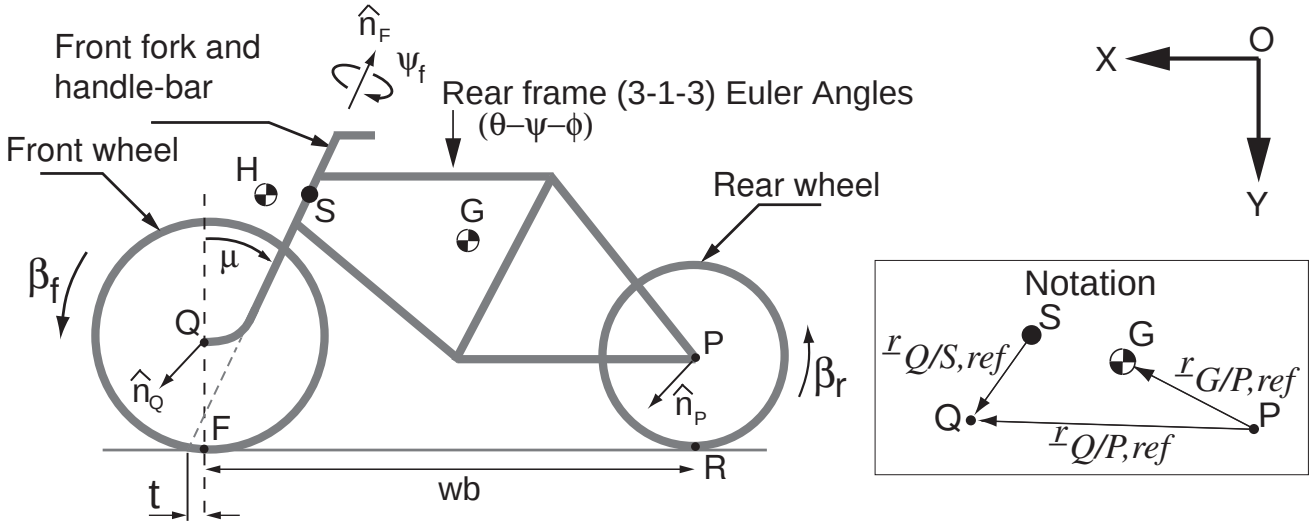

Figure 2.1: Sketch of the bicycle in its reference configuration. The bicycle is flat on the ground.

2.2.3 Reference configuration to instantaneous configuration

In the reference configuration chosen here (see figure 2.1), the bicycle is lying flat on the ground. Its lateral-symmetry plane coincides with the XY plane.

To reach an arbitrary instantaneous configuration, we proceed as follows. First, the rear frame is rotated by θ about e_3 (i.e., the Z-direction). This determines the eventual heading direction of the bicycle (it corresponds to a yawing motion). Next, the rear frame is rotated by ψ about the body-fixed e_1 axis (i.e., about what was the X-direction before the first rotation). This determines the tilt of the bicycle (it corresponds to a rolling motion). Finally, the rear frame is rotated by ϕ about the body-fixed e_3 axis (i.e., about what was the Z-direction before the two preceding rotations). This rotation is not really independently specifiable when the bicycle moves on flat ground. It corresponds to a pitching motion, and must take whatever value is needed for the front wheel to touch the ground.

After the three rotations given by the above Euler angles, the rear frame is translated so that the rear wheel axle center reaches the point (x, y, z).

Holding the rear frame fixed, the rear wheel is rotated by β_r, the front fork is rotated by ψ_f, and then the front wheel is rotated relative to the front fork by β_f.

Now the bicycle is in the instantaneous configuration. Note that z and ϕ cannot be independently specified: they must ensure contact between the wheels and ground. The bicycle thus has seven independent configuration variables, though we work with nine for convenience.

2.2.4 Velocity degrees of freedom

As discussed earlier, the configuration space of the bicycle is seven-dimensional. However, the bicycle has 4 nonholonomic constraints, 2 for each wheel. These constraints reduce the bicycle to only 3 degrees of freedom in the velocities. This velocity space is parameterized by the lean rate $\dot{\psi}$ of the rear frame, the steer rate $\dot{\psi}_f$ and the rear wheel spin rate $\dot{\beta}_r$ relative to the rear frame.

2.2.5 Parameters describing a bicycle

The parameters of all bicycles studied in this thesis are listed in appendix A. The number of design parameters is 25. Here, for academic interest, we discuss how to eliminate four of them without loss of generality. However, we will continue to work with all the 25 parameters for convenience.

See figure 2.2.

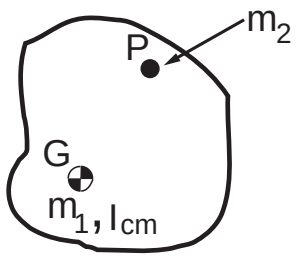

Figure 2.2: Adding a point mass to a rigid body.

An arbitrary rigid object has mass m_1, center of mass at G, and moment of inertia about center of mass I_{cm}. A point mass m_2 is added to this object at point P. The new composite object will have total mass $m_1 + m_2$. The new center of mass G' will satisfy

$$(m_1 + m_2)\,\underline{r}_{G'} = m_1\,\underline{r}_G + m_2\,\underline{r}_P.$$

The new moment of inertia matrix about G' can be found by applying the parallel axis theorem (3D version) to I_{cm} and adding on the further contribution of mass m_2 at P. These formulas continue to apply if a point mass is *removed* from the object: in this case, m_2 is simply negative.

The above can be used to reduce the size of the independent parameter set of the bicycle.

First, a point mass equal to the mass of the rear wheel can be transferred from the wheel to the rear frame, at the wheel axle. This alters the total mass, center of mass position, and moment of inertia matrix of the rear frame; but it does not change the

number of scalar parameters needed to specify them. However, now the mass of the rear wheel may be set to zero, thereby reducing the size of the parameter set by one. Note that the moment of inertia matrix of the rear wheel remains unchanged. A minor point here is that the moment of inertia matrix is supposed to be calculated about the center of mass, and now the center of mass of the wheel is indeterminate because its mass is zero. However, for exactly the same reason, the moment of inertia matrix becomes independent of center of mass location, as may be seen by applying the parallel axis theorem, and so the indeterminacy has no dynamical consequences. Another way to see the validity of this point mass transfer is to note that there is no change in either the kinetic or the potential energy of the system, and so Lagrange's equations remain the same. In writing Newton-Euler equations, on the other hand, the zero mass of the rear wheel makes a zero contribution to linear momentum balance equations (no ambiguity); and the zero mass also causes the relevant $\underline{r} \times m\underline{a}$ term in angular momentum balance equations to drop out regardless of the indeterminacy in $\underline{r}$ (again, no ambiguity).

In this way, one parameter has been eliminated.

We now consider the front fork. See figure 2.3 (left), which shows a side view.

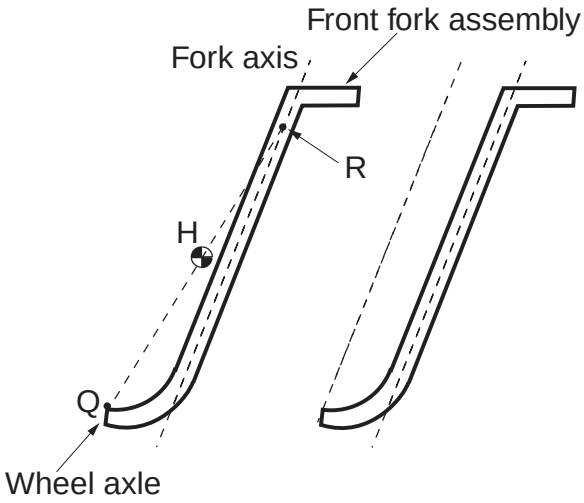

Figure 2.3: Front fork.

Let us draw a line from the wheel axle Q, through the front fork center of mass H,

to intersect the fork axis at some point R. That this is possible for typical bicycle designs is seen from the same figure (right), where a line parallel to the fork axis has been drawn through Q. Since all the mass lies to the right side of this line, the center of mass lies to its right as well.

Having identified points Q, H and R, we now seek two masses m_1 and m_2 that satisfy

$$m_1 + m_2 = m_{ff} \text{ (mass of front fork)}, \tag{2.1}$$

$$m_1\, \underline{r}_{Q/H} + m_2\, \underline{r}_{R/H} = \underline{0}. \tag{2.2}$$

Equation 2.2 looks like a vector equation, but effectively is a scalar equation because $\underline{r}_{Q/H}$ and $\underline{r}_{R/H}$ are collinear. Solving Eqs. 2.1 and 2.2, we obtain m_1 and m_2. We then transfer a point mass m_1 to the front wheel axle at Q. This changes the mass of the front wheel, but does not alter the number of free parameters required to describe it. After transferring this mass, the new mass of the front fork is m_2; and the new center of mass is at R. The front fork also has a new moment of inertia matrix about R, which can be calculated as described above. Finally, we transfer a point mass m_2 from the front fork to the rear frame at point R. This does not change the moment of inertia matrix of the front fork, but makes its mass zero (eliminating one parameter). The mass, center of mass position, and moment of inertia matrix about center of mass of the rear frame are now updated, but no new parameters are introduced there.

Finally, we note that the center of mass position of the front fork is now dynamically irrelevant, so it can (say) be set equal to the origin with no dynamical consequences. This, in effect, eliminates a further two scalar parameters.

We have, in this way, eliminated a total of four parameters, yielding a reduced set.

We mention that the front and rear wheels in bicycles are usually modeled as thin (as in [17]). In such cases, in the reference configuration, the polar moment of inertia I_{zz} (about the axis of a wheel) is double the value of the transverse moments of inertia $I_{xx} = I_{yy}$ (consistent with our choice of coordinate axes in the reference position; different from that of [17]). However, if one is interested in wheels where $I_{xx} = I_{yy} = \gamma\, I_{zz}$ with γ a positive free parameter different for each wheel, then these two parameters can be eliminated as well. This is because, e.g., the rear wheel's instantaneous moment of inertia matrix does not depend on its rotation with respect to the rear frame. Its rotational kinetic energy may

be split into two parts: one due to its angular velocity component in the axial direction, which depends on the polar moment of inertia, and the other due to the transverse or in-wheel-plane component of angular velocity, which depends on the transverse moment of inertia, i.e., on γ. This latter part of the kinetic energy may be transferred to the rear frame by transferring the γ-dependent portion of the wheel's moment of inertia to the rear frame. Since there is no change in the Lagrangian, there is no change in the equations of motion. The contribution of γ gets absorbed into the inertia properties of the rear frame, and the parameter set is reduced by one. A similar process of transferring rotational inertia from the front wheel to the front fork can eliminate yet another free parameter, bringing the total reduction to six. In practical bicycle designs with thin wheels, as mentioned above, elimination of the last two parameters may be superfluous (because γ is fixed at $1/2$, and not free). However, this may be of interest in the dynamics of motorcycles with fatter wheels.

It may be noted that the above discussion of reduction of the parameter set by as much as six independent parameters is for academic interest only, and is not used in the rest of this thesis.

2.2.6 Notation for rotations

We work with a fixed inertial reference frame XYZ, and use a single coordinate system for all calculations so that vectors are equivalent to their 3×1 matrices of components. To emphasize this for clarity, we write

$$\mathbf{r} = \underline{r} \equiv r,$$

where r denotes the matrix of components of the vector $\mathbf{r}$ or $\underline{r}$.

Our notation for rotations, though not new, is presented briefly below for completeness.

Let a body be rotated about a unit vector $\underline{n}$ through an angle θ. Then a vector r embedded in the body gets rotated into a new vector r' given by the matrix relation

$$r' = \Big[\cos\theta\, I + (1 - \cos\theta) nn^T + \sin\theta\, S(n)\Big]\, r\,,$$

where

$$S(a) = \begin{bmatrix} 0 & -a_3 & a_2 \\ a_3 & 0 & -a_1 \\ -a_2 & a_1 & 0 \end{bmatrix} .$$

We define

$$R(n,\theta) \equiv \cos\theta\, I + (1-\cos\theta) nn^T + \sin\theta\, S(n) . \tag{2.3}$$

All rotation matrices used below are built up using the above "axis-angle" formula.

2.3 Lagrange's Equations

2.3.1 Kinetic and potential energies

We require the kinetic and potential energies of each of the four rigid bodies constituting the bicycle. The appropriate constraint equations are also required.

2.3.1.1 Rear frame

Defining (see subsection 2.2.6 for a slightly offbeat but compact notation) $R_1 = R(e_3, \theta)$, $R_2 = R(R_1 e_1, \psi)$ and $R_3 = R(R_2 R_1 e_3, \phi)$, the final rotation matrix R_{rf} for the rear frame is given by

$$R_{rf} = R_3 R_2 R_1 . \tag{2.4}$$

The above matrices are individually computed and reliably multiplied through in Maple. We obtain the angular velocity ω_{rf} of the rear frame *via*

$$S(\omega_{rf}) = \dot{R}_{rf} R_{rf}^T . \tag{2.5}$$

From $S(\omega_{rf})$, the elements of ω_{rf} are picked out individually. The entire calculation is easily programmed in Maple, and actual expressions are not presented here.

The mass moment of inertia matrix of the rear frame in the rotated configuration, $I_{cm,rf}$, is given by

$$I_{cm,rf} = R_{rf} I_{cm,rf,ref} R_{rf}^T , \tag{2.6}$$

where $I_{cm,rf,ref}$ is the mass moment of inertia matrix about the center of mass of the rear frame in its reference configuration. The rotational kinetic energy of the rear frame is (again in Maple)

$$KE_{rf,rot} = \frac{1}{2}\omega_{rf}^T I_{cm,rf}\omega_{rf}\,. \tag{2.7}$$

For the translational kinetic energy of the rear frame, we need the velocity $\underline{v}_G$ of the centre of mass G of the rear frame. The centre of mass of the rear wheel is at P, as shown in figure 2.1. Thus,

$$\underline{r}_G = \underline{r}_P + R_{rf}.\underline{r}_{G/P,ref}, \tag{2.8}$$

where $\underline{r}_{G/P,ref}$ is the position vector of G relative to P in the reference configuration of the bicycle. Having $\underline{r}_G$, we differentiate to obtain $\underline{v}_G$. The translational kinetic energy, $KE_{rf,trans}$, of the rear frame is

$$KE_{rf,trans} = \frac{1}{2}m_{rf}v_G^T v_G\,, \tag{2.9}$$

where m_{rf} is the mass of the rear frame including the rigidly attached rider. The total kinetic energy of the rear frame is then

$$KE_{rf} = KE_{rf,trans} + KE_{rf,rot}. \tag{2.10}$$

The potential energy, PE_{rf} of the rear frame is

$$PE_{rf} = m_{rf}g\,\underline{r}_{G,z}, \tag{2.11}$$

where $\underline{r}_{G,z}$ is the z-component of $\underline{r}_G$.

2.3.1.2 Front frame

The rotation matrix for the front frame is

$$R_{ff} = R(R_{rf}n_f, \psi_f)R_{rf}. \tag{2.12}$$

In the above equation, $n_f = \{-\sin\mu, -\cos\mu, 0\}^T$, is the unit vector pointing along the axis of the fork when the bicycle is in the reference configuration. As before,

$$S(\omega_{ff}) = \dot{R}_{ff}R_{ff}^T\,. \tag{2.13}$$

The mass moment of inertia matrix is

$$I_{cm,ff} = R_{ff} I_{cm,ff,ref} R_{ff}^T \,. \tag{2.14}$$

The rotational kinetic energy is

$$KE_{ff,rot} = \frac{1}{2} \omega_{ff}^T I_{cm,ff} \omega_{ff} \,. \tag{2.15}$$

The velocity of point H, the centre of mass of the front frame, is found as follows. First,

$$\underline{r}_S = \underline{r}_P + R_{rf}.\underline{r}_{S/P,ref}. \tag{2.16}$$

In the above equation S is any point on the fork axis. Then,

$$\underline{r}_H = \underline{r}_S + R_{ff}.\underline{r}_{H/S,ref}. \tag{2.17}$$

Having obtained $\underline{r}_H$, differentiation gives $\underline{v}_H$. The translational kinetic energy of the front frame is then given by

$$KE_{ff,trans} = \frac{1}{2} m_{ff} v_H^T v_H \,, \tag{2.18}$$

where m_{ff} is the mass of the front frame.

The total kinetic energy is

$$KE_{ff} = KE_{ff,trans} + KE_{ff,rot}. \tag{2.19}$$

The potential energy of the front frame is

$$PE_{ff} = m_{ff} g \, \underline{r}_{H,z}, \tag{2.20}$$

where $\underline{r}_{H,z}$ is the z-component of $\underline{r}_H$.

2.3.1.3 Front wheel

Finally, for the front wheel, we write

$$R_{fw} = R(R_{ff} e_3, \beta_f) R_{ff}, \tag{2.21}$$

$$I_{cm,fw} = R_{fw} I_{cm,fw,ref} R_{fw}^T \,, \tag{2.22}$$

$$S(\omega_{fw}) = \dot{R}_{fw} R_{fw}^T \,, \tag{2.23}$$

and

$$KE_{fw,rot} = \frac{1}{2} \omega_{fw}^T I_{cm,fw} \omega_{fw} \,. \tag{2.24}$$

As before, we write

$$\underline{r}_Q = \underline{r}_S + R_{ff} . \underline{r}_{Q/S,ref}, \tag{2.25}$$

where Q is the centre of the front wheel. Then we differentiate to obtain $\underline{v}_Q$. The translational kinetic energy is

$$KE_{fw,trans} = \frac{1}{2} m_{fw} v_Q^T v_Q \,. \tag{2.26}$$

The total kinetic energy KE_{fw} of the front wheel is then

$$KE_{fw} = KE_{fw,trans} + KE_{fw,rot}. \tag{2.27}$$

The potential energy of the front wheel is

$$PE_{fw} = m_{fw} g \, \underline{r}_{Q,z}. \tag{2.28}$$

2.3.1.4 Rear wheel

The rotation matrix of the rear wheel is

$$R_{rw} = R(R_{rf} e_3, \beta_r) R_{rf}. \tag{2.29}$$

The angular velocity vector ω_{rw} of the rear wheel is obtained from

$$S(\omega_{rw}) = \dot{R}_{rw} R_{rw}^T \,. \tag{2.30}$$

The instantaneous mass moment of inertia matrix about the center of mass of the rear wheel, $I_{cm,rw}$, is

$$I_{cm,rw} = R_{rw} I_{cm,rw,ref} R_{rw}^T \,. \tag{2.31}$$

The rotational kinetic energy of the rear wheel is

$$KE_{rw,rot} = \frac{1}{2} \omega_{rw}^T I_{cm,rw} \omega_{rw} \,. \tag{2.32}$$

The translational kinetic energy of the rear wheel is (recall our choice of generalized coordinates)

$$KE_{rw,trans} = \frac{1}{2} m_{rw}(\dot{x}^2 + \dot{y}^2 + \dot{z}^2). \tag{2.33}$$

The total kinetic energy of the rear wheel is

$$KE_{rw} = KE_{rw,trans} + KE_{rw,rot}. \tag{2.34}$$

The potential energy of the rear wheel is

$$PE_{rw} = m_{rw} g z. \tag{2.35}$$

2.3.1.5 Lagrangian

Let the total kinetic energy of the bicycle be T and the total potential energy be V. Then T and V are given as follows:

$$T = KE_{rf} + KE_{rw} + KE_{ff} + KE_{fw}, \tag{2.36}$$

$$V = PE_{rf} + PE_{rw} + PE_{ff} + PE_{fw}. \tag{2.37}$$

The Lagrangian is

$$\mathcal{L} = T - V. \tag{2.38}$$

It remains to write the constraint equations for the two wheels.

2.3.2 Constraint equations for the wheels

2.3.2.1 Rear wheel

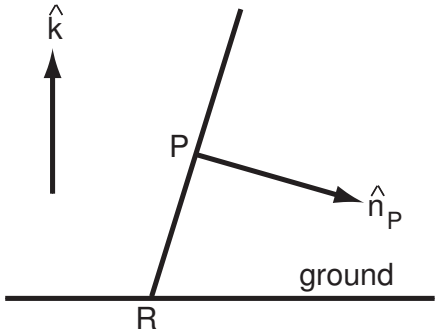

Figure 2.4: The rear wheel. The lowermost point on the wheel touches ground. The unit vector along $\hat{n}_P \times \hat{k}$, say $\hat{\lambda}_r$, points out of the page.

We begin by setting *all three* components of the contact point velocity to zero. The equation for the vertical component of the velocity is of course just the differentiated form of a holonomic constraint: we remain alert to that.

At an arbitrary configuration of the rear wheel, its plane intersects the ground along some line. If we view the wheel along this line, both the wheel and the ground reduce to straight lines. This 2D view is shown in figure 2.4. The centre of the wheel is at P, and the instantaneous point of contact is at R. A unit vector normal to the plane of the wheel is shown, and denoted by $\underline{n}_P$. In the reference configuration, $\underline{n}_P$ was aligned with $\hat{k}$ (the same as e_3); it is now, in matrix notation, given by $R_{rw}e_3$.

Assuming the wheel is *not* flat on the ground (which also happens to be the singular configuration for (3-1-3) Euler angles), the vector

$$\underline{p} = \underline{n}_P \times \hat{k} \tag{2.39}$$

is nonzero and points out of the plane of the paper. Now, from the figure, we see that[1]

$$\underline{r}_{P/R} = \frac{r_1}{\left|\underline{p}\right|}\underline{p} \times \underline{n}_P, \tag{2.40}$$

where r_1 is the radius of the rear wheel.

Using $\underline{r}_{P/R}$, the velocity of P can be written in two equivalent ways:

$$\underline{v}_P \equiv \dot{x}\hat{i} + \dot{y}\hat{j} + \dot{z}\hat{k} \equiv \underline{v}_R + \underline{\omega}_{rw} \times \underline{r}_{P/R}. \tag{2.41}$$

The constraint that $\underline{v}_R = \underline{0}$ is thus expressible as

$$\dot{x}\hat{i} + \dot{y}\hat{j} + \dot{z}\hat{k} - \underline{\omega}_{rw} \times \underline{r}_{P/R} = \underline{0}. \tag{2.42}$$

The above vector equation has three components. The vertical component is identifiable (on calculating it in Maple) as the derivative of

$$z = r_1 \sin\psi, \tag{2.43}$$

which is a holonomic constraint; we use it to eliminate z and reduce the number of degrees of freedom to eight.

The two other components turn out to be nonholonomic constraint equations:

$$\dot{x} + r_1 \cos\theta\dot{\beta}_r + r_1 \cos\theta\dot{\phi} - r_1 \sin\theta \sin\psi\dot{\psi} + r_1 \cos\theta \cos\psi\dot{\theta} = 0, \tag{2.44}$$

$$\dot{y} + r_1 \sin\theta\dot{\beta}_r + r_1 \sin\theta\dot{\phi} + r_1 \sin\psi \cos\theta\dot{\psi} + r_1 \sin\theta \cos\psi\dot{\theta} = 0. \tag{2.45}$$

2.3.2.2 Front wheel

The constraint equations for the front wheel are similarly obtained. The analog for $n_P = R_{rw}e_3$ is $n_Q = R_{fw}e_3$. The analog for the ground contact point R is point F. The analog for Eq. 2.42 is

$$\underline{v}_Q - \underline{\omega}_{fw} \times \underline{r}_{Q/F} = \underline{0}.$$

The vertical component of the above equation, though known theoretically to be a holonomic constraint, was retained in differentiated form (like a nonholonomic constraint) in this work due to its apparent analytical intractability.

[1]This offbeat approach requires no bicycle-specific 3D visualization and avoids errors.

Chapter 3

Newton-Euler Equations of Motion

3.1 Introduction

In this chapter, we use a Newton-Euler formulation for deriving the equations of motion. Here we write the linear and angular momentum balance equations for the rigid bodies constituting the bicycle. The constraint equations are then derived in the same way as they were derived for Lagrange's equations. Then we derive kinematic relations through which the linear and angular accelerations of the centres of mass of the various rigid bodies constituting the bicycle are related. Finally we end up with a system of linear equations in the unknowns. The Newton-Euler approach can also be used with Maple, but it is conveniently programmed into Matlab for a fast, fully numerical evaluation of the second derivatives needed for numerical integration. While the basic principles are straightforward, the actual implementation is less routine than obtaining Lagrange's equations. While our discussion is around using Matlab, the use of Matlab here is notional. All calculations here are transferable to other computing environments.

3.2 Momentum Balance

We begin with free body diagrams of the front wheel, the rear wheel, and the rear wheel along with the rear frame (figures 3.1 (A), (B) and (C) below).

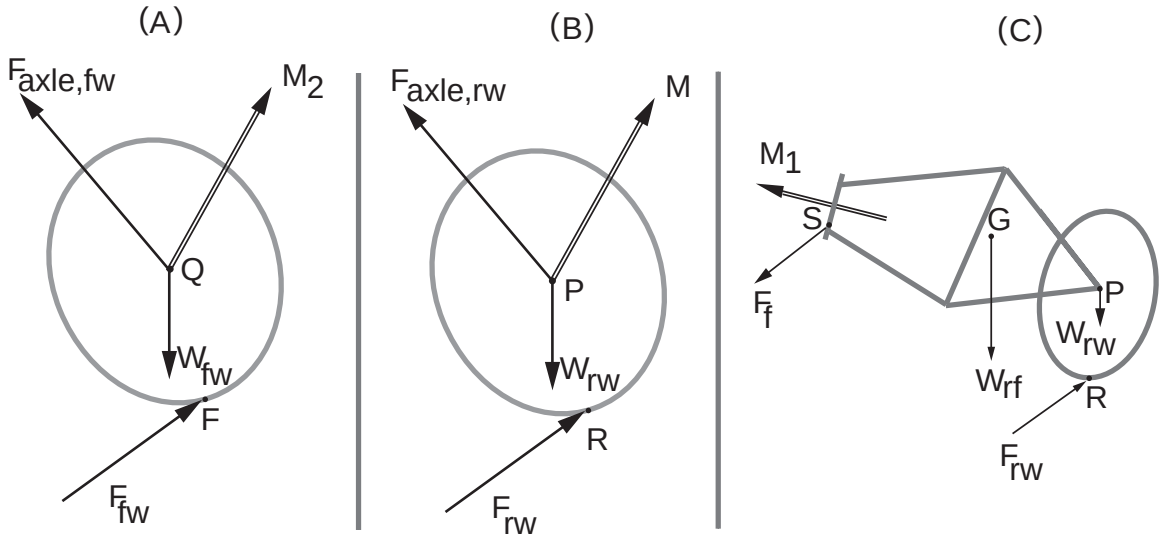

Figure 3.1: Free body diagrams. (A) shows the FBD of the front wheel, (B) shows the same for the rear wheel while (C) shows the FBD of the rear wheel and rear frame.

Consider the rear wheel (figure 3.1 (B)). There are three forces acting on it: its weight through P; an axle force $\underline{F}_{axle,rw}$ also at P; and a force $\underline{F}_{rw}$ at the ground contact R. There is also an unknown bearing moment $\underline{M}$ with no component along the bearing axis or $\hat{n}_P$. Angular momentum balance about P gives

$$\underline{r}_{R/P} \times \underline{F}_{rw} + \underline{M} = \underline{I}_{cm,rw}\underline{\alpha}_{rw} + \underline{\omega}_{rw} \times \underline{I}_{cm,rw}\underline{\omega}_{rw},$$

which in matrix notation is

$$S(r_{R/P})F_{rw} + M = I_{cm,rw}\alpha_{rw} + S(\omega_{rw})I_{cm,rw}\omega_{rw}. \tag{3.1}$$

In the above, α denotes angular acceleration (a vector). We eliminate $\underline{M}$ by taking the dot product of Eq. 3.1 with $\hat{n}_P$, obtaining

$$-n_P^T I_{cm,rw}\alpha_{rw} + n_P^T S(r_{R/P})F_{rw} = n_P^T S(\omega_{rw})I_{cm,rw}\omega_{rw}. \tag{3.2}$$

The above is a scalar equation, with terms rearranged so that unknowns appear on the left side so that it facilitates the assembly of the system of equations.

In Eq. 3.2, we could have written $-S(F_{rw})r_{R/P}$ in place of $S(r_{R/P})F_{rw}$, but the latter is preferred because the unknown F_{rw} now appears on the right; its coefficient matrix can be computed numerically and used directly while assembling the system equations. We will reuse this idea.

We now write the angular momentum balance equation for the rear wheel and the rear frame, together, about the point S on the fork axis (figure 3.1 (C)). Directly in matrix notation, we have (with unknowns on the left hand side)

$$\begin{aligned} S(r_{R/S})F_{rw} - m_{rw}gS(r_{P/S})e_3 - m_{rf}gS(r_{G/S})e_3 + M_1 = I_{cm,rf}\alpha_{rf} + S(\omega_{rf})I_{cm,rf}\omega_{rf} \\ + m_{rf}S(r_{G/S})a_G + I_{cm,rw}\alpha_{rw} + S(\omega_{rw})I_{cm,rw}\omega_{rw} + m_{rw}S(r_{P/S})a_P, \end{aligned} \quad (3.3)$$

where a denotes acceleration (a vector). We eliminate M_1 by taking the dot product of Eq. 3.3 with $\hat{n}_f$, getting the scalar equation

$$\begin{aligned} & n_f^T(S(r_{R/S})F_{rw} - I_{cm,rf}\alpha_{rf} - I_{cm,rw}\alpha_{rw} - S(r_{G/S})m_{rf}a_G - S(r_{P/S})m_{rw}a_P) \\ = & \, n_f^T(S(r_{P/S})m_{rw}ge_3 + S(r_{G/S})m_{rf}ge_3 + S(\omega_{rf})I_{cm,rf}\omega_{rf} + S(\omega_{rw})I_{cm,rw}\omega_{rw}). \end{aligned} \quad (3.4)$$

Finally, we write the angular momentum balance equation for the front wheel about Q. The free body diagram is shown in figure 3.1 (A) above. The resulting scalar equation in matrix notation is (with unknowns on the left)

$$-n_Q^T I_{cm,fw}\alpha_{fw} + n_Q^T S(r_{F/Q})F_{fw} = n_Q^T S(\omega_{fw})I_{cm,fw}\omega_{fw}. \quad (3.5)$$

We now write the linear momentum balance and the angular momentum balance equations for the entire bicycle about G, the centre of mass of the rear frame.

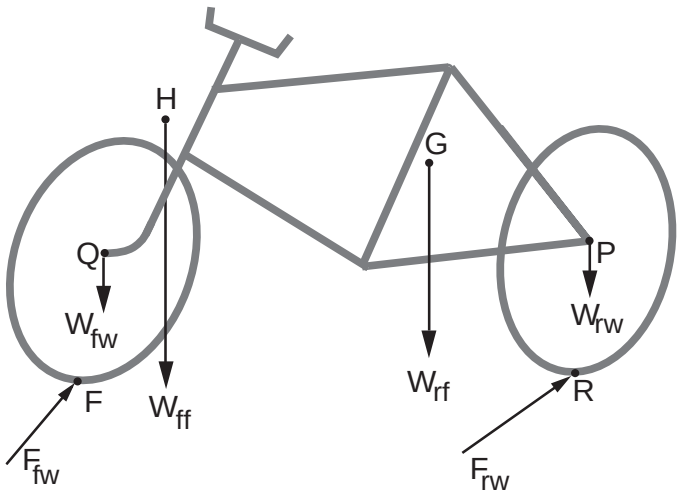

Figure 3.2: Free body diagram of the entire bicycle.

Linear momentum balance gives

$$F_{rw} + F_{fw} - m_{rw}a_P - m_{rf}a_G - m_{ff}a_H - m_{fw}a_Q = m_{tot}ge_3, \tag{3.6}$$

where m_{tot} is the total mass of the bicycle. Angular momentum balance about G gives

$$\begin{aligned} S(r_{R/G})F_{rw} + S(r_{F/G})F_{fw} - S(r_{P/G})m_{rw}a_P - I_{cm,rw}\alpha_{rw} - I_{cm,rf}\alpha_{rf} - \\ S(r_{H/G})m_{ff}a_H - I_{cm,ff}\alpha_{ff} - S(r_{Q/G})m_{fw}a_Q - I_{cm,fw}\alpha_{fw} = S(r_{P/G})m_{rw}ge_3 + \\ S(r_{H/G})m_{ff}ge_3 + S(r_{Q/G})m_{fw}ge_3 + S(\omega_{rw})I_{cm,rw}\omega_{rw} + S(\omega_{rf})I_{cm,rf}\omega_{rf} + \\ S(\omega_{ff})I_{cm,ff}\omega_{ff} + S(\omega_{fw})I_{cm,fw}\omega_{fw}. \end{aligned} \tag{3.7}$$

The above two equations are vector equations, with three scalar components each. Thus, we have so far obtained nine scalar equations.

3.3 Constraint Equations

The constraints are the same as before, but now we will not eliminate one coordinate using the holonomic constraint of ground contact for the rear wheel. That is, we will retain *six*

constraint equations. Corresponding to the differentiation of the five velocity constraint equations in the Lagrangian formulation before, we will now directly differentiate the two vector constraint equations.

To begin, we rewrite Eq. 2.40 as follows:

$$\underline{r}_{P/R} = r_1(\underline{\lambda}_r \times \hat{n}_P), \tag{3.8}$$

where

$$\underline{\lambda}_r = \frac{\hat{n}_P \times \hat{k}}{\left|\hat{n}_P \times \hat{k}\right|}.$$

Now we differentiate Eq. 2.41 to get

$$\underline{a}_P = \underline{\alpha}_{rw} \times \underline{r}_{P/R} + \underline{\omega}_{rw} \times r_1(\underline{\dot{\lambda}_r} \times \hat{n}_P + \underline{\lambda}_r \times \dot{\hat{n}}_P). \tag{3.9}$$

In matrix notation the above equation becomes

$$a_P + S(r_{P/R})\alpha_{rw} = r_1 S(\omega_{rw})(S(\dot{\lambda}_r)n_P + S(\lambda_r)\dot{n}_P), \tag{3.10}$$

where $\dot{n}_P$, λ_r and $\dot{\lambda}_r$ in matrix notation are given as follows:

$$\dot{n}_P = S(\omega_{rw})n_P. \tag{3.11}$$

$$\lambda_r = \frac{-S(e_3)n_P}{\sqrt{n_P^T S^T(e_3)S(e_3)n_P}}. \tag{3.12}$$

$$\dot{\lambda}_r = \frac{-S(e_3)\dot{n}_P}{\sqrt{n_P^T S^T(e_3)S(e_3)n_P}} + \frac{S(e_3)n_P\dot{n}_P^T S^T(e_3)S(e_3)n_P}{(n_P^T S^T(e_3)S(e_3)n_P)^{3/2}}. \tag{3.13}$$

The above equation could be simplified a little, but we leave it in this form for the sake of transparency. Similarly, for the front wheel we can write the constraint equations in matrix form as follows:

$$a_Q + S(r_{Q/F})\alpha_{fw} = r_2 S(\omega_{fw})(S(\dot{\lambda}_f)n_Q + S(\lambda_f)\dot{n}_Q), \tag{3.14}$$

with similar expressions for $\dot{n}_Q$, λ_f and $\dot{\lambda}_f$. They are given below.

$$\dot{n}_Q = S(\omega_{fw})n_Q. \tag{3.15}$$

$$\lambda_f = \frac{-S(e_3)n_Q}{\sqrt{n_Q^T S^T(e_3)S(e_3)n_Q}}. \tag{3.16}$$

$$\dot{\lambda}_f = \frac{-S(e_3)\dot{n}_Q}{\sqrt{n_Q^T S^T(e_3)S(e_3)n_Q}} + \frac{S(e_3)n_Q\dot{n}_Q^T S^T(e_3)S(e_3)n_Q}{(n_Q^T S^T(e_3)S(e_3)n_Q)^{3/2}}. \tag{3.17}$$

We thus have six more scalar equations (Eqs. 3.10 and 3.14).

Pausing to take stock, we note that we so far have the following unknown vectors: $\underline{a}_P$, $\underline{a}_G$, $\underline{a}_H$, $\underline{a}_Q$, $\underline{\alpha}_{rw}$, $\underline{\alpha}_{rf}$, $\underline{\alpha}_{ff}$, $\underline{\alpha}_{fw}$, $\underline{F}_{rw}$ and $\underline{F}_{fw}$. Thus, we have 30 scalar unknowns so far. We also have 15 equations so far. The additional equations needed will come from kinematic relations among the nonminimal set of unknowns.

3.4 Further Kinematic Relations

We begin with

$$\underline{v}_G = \underline{v}_P + \underline{\omega}_{rf} \times \underline{r}_{G/P}.$$

Differentiating, we get

$$\underline{a}_G = \underline{a}_P + \underline{\alpha}_{rf} \times \underline{r}_{G/P} + \underline{\omega}_{rf} \times \underline{\omega}_{rf} \times \underline{r}_{G/P},$$

which in matrix notation is

$$a_G - a_P + S(r_{G/P})\alpha_{rf} = S(\omega_{rf})S(\omega_{rf})r_{G/P}. \tag{3.18}$$

In the above, as before, we use the trick of writing $S(r_{G/P})\alpha_{rf}$ instead of $-S(\alpha_{rf})r_{G/P}$, so that the unknown quantities stay on the right side of the matrix product, while the premultiplying coefficient matrices may be input easily into Matlab.

Similarly, we can write relations between a_H and a_G and between a_Q and a_H.

$$a_H - a_G + S(r_{S/G})\alpha_{rf} + S(r_{H/S})\alpha_{ff} = S(\omega_{rf})S(\omega_{rf})r_{S/G} + S(\omega_{ff})S(\omega_{ff})r_{H/S}. \tag{3.19}$$

$$a_Q - a_H + S(r_{Q/H})\alpha_{ff} = S(\omega_{ff})S(\omega_{ff})r_{Q/H}. \tag{3.20}$$

We have thus added 9 scalar equations (Eqs. 3.18, 3.19 and 3.20), and are presently short by 6.

Now we write relations connecting the angular accelerations of the four rigid bodies. We have

$$\underline{\omega}_{rw} = \underline{\omega}_{rf} + \dot{\beta}_r \hat{n}_P.$$

Differentiating with respect to time, we have

$$\underline{\alpha}_{rw} = \underline{\alpha}_{rf} + \ddot{\beta}_r \hat{n}_P + \dot{\beta}_r (\underline{\omega}_{rf} \times \hat{n}_P),$$

which in matrix notation is

$$\alpha_{rw} - \alpha_{rf} - \ddot{\beta}_r n_P = \dot{\beta}_r S(\omega_{rf}) n_P. \tag{3.21}$$

Note that, when assembling the final set of equations, the left hand side above will be written as

$$I\alpha_{rw} - I\alpha_{rf} - n_P \ddot{\beta}_r,$$

where I is the 3×3 identity matrix; this helps identify the coefficient matrices of unknown quantities.

Similarly we can write

$$\alpha_{ff} - \alpha_{rf} - \ddot{\psi}_f n_f = \dot{\psi}_f S(\omega_{rf}) n_f. \tag{3.22}$$

$$\alpha_{fw} - \alpha_{ff} - \ddot{\beta}_f n_Q = \dot{\beta}_f S(\omega_{ff}) n_Q. \tag{3.23}$$

Thus we have introduced 3 more unknowns, $\ddot{\beta}_r$, $\ddot{\psi}_f$ and $\ddot{\beta}_f$, giving a total of 33 unknowns. But we have added Eqs. 3.21, 3.22 and 3.23, which are all vector equations, to our previously obtained 24 scalar equations. So we now have 33 independent equations as well. This system of 33 linear equations in 33 variables can be solved numerically.

3.5 Second Derivatives of Euler Angles from Angular Accelerations

A key step remains. We have now obtained $\ddot{\beta}_r$, $\ddot{\psi}_f$ and $\ddot{\beta}_f$ (second derivatives of 3 angles), along with $\ddot{x}$, $\ddot{y}$ and $\ddot{z}$. We also have $\underline{\alpha}_{rf}$, the angular acceleration of the rear frame. However, we need the second derivatives of the (3-1-3) Euler angles, i.e., $\ddot{\theta}$, $\ddot{\psi}$ and $\ddot{\phi}$. These are obtained as follows.

We again use the framework of (3-1-3) Euler angle rotations of an arbitrary rigid body. Let the reference position of the rigid body denote a reference frame F_1. Let F_2 be a frame that is always rotated about the e_3 axis through θ relative to F_1. Let frame F_3 be always rotated about the θ-rotated e_1 axis through ψ relative to F_2. Finally, let F_4 be always rotated about the first-θ-then-ψ-rotated e_3 axis through ϕ relative to F_3. It is clear that F_4 is attached to the moving rigid body.

It can be shown that the angular velocity of the rear frame is

$$\omega = \left[\begin{array}{ccc} e_3 & R_1 e_1 & R_2 R_1 e_3 \end{array} \right] \left\{ \begin{array}{c} \dot{\theta} \\ \dot{\psi} \\ \dot{\phi} \end{array} \right\},$$

which we abbreviate to $\omega = A\dot{\Theta}$. Then we can show that

$$\alpha_{rf} = A\ddot{\Theta} + q\,,$$

where

$$q = S(R_1 e_1 \dot{\psi} + e_3 \dot{\theta}) R_2 R_1 e_3 \dot{\phi} + S(e_3 \dot{\theta}) R_1 e_1 \dot{\psi}\,.$$

The above can be used to solve for $\ddot{\Theta}$, once α_{rf} has been obtained from the Newton-Euler equations.

We now have a numerical procedure for obtaining the second derivatives of the system coordinates. The choice of initial conditions is subject to the same constraints as discussed in detail already for the Lagrange's equations case, except that z has not been eliminated in the Newton-Euler formulation, and so the initial conditions for z and $\dot{z}$ must also satisfy the system constraints. This straightforward issue is not discussed in any further detail.

Chapter 4

Numerical Solution of the Equations of Motion and Related Issues

4.1 Introduction

We have so far obtained the equations of motion for the bicycle in two different ways. Before proceeding to solve them numerically, we first need to verify that both the sets of derived equations are correct and exactly equivalent. Lagrange's equations, in our case are very long and have been obtained analytically using computer algebra. On the other hand, the Newton-Euler equations are shorter, and implemented numerically. The two independent sets of equations differ greatly in length and defy full manual comparison. We advocate the view, therefore, that numerical agreement to many digits (say, 10 or more) between outputs (accelerations) from two sets of equations for several sets of randomly generated inputs may be taken as a reliable demonstration of equivalence; and we will use such checks below. Before using such checks, we start with a discussion of how we have calculated the value of ϕ, which is our third Euler-angle.

4.2 Calculation and Uniqueness of $\phi(0)$.

Taking the point of contact of the front wheel with the ground to be F, we have

$$\underline{r}_F = \underline{r}_P + R_{rf}\underline{r}_{S/P,ref} + R_{ff}\underline{r}_{Q/S,ref} + \underline{r}_{F/Q}, \tag{4.1}$$

where, as mentioned earlier, R_{rf} and R_{ff} are the rotation matrices for the rear frame and front frame respectively. Also $\underline{r}_{F/Q}$ is given as

$$\underline{r}_{F/Q} = -r_2\,(\underline{\lambda}_f \times \hat{n}_Q), \tag{4.2}$$

where r_2 is the radius of the front wheel and

$$\underline{\lambda}_f = \frac{\hat{n}_Q \times \hat{k}}{\left|\hat{n}_Q \times \hat{k}\right|}.$$

P, S, Q and $\hat{n}_Q$ are as shown in figure 2.1. The z-component of $\underline{r}_F$, if equated to zero, yields an implicit relation in ϕ, ψ and ψ_f only. This equation is nonlinear (with trigonometric terms) but independent of velocities. Solving this equation numerically, we obtain $\phi(0)$ for given initial conditions on the remaining coordinates.

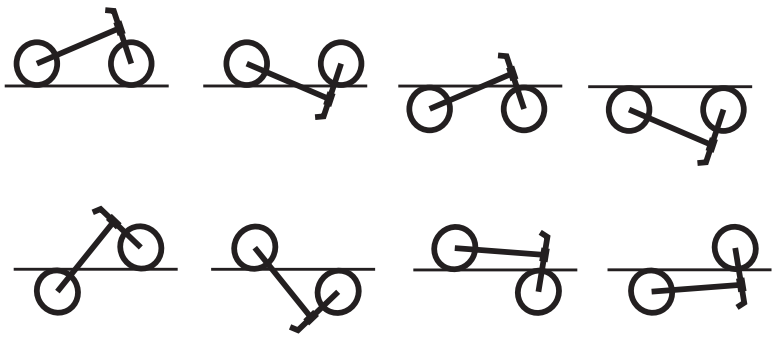

Figure 4.1: Eight possible ways in which the wheels of a vertical bicycle may, mathematically, touch the ground. Of these, only the first two from the left in the first row are recognized in our formulation, because we explicitly take the lowermost point on each wheel to be touching the ground. Of those two, the first is of interest here.

There are actually four ways in which a vertical and upright bicycle's wheels may touch the ground: these involve each wheel, independently, being either below the ground (touching the ground at its topmost surface) or above the ground (touching the ground at its lowermost surface). Holding the bicycle vertical but upside down, there are four more possible configurations where both wheels touch the ground. Thus, there are a total of eight possible configurations, as sketched in figure 4.1, with only two being recognized in our formulation and one of those two being of actual interest.

For a vertical, straight-running bicycle, the appropriate initial condition is $\phi(0) = \pi$ (figure 4.1, top left). This is a direct consequence of the fact that in the reference configuration (figure 2.1), both wheels touch the x-axis, and the bicycle lies in the negative-y half plane. Choosing $\phi(0) = 0$ in this situation corresponds to the configuration of figure 4.1 (first row, second from left).

It appears, from our numerical simulations and animations, that in general (non-vertical, non-straight) choices of initial values of coordinates, there are again two possible choices of $\phi(0)$. Of these, choosing the one closer to π seems to give the solution of interest, which we verify post facto from the animation of the moving bicycle.

There exist geometries (e.g., very large rear wheels with all other component sizes small) and initial configurations for which there are no solutions for $\phi(0)$. These fall outside the purview our study.

4.3 Checking the Equivalence of the Two Sets of Equations

Having discussed the procedure which gives us the initial value of ϕ, we are now in a position to check the equivalence of our two independent sets of equations. For several arbitrary (random) choices of coordinates and their first derivatives, the second derivatives obtained from the Lagrange and Newton-Euler sets of equations matched to machine precision; see table 4.1. We conclude that our two sets of equations are exactly equivalent.

Input		Output	
q	$\dot{q}$	Lagrange ($\ddot{q}$)	Newton-Euler ($\ddot{q}$)
$x = 0$	-2.8069345714545	-0.5041626315047	-0.5041626315047
$y = 0$	-0.1480982396001	-0.3449706619454	-0.3449706619454
$z = 0.2440472102925$	0.1058778746261	-	-1.4604528332980
$\theta = 0$	0.7830033527065	0.8353281706379	0.8353281706379
$\psi = 0.9501292851472$	0.6068425835418	-7.8555281128244	-7.8555281128244
$\phi = 3.1257073014894$	-0.0119185528069	0.1205543897884	0.1205543897884
$\psi_f = 0.2311385135743$	0.4859824687093	-4.6198904039403	-4.6198904039403
$\beta_r = 0$	8.9129896614890	1.8472554144217	1.8472554144217
$\beta_f = 0$	8.0133620584155	2.4548072904550	2.4548072904550

Table 4.1: Comparison of the results obtained using Lagrange and Newton-Euler. The initial conditions are consistent with the constraints. The first and the second columns represent the inputs, while the third and the fourth columns represent the outputs.

4.4 Nonlinear Dynamic Simulation

Having checked the equivalence of the two sets of equations, we now integrate our Newton-Euler equations with one set of initial conditions which are consistent with the constraints. This simulation matches the one presented in [17], and the (visual) match with their results provides further support for the correctness of the equations that we use here. For comparison and reference, we list the initial conditions here. The *nonzero* initial conditions at $t = 0$ are (all given values taken to 16 digits; all others taken as zero)

$$\begin{gathered}\dot{x}(0) = -4.6\,\mathrm{m/s},\ \dot{\mathrm{y}}(0) = -0.15\,\mathrm{m/s},\ \psi(0) = \pi/2,\ \dot{\psi}(0) = 0.5\,\mathrm{s}^{-1},\\ \phi(0) = \pi,\ \dot{\beta}_r(0) = 15.333\,\mathrm{s}^{-1},\ \dot{\beta}_\mathrm{f}(0) = 13.143\,\mathrm{s}^{-1}.\end{gathered} \tag{4.3}$$

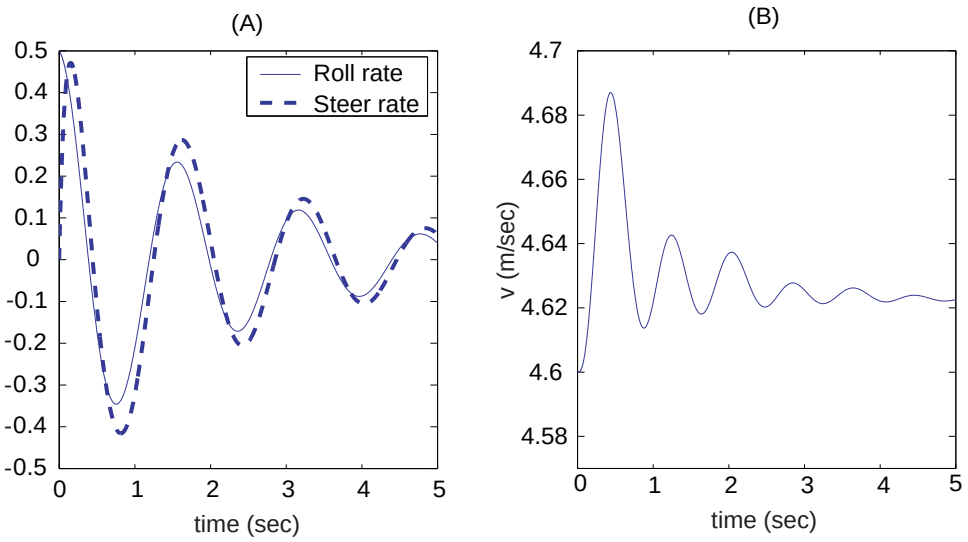

Figure 4.2: (A) Here roll rate means $\dot{\psi}$, steer rate means $\dot{\psi}_f$. (B) Forward speed v is taken as $\dot{\beta}_r\, r_1$.

The velocity initial conditions chosen here are $\dot{\beta}_r(0)$, $\dot{\psi}(0)$ and $\dot{\psi}_f(0)$. Of these, the first sets the forward speed ($v(0) = \dot{\beta}_r(0) r_1$); the second sets the initial roll (or lean) rate; and the third sets the initial steer rate. On specifying these three arbitrarily, the remaining five are found from the velocity constraint equations.

In the initial conditions of Eq. 4.3, $\dot{\beta}_r(0)$ sets $v = 4.6$ m/s, which falls within the hands-free stable speed range of the bicycle. We will find the stable speed range in chapter 5. There is a perturbation of $\dot{\psi} = 0.5$ rad/s to the roll rate. Results are plotted in figure 4.2.

When an uncontrolled bicycle is within its stable speed range, roll and steer perturbations die away in a seemingly damped fashion. However, the system has no true energy dissipation and hence conserves energy. A non-linear dynamic analysis was performed on the bicycle model to demonstrate the transfer of energy from lateral perturbations into forward speed. Figure 4.2 (B) shows a small increase in the forward speed v while the lateral motions die out, as expected. Figure 4.2 (A) also shows that the period for the roll and steer oscillations is approximately 1.60 s. The steering motion $\dot{\psi}_f$ has a small phase

lag relative to the roll motion $\dot{\psi}$ visible in the solution in figure 4.2 (A). The match with [17] is, as far as we can tell, exact.

4.5 Post-facto Coordinate Partitioning on Velocities

For general initial conditions, the holonomic and nonholonomic constraints are not always numerically satisfied to high accuracy over long times if the constraint equations have been incorporated after differentiation. These constraint equations can be satisfied much more accurately using coordinate partitioning on velocities. For nonholonomic constraints, we can use the equations (and Matlab code) that we already have. The holonomic constraint, if treated as a nonholonomic constraint after one differentiation, can be included here. Direct enforcement of the holonomic constraint involves differential algebraic equations (DAEs) which are not discussed here.

Let $\hat{q}$ (as distinct from the previously used symbol q) denote the generalized coordinates. Given an N-dof system with p nonholonomic constraints of the form

$$\sum_{j=1}^{N} a_{ij}(\hat{q})\dot{\hat{q}}_j + a_{it}(\hat{q}) = 0, \quad i = 1, 2, \cdots, p,$$

we may solve (after possible renumbering) for the first p rates, i.e., for

$$\dot{\hat{q}}_1, \dot{\hat{q}}_2, \cdots, \dot{\hat{q}}_p$$

in terms of the other $N - p$ rates and the full vector of generalized coordinates $\hat{q}$. We may now treat the actual state vector as composed of $\hat{q}$ along with the latter $N - p$ rates, i.e.,

$$\tilde{q} = \{\hat{q}^T, \dot{\hat{q}}_{p+1}, \dot{\hat{q}}_{p+2}, \cdots, \dot{\hat{q}}_N\}^T.$$

Given this state vector, we use the nonholonomic constraint equations to obtain a full set of $\dot{\hat{q}}$'s. Constructing a new augmented state vector $\{\hat{q}^T, \dot{\hat{q}}^T\}^T$ (nothing but our old q), we use our existing equations of motion to find the full set of $\ddot{\hat{q}}$'s. We then discard the first p second derivatives, and use $\dot{\tilde{q}}$. In this way the first p rates are chosen to constantly satisfy the nonholonomic constraints. There is little added conceptual complication or computational load. We have adopted this procedure for our simulations, but not a DAE solver for the holonomic constraints in their undifferentiated form.

Chapter 5

Linearized Equations of Motion

5.1 Introduction

In this chapter, we study the stability of straight motion of the bicycle. We have two sets of equations at our disposal. We choose Lagrange's equations for linearization. After linearizing them, we examine the corresponding eigenvalue problem. The characteristic polynomial is a quartic, giving four nontrivial eigenvalues. Several eigenmodes like weave, capsize and a stable mode called caster have been identified and the speed ranges in which they are dominant are computed. This leads to the determination of a stable speed range for the uncontrolled bicycle. Our approach, based on explicit linearization of Lagrange's equations in Maple, differs significantly from [17]. However, the results match exactly.

5.2 Stability of Straight Motion

The Newton-Euler procedure discussed in chapter 3 is good for simulating general (nonlinear) motions, but not amenable to analytical linearization for near-straight motions. Here, we use the Lagrangian approach. Since the equations are very long, we found it necessary to substitute the numerical values of system parameters of the bicycle before the linearized equations were obtained. The bicycle design parameters are listed in tables A.1 and A.2 in

the appendix.

We make the following substitutions into the equations of motion:

$$\{\theta = \epsilon\tilde{\theta},\, \psi = \pi/2 + \epsilon\tilde{\psi},\, \phi = \pi + \epsilon\tilde{\phi},\, \psi_f = \epsilon\tilde{\psi}_f,\, x = -v\,t + \epsilon\tilde{x},$$
$$y = \epsilon\tilde{y},\, \beta_r = v\,t/r_1 + \epsilon\tilde{\beta}_r,\, \beta_f = -v\,t/r_2 + \epsilon\tilde{\beta}_f\},$$

where ϵ is infinitesimal, v is the nominal forward velocity of the bicycle, and t is time. Setting $\epsilon = 0$ gives the solution corresponding to exactly straight line motion.

The constraint forces, represented here by λ's, still need to be solved for from a straightforward set of linear equations. We find that, barring $\lambda_5 = 309.30353\cdots$, all of them are zero. Accordingly, for near-straight motions, we substitute into the equations of motion:

$$\{\lambda_1 = \epsilon\tilde{\lambda}_1, \lambda_2 = \epsilon\tilde{\lambda}_2, \lambda_3 = \epsilon\tilde{\lambda}_3, \lambda_4 = \epsilon\tilde{\lambda}_4, \lambda_5 = 309.30353\cdots + \epsilon\tilde{\lambda}_5\}.$$

We now expand the equations of motion in a Taylor series (Maple) about $\epsilon = 0$ and drop terms of $\mathcal{O}(\epsilon^2)$. For completeness, we present these equations below. Numerical values are shown accurate to 5 places of decimals here; numbers with fewer decimal places signify additional zeros not presented to save space; in our actual calculations, 20 total digits of precision were retained. Finally, we have dropped the tildes because all quantities shown below have them.

$$94\,\ddot{x} - 52.75\,\ddot{\phi} - \lambda_1 - \lambda_3 = 0. \tag{5.1}$$

$$94\,\ddot{y} - 52.75\,\ddot{\psi} - 32.16\,\ddot{\theta} - 0.20062\,\ddot{\psi}_f - \lambda_2 - \lambda_4 = 0. \tag{5.2}$$

$$-52.75\,\ddot{x} + 56.7187\,\ddot{\phi} + 0.12\,\ddot{\beta}_r + 0.28\,\ddot{\beta}_f - 502.01232\,\phi - 0.3\,\lambda_3 - 0.3\,\lambda_1 + 1.02\,\lambda_5 = 0. \tag{5.3}$$

$$-52.75000\,\ddot{y} + 19.28544\,\ddot{\theta} + 40.70722\,\ddot{\psi} + 0.10101\,\ddot{\psi}_f + 0.76085\,v\,\dot{\psi}_f$$
$$+1.20\,v\,\dot{\theta} - 25.50126\,\psi_f - 794.1195\,\psi - 0.3\,\lambda_2 - 0.3\,\lambda_4 = 0. \tag{5.4}$$

$$-32.16\,\ddot{y} + 17.01908\,\ddot{\theta} + 19.28544\,\ddot{\psi} + 0.33012\,\ddot{\psi}_f - 0.24721\,v\,\dot{\psi}_f - 1.2\,v\,\dot{\psi} + 1.02\,\lambda_4 = 0. \tag{5.5}$$

$$-0.20062\,\ddot{y} + 0.33012\,\ddot{\theta} + 0.15390\,\ddot{\psi}_f + 0.10101\,\ddot{\psi} + 0.24721\,v\,\dot{\theta}$$
$$-0.76085\,v\,\dot{\psi} - 7.88032\,\psi_f - 25.50126\,\psi - 0.07608\,\lambda_4 = 0. \tag{5.6}$$

$$0.12\,\ddot{\phi} + 0.12\,\ddot{\beta}_r - 0.3\,\lambda_1 = 0. \tag{5.7}$$

$$0.28\,\ddot{\phi} + 0.28\,\ddot{\beta}_f - 0.35\,\lambda_3 = 0. \tag{5.8}$$

Also the constraint equations are as follows:

$$\dot{x} + 0.3\,\dot{\phi} + 0.3\,\dot{\beta}_r = 0. \tag{5.9}$$

$$\dot{y} + 0.3\,\dot{\psi} + v\,\theta = 0. \tag{5.10}$$

$$\dot{x} + 0.35\,\dot{\beta}_f + 0.3\,\dot{\phi} = 0. \tag{5.11}$$

$$\dot{y} + 0.07608\,\dot{\psi}_f + 0.3\,\dot{\psi} - 1.02\,\dot{\theta} + 0.95106\,v\,\psi_f + v\,\theta = 0. \tag{5.12}$$

$$1.02\,\dot{\phi} = 0. \tag{5.13}$$

Note that we do not differentiate the five velocity constraint equations. Instead, we solve them for $\dot{\tilde{x}}$, $\dot{\tilde{y}}$, $\dot{\tilde{\phi}}$ $\dot{\tilde{\theta}}$ and $\dot{\tilde{\beta}}_r$, and substitute into Lagrange's equations of motion, differentiating as needed (e.g., differentiating $\dot{\tilde{x}}$ where $\ddot{\tilde{x}}$ is needed). We solve the resulting 8 linear equations for the 5 $\tilde{\lambda}$'s, $\ddot{\tilde{\beta}}_f$, $\ddot{\tilde{\psi}}$ and $\ddot{\tilde{\psi}}_f$. The solutions for the $\tilde{\lambda}$'s are not needed further in our analysis. Hence we discard them. Also we find that $\ddot{\tilde{\beta}}_f \equiv 0$. There remain 2 equations giving $\ddot{\tilde{\psi}}$ and $\ddot{\tilde{\psi}}_f$. Dropping tildes, they are (we retained more decimal places than shown here):

$$\ddot{\psi} = -0.10552\,v\,\dot{\psi} - 0.33052\,v\,\dot{\psi}_f + 9.48977\,\psi - (0.57152 + 0.89120\,v^2)\,\psi_f \tag{5.14}$$

$$\ddot{\psi}_f = 3.67681\,v\,\dot{\psi} - 3.08487\,v\,\dot{\psi}_f + 11.71948\,\psi + (30.90875 - 1.97172\,v^2)\,\psi_f \tag{5.15}$$

The last two equations can also be written in the form:

$$\mathbf{M}\,\ddot{q} + v\,\mathbf{C}\,\dot{q} + [g\,\mathbf{K_1} + v^2\,\mathbf{K_2}]\,q = \mathbf{0} \tag{5.16}$$

The elements of the individual matrices $\mathbf{M}$, $\mathbf{C}$, $\mathbf{K_1}$ and $\mathbf{K_2}$ are defined in terms of the parameters of the bicycle as can be found in [17]. Also it is to be noted that $\mathbf{M}$ is a symmetric mass matrix which gives the kinetic energy of the bicycle system at zero forward speed. The damping-like matrix $\mathbf{C_{eq}} = v\,\mathbf{C}$ is linear in the forward speed v. The stiffness matrix $\mathbf{K_{eq}}$ is the sum of two parts: a velocity- independent symmetric part $g\,\mathbf{K_1}$ proportional to the gravitational acceleration, which can be used to calculate changes in potential energy and a part $v^2\,\mathbf{K_2}$, which is quadratic in the forward speed and is due to centrifugal effects.

5.2.1 Stability results

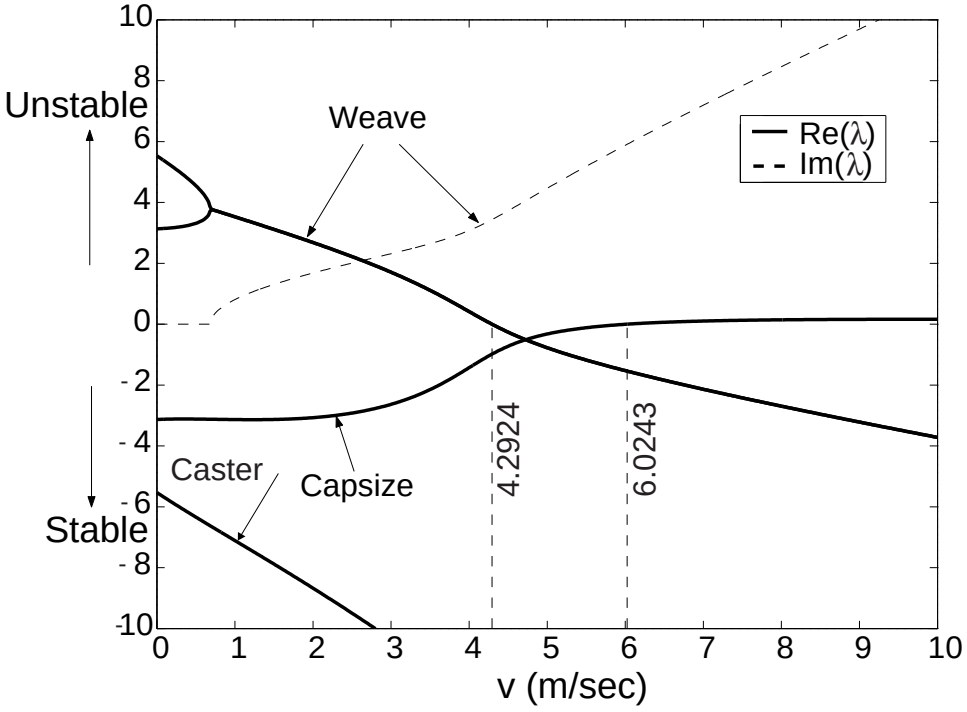

Figure 5.1: Plot of eigenvalues versus forward speed v as obtained from the linear stability analysis.

The discussion in this paragraph has substantial similarities to the one in [17]. Stability eigenvalues are independent of the choice of coordinates and also independent of the form of the equations. Any non-singular change of variables yields equations with the same linearized stability eigenvalues. Thus stability eigenvalues serve well as convenient benchmark results permitting comparison between different approaches. The stability eigenvalues are calculated by assuming an exponential solution of the form $q = q_0 \exp(\lambda t)$ for the homogeneous equations in Eqs. 5.14 and 5.15. This leads to the characteristic polynomial, which is a polynomial of degree 4 in λ. The solutions λ of the characteristic polynomial for a range of forward speeds are shown in figure 5.1. Eigenvalues with a positive real part correspond to unstable motions whereas eigenvalues with a negative real part correspond to asymptotically stable motions for the corresponding mode. Imaginary eigenvalues cor-

respond to oscillatory motions. The time-reversal nature of these conservative dynamical equations leads to symmetry in the characteristic equation and in the parameterized solutions: if (v, λ) is a solution then $(-v, -\lambda)$ is also a solution. This means that figure 5.1 is symmetric about the origin.

This fourth order system has four distinct eigenmodes except at special parameter values associated with multiple roots. A complex (oscillatory) eigenvalue pair is associated with a pair of complex eigenmodes. For large speeds, the two modes which play a vital role in determining the stability of the bicycle are traditionally called the capsize mode and weave mode. The capsize mode corresponds to a real eigenvalue: when unstable, a capsizing bicycle leans progressively from the vertical with steer and lean both increasing until it falls over like a capsizing ship. The weave mode is an oscillatory motion in which the bicycle steers tortuously about the headed direction with a slight phase lag relative to leaning. The third eigenvalue is large, real and negative. It corresponds to a stable mode called castering.

At small speeds, say between $0 < v < 0.5$ m/s, there are two pairs of real eigenvalues. Each pair consists of a positive and a negative eigenvalue and corresponds to an inverted-pendulum-like falling of the bicycle. The positive root in each pair corresponds to falling, whereas the negative root corresponds to the time reversal of this falling. When speed is increased to $v_d = 0.684$ m/s, two real eigenvalues coalesce and form a complex conjugate pair; this is where the oscillatory weave motion emerges. At first this motion is unstable but at $v_w = 4.292$ m/s, the weave eigenvalues cross the imaginary axis in a Hopf bifurcation and this mode becomes stable. At a higher speed the capsize eigenvalue crosses the origin in a pitchfork bifurcation at $v_c = 6.024$ m/s, the capsize speed, and the bicycle becomes mildly unstable. The speed range for which the uncontrolled bicycle shows asymptotically stable behaviour, with all eigenvalues having negative real part, is $v_w < v < v_c$.

5.2.2 The *other* straight motion

The bicycle also has straight motions where the handle rotation is $\pm\pi$ (we use $-\pi$ here and below). The linearized equations governing stability of such straight motions are:

$$\ddot{\psi} = -0.16392\, v\, \dot{\psi} - 0.33879\, v\, \dot{\psi}_f + 9.19308\, \psi - (1.59980 + 0.90354\, v^2)\, \psi_f \tag{5.17}$$

$$\ddot{\psi}_f = 3.19888\, v\, \dot{\psi} - 3.11851\, v\, \dot{\psi}_f + 11.17234\, \psi + (41.76704 - 1.79831\, v^2)\, \psi_f \tag{5.18}$$

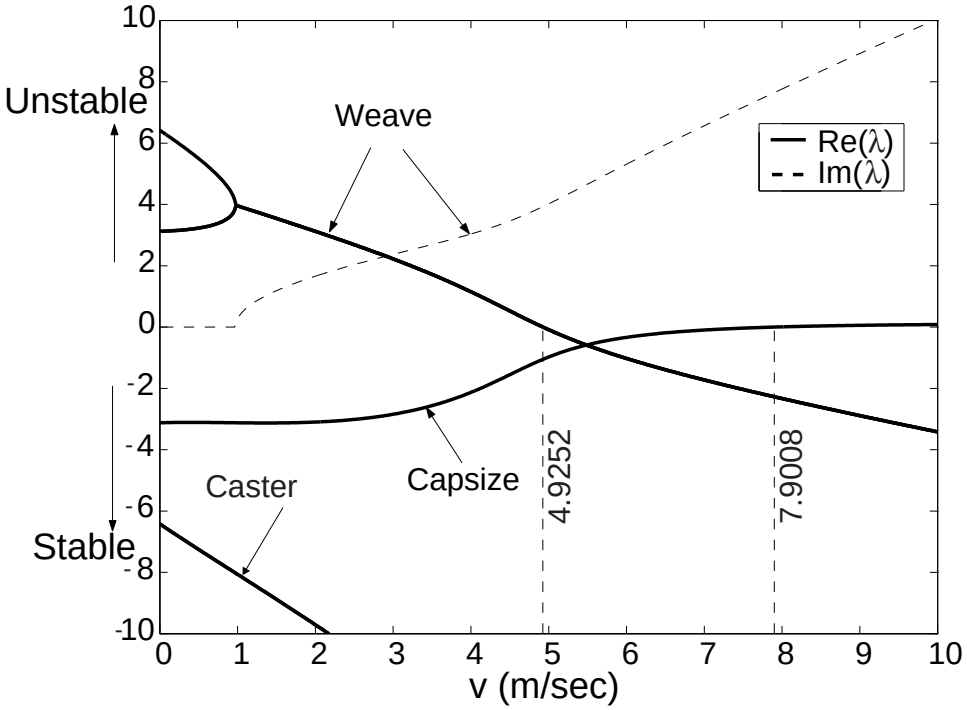

Figure 5.2: Eigenvalues governing stability of straight motion with $\psi_f = -\pi$, versus forward speed v.

Qualitatively, the figure is similar to that obtained for stability of straight motion with $\psi_f = 0$. Two key numerical values are the speeds limiting the stable range: these are 4.9252 and 7.9008 m/s.

Chapter 6

Circular Motions of the Bicycle

6.1 Introduction

In this chapter, we study hands-free circular motions of the bicycle. The topic of hands-free circular motions might be initially misunderstood because human riders can follow a wide range of circles at arbitrary speeds. However, this is only possible by the imposition of handlebar torques and the displacement of the torso of the rider about the vertical symmetry plane of the bicycle. With zero handle torque and a rigid rider, only a few discrete lean angles are possible at each speed. Circular motions can be parameterized by a radius, say the radius R traversed by the rear wheel centre. A particular value of the radius is chosen and based on that the lean angle ψ, the steer angle ψ_f and the rear wheel spin rate $\dot{\beta}_r$ which lead to the circular motion can be computed based on the satisfaction of certain conditions. Then the radius is changed by a small amount from its existing value and the same process is repeated. In this way, we get $(\psi, \psi_f, \dot{\beta}_r)$ for each value of the parameter R.

6.2 Circular Motions

6.2.1 Finding hands-free circular motions

In circular motions, x and y vary sinusoidally and z is constant. The rear wheel center traverses a circle of radius (say) R. The first Euler angle θ (heading) grows linearly with time. The second Euler angle ψ (roll), the third Euler angle ϕ (pitch), the steering rotation angle ψ_f, and the wheel spin rates $\dot{\beta}_f$ and $\dot{\beta}_r$ are all constants.

We seek a triple $(\psi, \psi_f, \dot{\beta}_r)$ subject to some conditions, dependent on a free parameter R, as follows.

(1) Given ψ and ψ_f, ϕ is found as discussed earlier. **(2)** ψ determines z (used in our Newton-Euler equations); and $\dot{z} = 0$. **(3)** The initial values of θ, x, y, β_r and β_f are arbitrarily taken as zero. **(4)** Setting $\dot{\psi} = \dot{\psi}_f = 0$, and with $\dot{\beta}_r$ given (or chosen), the velocity constraint equations give $\dot{x}$, $\dot{y}$, $\dot{\theta}$, $\dot{\phi}$ and $\dot{\beta}_f$. (We find that $\dot{\phi} = 0$.) **(5)** Having all initial conditions required for the Newton-Euler equations, we find the second derivatives of the coordinates. **(6)** Finally, we define a vector function with R as a parameter:

$$\left\{\psi, \psi_f, \dot{\beta}_r\right\}^T \mapsto \left\{\sqrt{\dot{x}^2 + \dot{y}^2} - R\dot{\theta}, \ddot{\psi}, \ddot{\psi}_f\right\}^T.$$

(7) We numerically find an R-parameterized family of zeroes of the above map, where steer and lean acceleration vanish.

6.2.2 Symmetries in the circular motion families

We note here that the existence of one circular hands-free motion implies the existence of three others, by symmetry. Firstly, one may create a mirror image of the configuration, for example leaning and steering rightwards instead of leftward. Secondly, the rotational velocities of both wheels may be reversed, without affecting inertial forces and moments. Thus we have four-way symmetry in the solutions of all circular motions.

6.2.3 Plotting hands-free circular motions

The number of families of circular motion solutions, not counting symmetries, is three or four depending on how we count. Consider, initially, the schematic in figure 6.1, depicting lean (left) and steer (right), as a function of front-wheel speed.

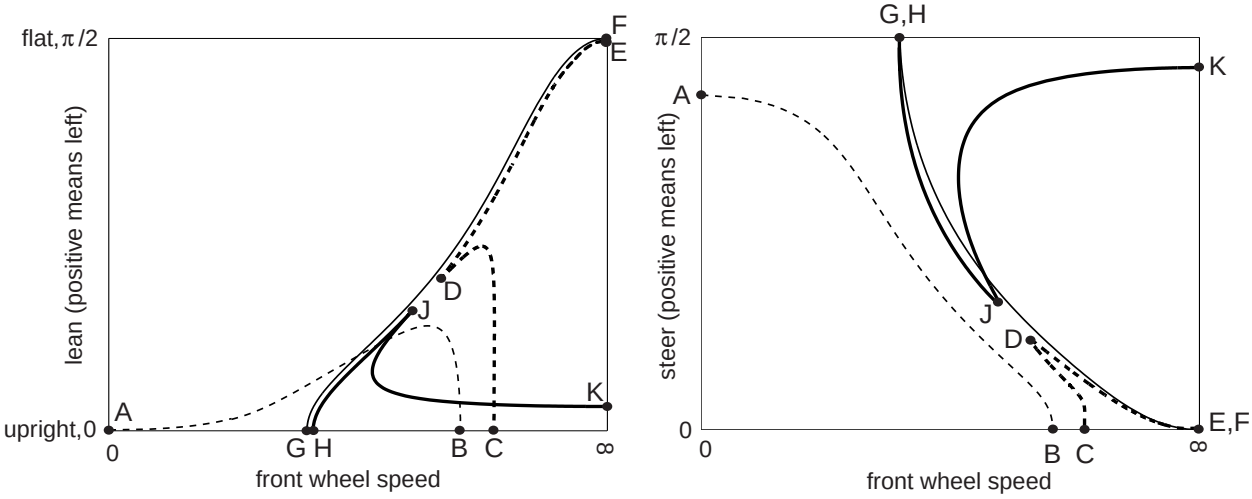

Figure 6.1: Circular motion families (schematic). Left: lean. Right: steer.

In the left figure, lean is defined as $\psi - \pi/2$, positive when the bicycle leans left, and shown here from 0 (upright) to $\pi/2$ (flat on the ground). In the right figure, steer angle is plotted from 0 (straight) to $\pi/2$ (perpendicular leftwards). Front wheel speed (really, speed of the front contact point) is $\dot{\beta}_f r_2$, and is plotted from 0 to ∞ in a nonuniform scaling ($\dot{\beta}_f$ is obtained from $\dot{\beta}_r$ using the velocity constraint equations).

For the two heavy curves (one solid, one dashed) $\dot{\beta}_f r_2 < 0$, and $-\dot{\beta}_f r_2$ is plotted instead. For these heavy curves, $\dot{\beta}_f r_2 < 0$ corresponds to the bicycle moving forward with a reversed handlebar (i.e. turned beyond $\pi/2$). In figure 6.1 (right), for the heavy curves corresponding to reversed handlebars, π has been added to the steer ψ_f.

For visualization, separation between nearly-coincident portions of light and heavy curves is exaggerated. Points E and F coincide in reality, as do G and H.

Handlebar asymmetry plays a role in the solutions obtained. Turning the handle by π (i.e., reversing the handlebar) effectively gives a slightly different bicycle. If the front wheel center was exactly on the fork axis; the front fork plus handlebar center of mass was exactly on the fork axis; and an eigenvector of the front fork assembly's central moment of inertia matrix coincided with the front fork axis; then handlebar reversal would give exactly the same bicycle. The reader might wish to consider the heavy lines in figure 6.1 not as alternatively-plotted curves at all, but regularly-plotted curves for a different bicycle whose front assembly is a reversed version of the benchmark's. Here, we avoid this expedient in favour of consistency.

6.2.4 Limiting motions

We now discuss various special motions and limiting configurations that help to understand the hands-free circular motions of the bicycle.

HF and HR bifurcations to large-radius turns: By Eqs. 5.14 and 5.15, 4 eigenvalues govern stability of straight motion. For hands-free circular motions with very large radii, all sufficiently small leans must give steady solutions, implying a zero eigenvalue. There is only one such point with handlebar forward (HF): the 'capsize' bifurcation at the upper limit of the stable speed range for straight motion (noted by [23]). With the handlebar reversed (HR), there is a similar stable speed range with its own capsize point. These points are labeled B and C in figure 6.1. Near these points, lean and steer (off 0 or $-\pi$ as appropriate) are both small, and the radius is large.

HF and HR flat spinning: There are limiting circular motions where the lean approaches $\pi/2$ (i.e., lying flat on the ground), steer approaches zero, turn radius approaches a small finite limit, and velocity approaches infinity. (The contact points are substantially displaced around each wheel.) Such solutions exist for both HF and HR configurations, i.e., with steer approaching 0 and $-\pi$. These points are labeled F and E, respectively, in figure 6.1. These limits require infinite friction.

HF upright static equilibrium: With the handlebar turned almost $\pi/2$, there is a static equilibrium with a lean angle of *exactly* zero, labeled A in figure 6.1. With a symmetric handlebar, it is obvious that an upright equilibrium exists with exactly $\pi/2$ steer.

But with the left-right asymmetry due to finite steer of an asymmetric handlebar, it seems surprising that the lean remains exactly zero, because equilibrium implies two conditions (handlebar torque and net bicycle-tipping torque both zero) on the one remaining variable (steer). To understand this, imagine locking the handlebar at a variety of near-$\pi/2$ steer angles, at each of which the equilibrium lean angle is determined. Select the locked steer angle that gives tipping-equilibrium with zero lean. Equilibrium ensures zero net moment on the bicycle about the line (say L) of intersection between the rear frame symmetry plane and ground. Of all forces on the bicycle, the two not in the symmetry plane are the front fork assembly weight and the front wheel ground contact force: they are therefore in moment equilibrium about L. But these two forces are then in moment equilibrium about the handle axis as well, and locking is not needed, explaining the zero lean at A. A detailed and alternative discussion follows later on.

Pivoting about a fixed rear contact point: It seems possible, for each steer angle, to find an angle of lean such that the normal to the front wheel rolling direction passes through the rear contact; in such a configuration, the bicycle rotates about the rear contact, which remains stationary. One imagines that by properly choosing both steer angle and front-wheel speed, we might simultaneously achieve roll and steer balance. Such a motion does exist: the steer is close to $\pi/2$ (handle turned left), the rear frame is nearly upright, and the front wheel follows a circle at a definite speed, and the bicycle pivots about a vertical axis through the rear wheel contact. Such motions were found for both HF and HR configurations (steer: $-\pi/2$). Nearby points, defined for plotting convenience at exactly zero lean, are labeled G and H, respectively, in figure 6.1. Noting that all motions of the bicycle are time-reversible, a pivoting motion can be reversed to give another where the front wheel speed and the handlebar are both reversed. Thus the HF and HR pivoting solutions coincide, as do G and H, although they are sketched distinct for visualization.

High speed dynamic equilibrium: Envisioning that terminal points occur in pairs, an expected eighth is found as K in figure 6.1. This configuration involves small lean, near-$\pi/2$ steer, and speed approaching infinity. It may be viewed as a perfectly dynamic counterpart to the static solution at A. It seems that the normal ground force at one wheel must become negative beyond some high speed for such a motion, but our analysis assumes sustained contact and ignores this question.

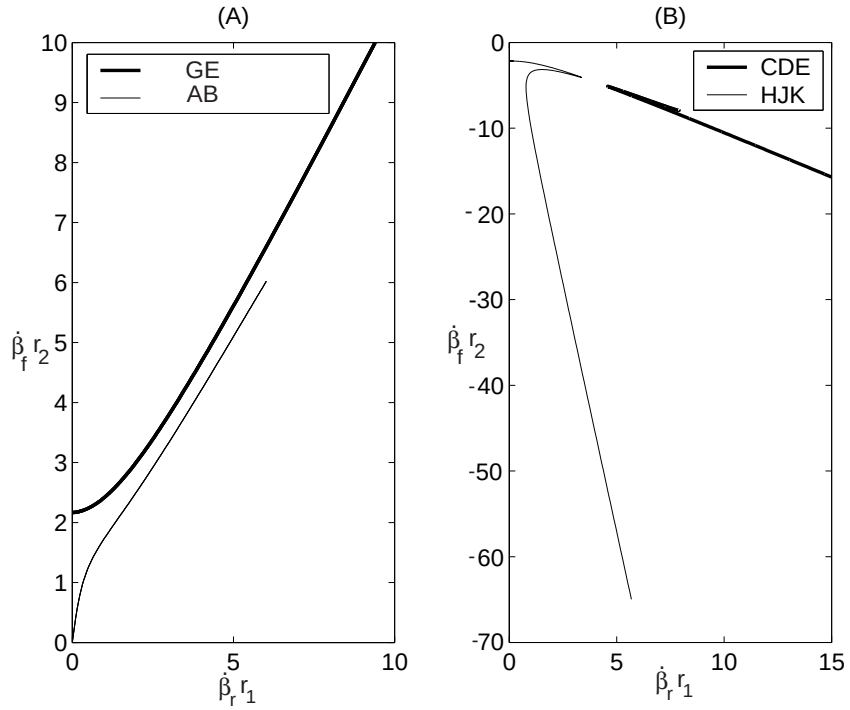

Figure 6.2: Variation of $\dot{\beta}_f\, r_2$ with $\dot{\beta}_r\, r_1$ for all the four circular motion families.

For easy visualization, we also plot the front wheel speed $\dot{\beta}_f\, r_2$ as a function of the rear wheel speed $\dot{\beta}_r\, r_1$. It can be seen that the plots suggest small rear-wheel-speeds for some circular motions where the front wheel is, in fact, moving rapidly. This turns out to be the case for the two families represented by the curves GE and HJK in figure 6.1. For the family represented by curve GE, we find $\dot{\beta}_f\, r_2$ is about 2.17 m/sec as the radius traversed by the rear wheel centre approaches 0, even though $\dot{\beta}_r\, r_1$ is quite small there. For the other family represented by curve HJK, $\dot{\beta}_f\, r_2$ is correspondingly about -2.17 m/sec, whereas $\dot{\beta}_r\, r_1$ is negligible there.

6.2.5 Description of the circular motion families

We can now connect appropriate pairs of endpoints to describe four circular motion families found for the bicycle.

One handlebar-forward family connects points B and A. The bicycle first bifurcates from HF straight motion, with steer and lean increasing while speed decreases, until a maximum lean angle is reached. Thereafter, steer continues to increase, and velocity continues to decrease, while lean decreases towards upright. The final perfectly upright state is approached via extremely slow motion, superficially like the pivoting points G = H but with the rear contact not quite fixed.

A handlebar-reversed family starts at C, bifurcating from HR straight motion. First the previous pattern is followed (attaining a maximum lean with continuously decreasing speed); but then at a near-cusp point labeled D, a qualitatively different curve is followed. The steer then decreases towards HR straightness, while lean and speed increase, as the bicycle approaches the flat and fast limit point E.

A third circular motion family, for continuity in the discussion, may be thought of as starting from the HF flat and fast limit F (the path radii of the rear wheel center differ at F and E). Velocity and lean angle decrease, while steer increasingly deviates until the rear frame is upright at pivoting motion G.

A fourth circular motion family starts with the identical pivoting motion at H (now considered HR), with lean increasing / steer decreasing up to a near-cusp at point J, and then reversing that trend to achieve a near upright lean and a nearly perpendicular steer, as the speed goes to infinity at K. But since G is essentially the same as H (except for an inconsequential speed reversal), the third and fourth families are actually one (G = H could be removed from the list of terminal points). This combined family – FGHJK – joins HF and HR configurations.

By this count, we have three circular motion families in all.

With this background, we consider qualitatively why heavy curves ED and JH lie so close to FG (figure 6.1). In both right and left plots, we actually see the broken curve FGHJ + DE *folded* at GH. In essence, this says that starting in an upright condition with the steer essentially $\pi/2$, an added leftward or rightward amount of steering leads to a bicycle with HR and HF configuration respectively; these two configurations may be viewed as almost-identical bicycles (due to 'small' handlebar asymmetry); and hence dynamic equilibria obtained are almost identical as well. Without handlebar asymmetry, the coincidence would be perfect.

In figure 6.1 (right), we have exaggerated the closeness of points G and H. In reality, due to the handlebar asymmetry, they have a small vertical separation, with G lying slightly above $\pi/2$ and H slightly below it. Actual numerical and graphical results presented below have no such misrepresentations.

Note that the hands-free-motion plots can also provide qualitative information about the sign of steer torque away from the plotted curves. For example, consider the light (HF) curves in the steer plot of figure 6.1. Recalling that the horizontal axis is also a line of zero steer torque, one can imagine increasing the steer angle at a speed just below B (such as 5 m/s in figure 6.3). The torque will become nonzero (negative, as it happens), attain a peak negative value, reduce to zero as the BA curve is crossed, then increase to a peak positive value, then drop again as the FG curve is approached. Thus, steer torque may vary significantly in both sign and slope (i.e., 'stiffness') as one alters turn radius, posing something of a control problem for the rider attempting to corner quickly at lean angles up to $\pi/4$ and steer angles up to $\pi/12$.

6.2.6 Accurate plots, with four-way symmetry

As mentioned above, for each circular motion, another is obtained if all speeds are reversed; and every left-leaning solution also implies a right-leaning one, where (ψ, ψ_f) are replaced by $(\pi - \psi, -\psi_f)$. The resulting four-way symmetry in the solutions is represented (actual numerics) in figure 6.3, where the infinite horizontal scale of $\dot{\beta}_f r_2$ is mapped to a finite range using the arctangent of $\dot{\beta}_f r_2/4$ (the 4 is an arbitrary scaling parameter chosen for better visualization).

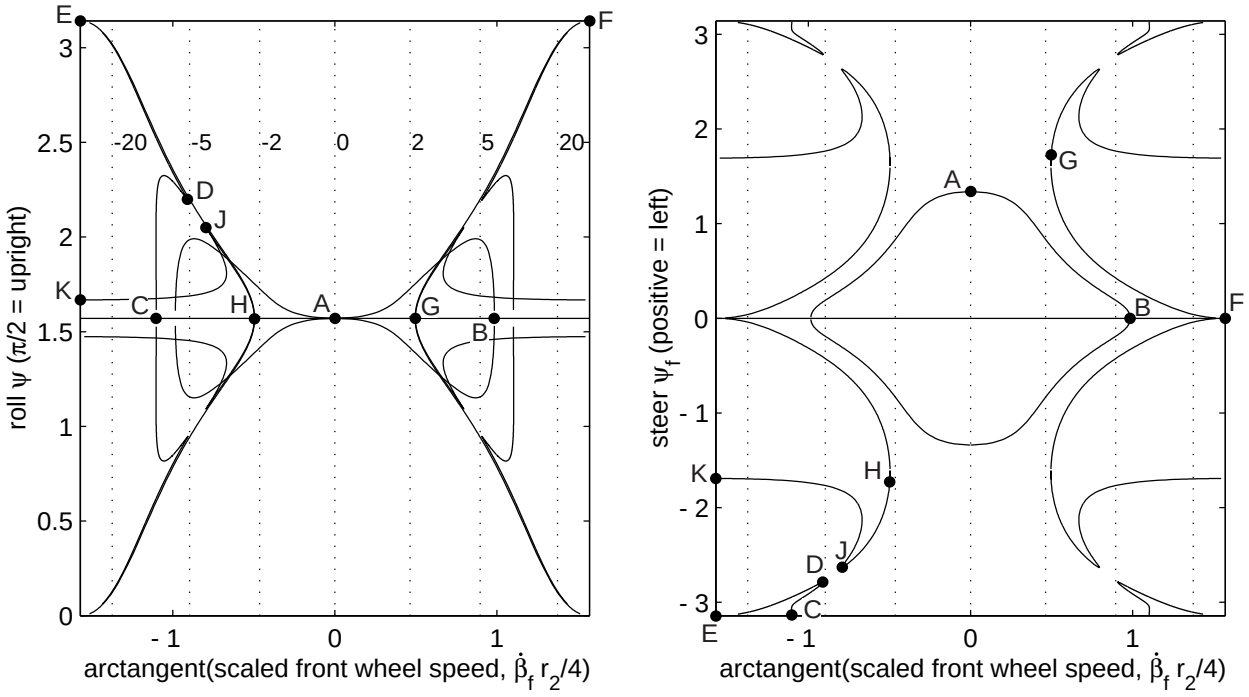

Figure 6.3: Circular motion families (numerics). Left: lean. Right: steer. The infinite speed range is mapped to a finite range using an arctangent mapping. Actual speeds at some locations are indicated using vertical dashed lines and labels (left). Curves plotted do not reach points B, C, E, F and K, and reflections thereof, because the numerical continuation calculation was stopped when the approach to these points was clear; in reality, they continue all the way to the indicated points.

All the curves represent numerically obtained solutions, while the labeled heavy dots indicate the correspondence with figure 6.1. Here, roll (ψ) has been plotted from 0 to π, instead of lean from $-\pi/2$ to $\pi/2$. Steer (ψ_f) has been plotted from $-\pi$ to π. As mentioned above, in figure 6.1 the heavy lines actually show $\pi + \psi_f$ against $-\dot{\beta}_f r_2$; in figure 6.3, we plot ψ_f against $\dot{\beta}_f r_2$, obtaining a curve in the third quadrant.

The steer curves provide another advantage on the earlier-described near-symmetry about $\pi/2$. The lean curves are harder to untangle, unless one reflects points HJK through the origin, and CDE through the vertical axis. Then a reflected curve (say C'D'E') is visible

No. (family)	Roll angle (ψ)	Steer angle (ψ_f)	Rear wheel spin rate ($\dot{\beta}_r$)	Radius traversed by rear wheel centre (R)
1 (CDE)	1.9893886377	−3.0755121969	26.3580011755	13.8724247186
2 (AB)	1.9178291654	0.4049333918	10.3899258905	2.2588798195
3 (AB)	1.7670024274	0.7254537952	5.5494771350	1.1408878065
4 (AB)	1.7183161276	0.8549190153	4.2289953550	0.8939154494
5 (GE)	2.1950752979	0.4266815552	14.4337001146	1.7525375246
6 (HJK)	2.0419972895	−2.6133787369	10.9563251310	1.4016100055
7 (CDE)	2.3535106155	−2.8688460258	19.4180569764	2.3503396652

Table 6.1: Some initial conditions for circular motion. $\dot{\beta}_r$ is in s^{-1} and R is in m. These were verified independently by Arend Schwab using SPACAR. These points are also plotted in figure 6.4. Stability-governing eigenvalues of these solutions are given in table 7.1.

in the first quadrant, and (similarly primed) K'J'H'GF appears in the first and fourth.

6.2.7 Some precise (benchmark) numerical values

The graphical results discussed above were presented, after some trial and error, in terms of variables allowing simple *post facto* interpretation. Here, in terms of our original variables, we report some precise numerical results for benchmarking.

Table 6.1 lists some initial conditions for steady circular hands-free motions. The radius R traversed by the rear wheel centre is also provided. These were independently verified through simulations by Arend Schwab (using SPACAR).

6.2.8 Benchmark circular motions

Along the lines of figure 6.3, figure 6.4 shows only steer versus front wheel speed; and also shows the 7 circular motions listed precisely in tables 6.1 and 7.1.

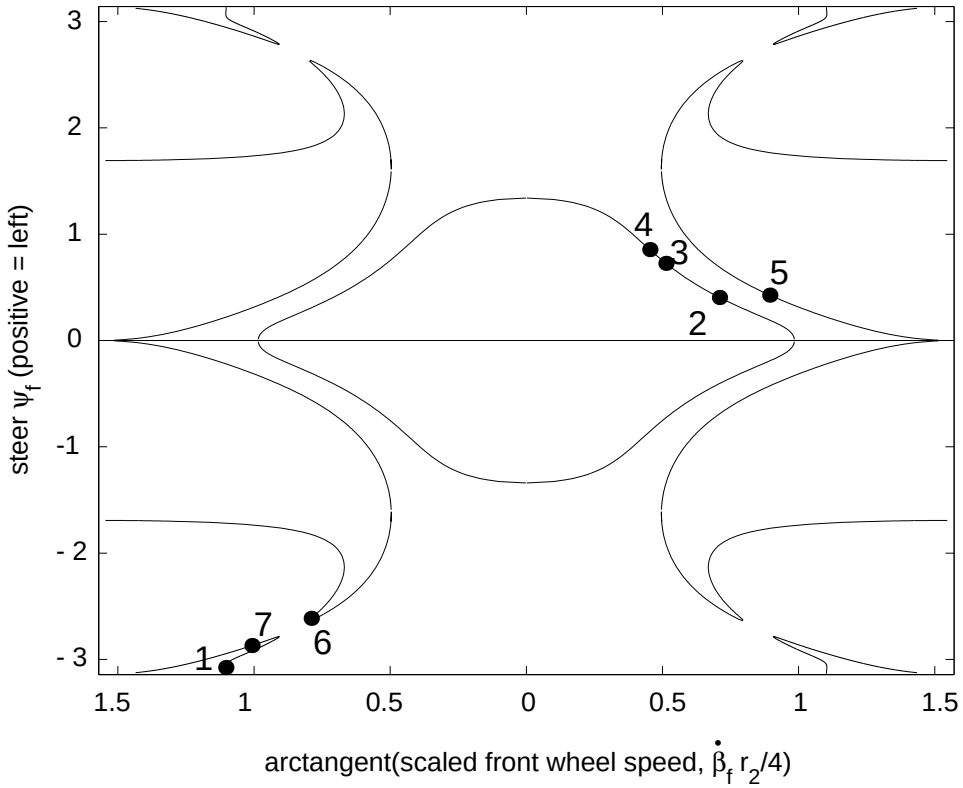

Figure 6.4: Benchmark circular motions from tables 6.1 and 7.1. Point 6 is slightly above the turning point, and not exactly on it.

In addition, we now list some special numerical values.

We have separately sought and found a static equilibrium of the bicycle at $\psi_f = 1.3397399115$ and $\psi = \pi/2$ (corresponding to point A in figures 6.1 and 6.3). The corresponding rear wheel center radius R is 0.2771720012 m.

Point B in figures 6.1 and 6.3 corresponds to a straight-ahead capsize speed of 6.0243 m/s. Point C corresponds to a straight-ahead (handlebar reversed) capsize speed of 7.9008 m/s. In linearized analysis of straight riding, capsize occurs at that speed where the handlebar 'torsional stiffness' vanishes, permitting any arbitrary turn to be maintained with zero handlebar torque. This forward speed is the unique solution of a linear equation in V^2.

Point E corresponds to a handlebar-reversed flat motion with $R \approx 3.3049$ m (from numerical extrapolation). Point F corresponds to another flat motion (handlebar forward) with $R \approx 3.0087$ m (numerical extrapolation). These configurations are hard to evaluate precisely due to geometrical (contact) and mathematical (Euler angles) singularities.

Point G (=H) represents the solution $\psi = \pi/2$, $\psi_f = 1.6416430491$, $\dot{\beta}_r = 0.2735815731$ and $R = -0.0415586589$ (here $R < 0$ because $\psi_f > \pi/2$ and the bicycle moves in a circle that curves right instead of left). Since this point is not a limiting motion, its definition is somewhat arbitrary: rather than an upright frame, we might instead specify minimum front-wheel velocity, or some other condition.

Point K can be found precisely by setting gravity to zero, choosing any nonzero speed, and seeking a unique circular motion. (This is asymptotically equivalent to finite gravity and infinite speed.) We have found $\psi = 1.6679684551$, $\psi_f = -1.6922153670$, and $R = 0.0666827859$ m.

6.2.9 Alternative plots of the same results

Here we plot the same results but now without using any arctangent transformation on the velocities. Also we keep the rear wheel speed as the abscissa in all the plots. We plot three quantities, namely lean, steer and the radius traversed by the rear wheel centre, as functions of the rear wheel speed for all the four circular motion families. Various special values are indicated in the plots.

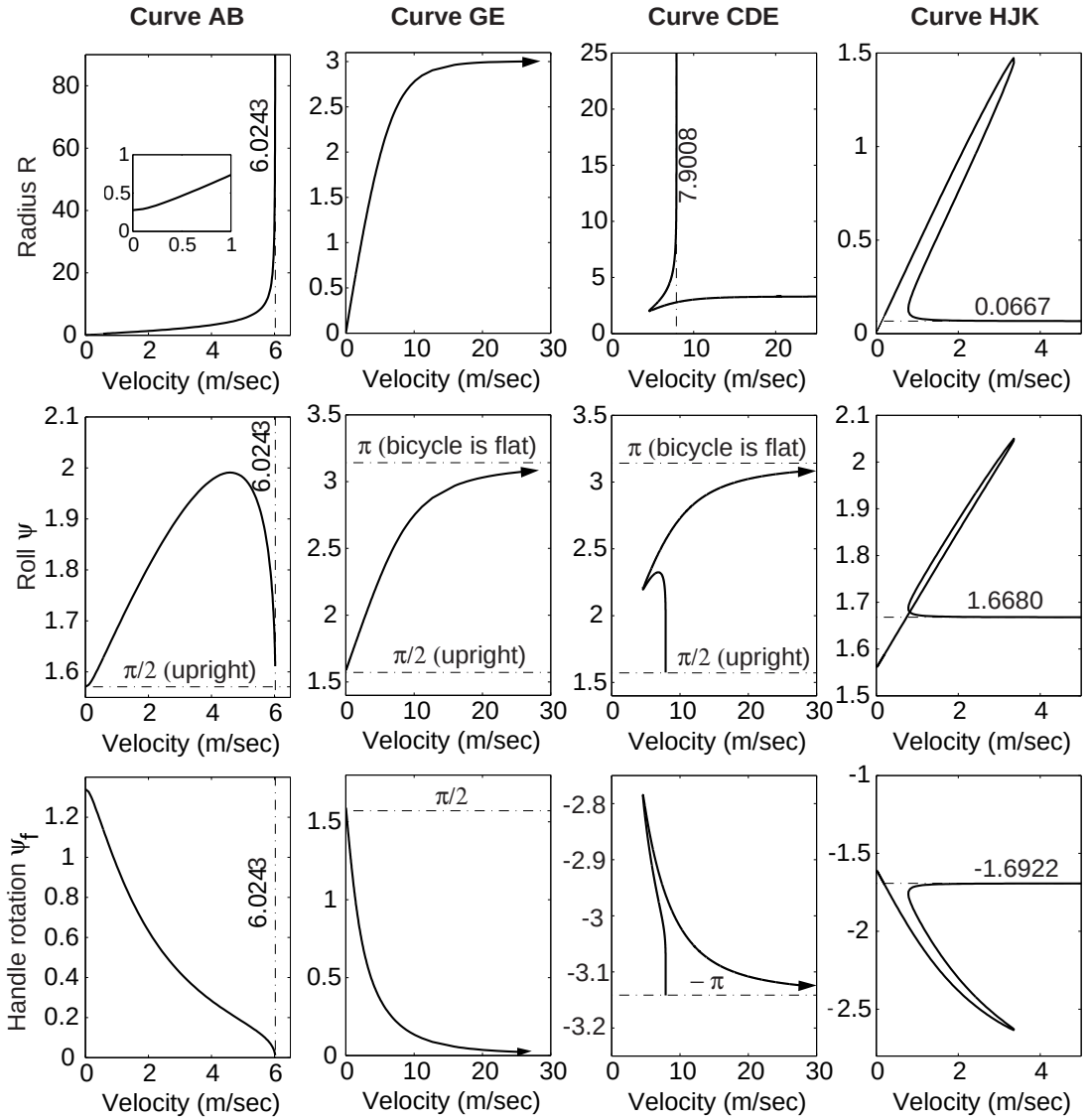

Figure 6.5: Four different one-parameter families of circular motions of the bicycle. Arrowheads indicate that solutions continue though not shown. The first column corresponds to curve AB in figure 6.1. The second, third and fourth columns correspond to curves GE, CDE and HJK respectively. Here "velocity" is $\dot{\beta}_r\, r_1$, which is not exactly the speed of the rear wheel center. Alternative measures of speed might be used; we choose this for simplicity. Inset in the top left plot shows a zoomed portion of the same.

6.2.10 Numerical simulation of one circular motion

For completeness, we pick one circular motion for full simulation, with initial conditions $\{\psi, \psi_f, \dot{\beta}_r\} = \{1.92746117082534,\ 0.38656355353653, 10.78186486867202\}$. In the simulation we found that $\dot{\psi}$, which is supposed to remain zero, actually increased exponentially until it became comparable to the rates of change of other coordinates (the circular motion is unstable). However, the relative change in total energy (kinetic plus potential), i.e.,

$$\frac{\text{instantaneous energy}}{\text{initial energy}} - 1,$$

remained on the order of 10^{-14} even as $\dot{\psi}$ increased through 10 orders of magnitude (a consistency check). The initial very-near-circular motion is shown in figure 6.6, and the change in total energy is shown in figure 6.7.

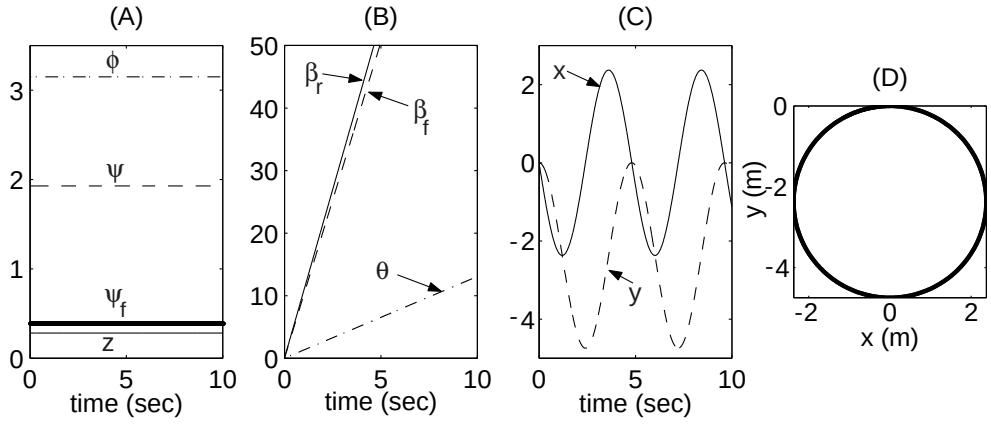

Figure 6.6: Numerical solution shows, at least for some time, the characteristics of circular motion. (A) z, ψ, ϕ and ψ_f are constant. (B) θ, β_r and β_f grow linearly. (C) x and y vary sinusoidally. (D) The rear wheel's center traverses a circle.

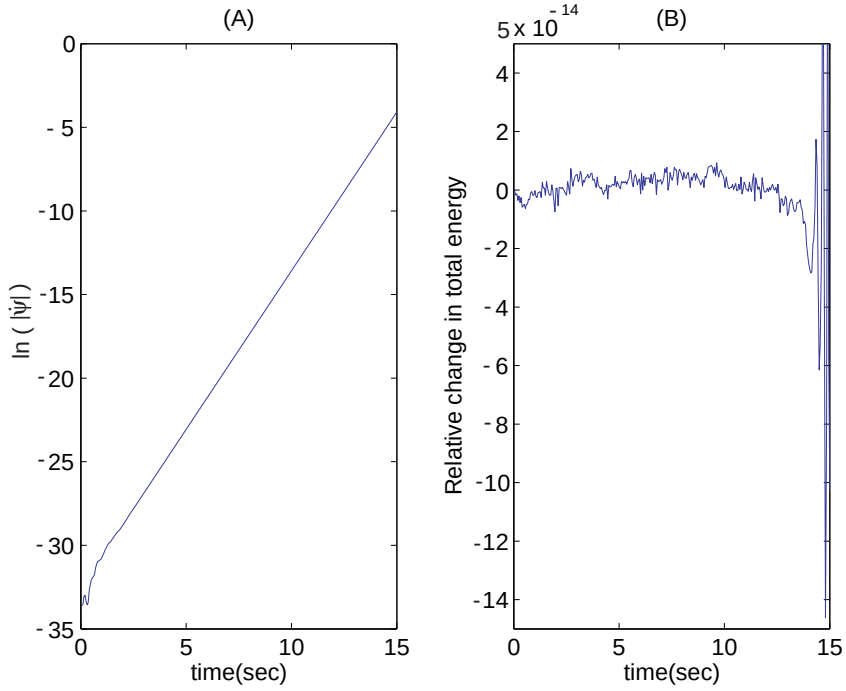

Figure 6.7: (A) $\dot{\psi}$ has exponential growth. (B) Total energy does not show changes until the bicycle falls over and passes through/near singular configurations (in the (3-1-3) Euler angles).

6.2.11 Unexpected equilibrium solution for the bicycle

In our study of circular motions, we found that one solution family ends at an unstable equilibrium position where $\psi_f \approx 1.3397$ and $\psi = \pi/2$. Here, we present a more detailed discussion of the same.

This exact $\pi/2$ value implies that the rear frame is exactly vertical in the equilibrium position, with the handle turned to some nonzero angle. Such an equilibrium initially seems surprising, because it seems that two equations are simultaneously satisfied by a single variable, as follows. Imagine that we lock the handle at some angle, and adjust the lean of the bicycle to achieve an unstable equilibrium. The lean of the rear frame is then

generically unequal to $\pi/2$. Now we unlock the handle, and relock it at some other angle, and repeat the procedure, to obtain a different value of the rear frame's lean. Adjusting the steer angle in this way, we might typically find an equilibrium at $\psi = \pi/2$, but the handle is *locked*. There seems to be no *a priori* guarantee that the handle torque is now zero, i.e., if we now unlock the handle, it seems that the equilibrium may in general be lost. But we can show that, in such a situation, the handle torque is zero as well.

We begin by assuming that an equilibrium exists with a vertical rear frame, and with the handlebar locked at some suitable angle. The rear wheel plane is then vertical as well. The ground contact force on the rear wheel will be vertical also, for two reasons. First, the component tangential to the wheel's circle must be zero to avoid a nonzero moment about the wheel center. Second, the component perpendicular to the wheel plane could potentially be nonzero; but for equilibrium of the entire bicycle we note that there must then be another equal and opposite force with the same line of action acting somewhere on the bicycle. However, for the particular bicycle chosen here or any similarly reasonable design, it is not geometrically possible for the front wheel to contact the ground anywhere along that line of action (see schematic of the top view in figure 6.8).

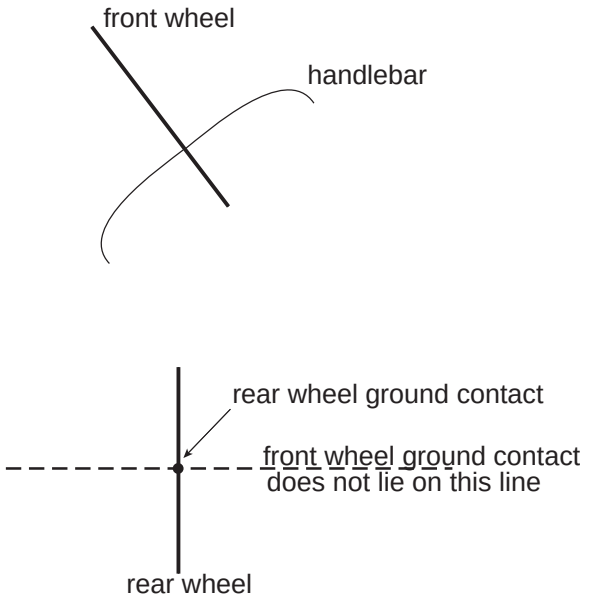

Figure 6.8: A schematic of the top view of the bicycle in an equilibrium position.

Given that the ground contact force at the rear wheel is vertical, and that gravity loading is vertical as well, it follows that the front wheel ground contact force is purely vertical.

Note that if any circular wheel (possibly tilted) touches the ground, then a vertical force at the contact point must pass through the wheel's axis (though not necessarily its center). Thus, both wheels are in equilibrium, and may be considered as connected rigidly to the bicycle in the remainder of this discussion.

In this equilibrium position, we ask if the torque at the locked handlebar is zero.

To see that the answer is yes, we consider equilibrium of only the rear assembly. The forces and moments on this assembly are the following.

1. There is a vertical ground reaction force at the rear wheel contact.
2. There is a vertical net weight of the rear assembly acting through its center of mass.
3. There is a force of interaction between the front and rear assemblies, which passes through the fork axis.
4. There is a vector moment exerted by the front assembly on the rear assembly, whose component along the fork axis is the handlebar torque required for equilibrium.

Since the rear frame is perfectly vertical, the first two forces are coplanar with the fork axis and contribute no moment about that axis. The third force also passes through the same axis. Thus, requiring the net moment about the fork axis to be zero for equilibrium even with a locked handlebar, we find that the handlebar torque is necessarily zero.

By the foregoing, we conclude that *if* it is possible to balance the bicycle with rear frame exactly vertical and with handle locked at some suitable angle, then that same equilibrium position survives even if the handle is unlocked. However, this is not entirely what we wish to show. Our numerics show an equilibrium position with rear frame lean ψ being *very* close to $\pi/2$. We have set out to demonstrate that the lean is in fact *exactly* $\pi/2$.

At this point we assume that, with the handle locked at various necessary angles, it

is in fact possible to balance the bicycle with rear frame lean values within some interval containing $\pi/2$ (the converse would be nongeneric). We note further that our numerical search for an equilibrium position was based on a Newton-Raphson iteration with numerically estimated Jacobian matrices. At the equilibrium position obtained numerically, we found that the Jacobian matrix was clearly invertible (its determinant was about -1013; its eigenvalues were about 15.9 and -63.6; and its singular values were about 188.1 and 5.4; though numerically estimated, these values are sufficiently far from zero to safely conclude invertibility). What Jacobian we obtain does depend on what equations we solve, but for any reasonable choice including ours which were based on zero values of angular accelerations, all we are interested in is that the Jacobian is invertible. Invertibility means that the equilibrium we have obtained numerically is *locally unique*, whether or not ψ is exactly $\pi/2$.

We finally have the following. By numerical demonstration, it is possible to balance the bicycle at a ψ value *extremely* close to $\pi/2$. By assumption, it is therefore possible to lock the handlebar at some suitable angle and then balance the bicycle with ψ exactly equal to $\pi/2$. By the foregoing discussion, at this balanced position, the handlebar torque is exactly zero, giving an equilibrium by demonstration. By invertibility of the Jacobian matrix, this demonstrated equilibrium is locally unique.

We conclude that at the equilibrium of interest, ψ is exactly $\pi/2$.

Chapter 7

Stability of Circular Motions

7.1 Introduction

The stability of circular motions can be studied along lines which are similar to those we adopted for studying the stability of straight motion. Here the generalized coordinates x and y are replaced by new ones defined by $x = -R\sin\chi$ and $y = R\cos\chi$. It is obvious that R and $\dot{\chi}$ remain constant during origin-centred circular motions. Thus we switch from a Cartesian coordinate system to a polar coordinate system. The in-ground-plane vector constraint equations are now not retained in terms of x and y components but instead retained in terms of components along $\hat{e}_R$ and $\hat{e}_\chi$, which are the unit vectors along the radial and circumferential directions. This has the advantage of making the constraint forces constant during the circular motions of interest. Now Lagrange's equations are obtained in the usual way for this new set of generalized coordinates.

7.2 Stability

For stability analysis of circular motions, we make a few changes for convenience. The generalized coordinates x and y are replaced by new ones defined by $x = -R\sin\chi$ and $y = R\cos\chi$. R and $\dot{\chi}$ remain constant during origin-centred circular motions. Also, two

new configuration dependent unit vectors are introduced while obtaining the equations of motion: these are

$$\hat{e}_R = -\sin\chi\,\hat{i} + \cos\chi\,\hat{j}, \text{ and } \hat{e}_\chi = -\cos\chi\,\hat{i} - \sin\chi\,\hat{j},$$

which are in radial and circumferential directions in the plane of the ground. Finally, the in-ground-plane vector constraint equations of no-slip are *not* retained in terms of x and y components, but instead retained in terms of components along $\hat{e}_R$ and $\hat{e}_\chi$. Here we give their expressions for completeness.

$$\begin{aligned}\dot{R} + r_1(\sin\chi\sin\theta\sin\psi + \cos\chi\sin\psi\cos\theta)\dot{\psi} - r_1(\sin\chi\cos\theta\cos\psi \\ - \cos\chi\sin\theta\cos\psi)\dot{\theta} + r_1(\cos\chi\sin\theta - \sin\chi\cos\theta)\dot{\beta}_r \\ -r_1(\sin\chi\cos\theta - \cos\chi\sin\theta)\dot{\phi} = 0 \end{aligned} \tag{7.1}$$

$$\begin{aligned}R\dot{\chi} + r_1(\cos\chi\sin\psi\sin\theta - \sin\chi\sin\psi\cos\theta)\dot{\psi} - r_1(\cos\chi\cos\theta\cos\psi \\ + \sin\chi\sin\theta\cos\psi)\dot{\theta} - r_1(\cos\chi\cos\theta + \sin\chi\sin\theta)\dot{\beta}_r \\ -r_1(\cos\chi\cos\theta + \sin\chi\sin\theta)\dot{\phi} = 0 \end{aligned} \tag{7.2}$$

Lagrange's equations are then obtained in the usual way, for the new set of generalized coordinates.

In these new equations, we seek circular motions by noting that R, ψ, ψ_f and ϕ are constants; $\dot{\theta} = \omega$ is a constant; $\dot{\chi} = \omega$ as well (i.e., not an extra unknown); $\dot{\beta}_r$ and $\dot{\beta}_f$ are constants; and all the 5 Lagrange multipliers are constants as well. Thus, there are 12 constants to be determined. Meanwhile, we have 8 equations of motion; 5 velocity constraint equations (including one that is actually a differentiated holonomic constraint); and a holonomic constraint equation to enforce front wheel contact with ground. That is, we have 14 equations and 12 unknowns. The following lines of thought help to clarify the situation.

The Lagrange multiplier (say λ_2) corresponding to the no-slip constraint at the rear wheel, in the $\hat{e}_\chi$ direction, turns out to be zero; this is expected because there is

no propulsive thrust; and one of the equations of motion reduces to exactly $\lambda_2 = 0$. We drop this equation, but retain λ_2 as an unknown and expect our subsequent calculation to rediscover that $\lambda_2 = 0$ (an automatic consistency check). So we now have 13 equations and 12 unknowns.

We retain the holonomic (front wheel contact) constraint equation in our calculations to ensure that a correct value for ϕ is obtained. But this automatically ensures that the velocity constraint equation in the normal direction at the front wheel contact is identically satisfied, and so we drop that equation. We then have 12 equations and 12 unknowns.

As may be anticipated, it turns out that the $\hat{e}_R$-direction no-slip equation is identically satisfied at the rear wheel, leaving 11 equations and 12 unknowns. This suggests, in line with prior calculations, that there are one or more one-parameter solution families. As before, we choose R, and solve 11 equations in 11 unknowns.

7.2.1 Stability results

All quantities of interest (including the Lagrange multipliers) are now treated as ϵ-order time varying perturbations of the nominal solutions corresponding to circular motion; the equations of motion (including velocity constraint equations) are linearized in terms of ϵ. The $\mathcal{O}(\epsilon)$ equations obtained from the velocity constraint equations are differentiated to get a full second order system. These are solved for the (perturbations in) Lagrange multipliers and second derivatives of generalized coordinates; and a constant coefficient system is obtained in terms of the 8 degrees of freedom used in our formulation. We then obtain a non-minimal set of 16 eigenvalues. Of these, 10 are zero. Of the remaining 6 nonzero eigenvalues, 2 are found to be exactly $\pm i\omega$ (where ω is already known for the circular motion). These 2 eigenvalues merely represent the same circular motion shifted to a nearby circle. There remain 4 nontrivial eigenvalues, which are tabulated below for the motions reported in table 6.1. These accurate eigenvalues can serve a benchmarking purpose. They are consistent to 3 or 4 decimal places with correspondingly (in)accurate eigenvalues found numerically using finite differences from the Newton-Euler equations. The latter, being quicker, were used to check the stability of the circular motions obtained above.

All of the circular motions of the bicycle with straight (forward) handlebar turn out to be unstable. Of the reversed-handlebar motions, relatively few are stable. These are shown in figure 7.1 (recognizable as the second-quadrant representation points D and J from figure 6.3), by means of individual heavy dots corresponding to our discrete sampling of the underlying continuous curves.

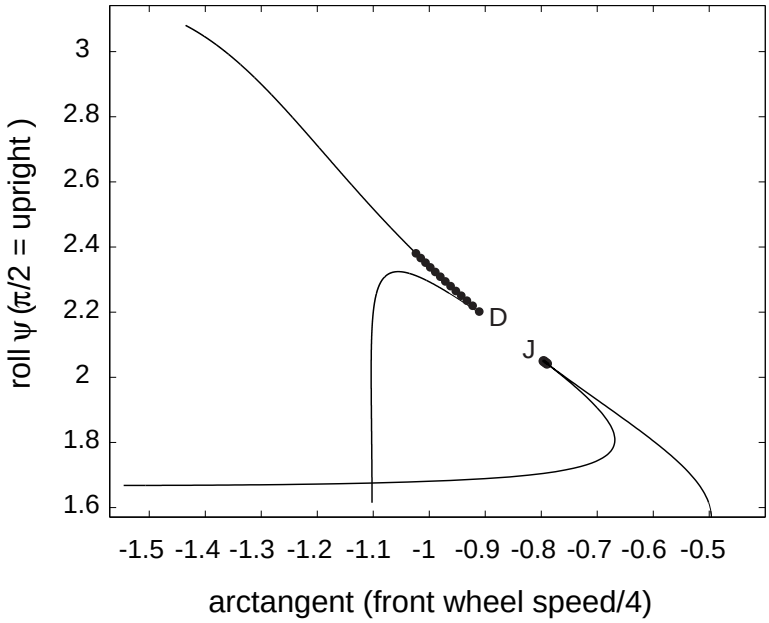

Figure 7.1: Stable hands-free circular motions of the bicycle.

We avoid here the sign change on speed used in figure 6.1; so the two curves are reflected versions of CDE and HJK of figure 6.1 (left).

We have also numerically simulated the bicycle starting from initial conditions corresponding to some of the circular motions obtained. For circular motions found to be unstable from the stability analysis, the numerical simulation results all showed divergence from the circular motion, at an exponential rate that matched the largest eigenvalue (real part). See figure 7.2.

No.	R (m)	Eigenvalues of the linearized equations of motion		
1	13.872424719	0.038127379	-21.152660576	$-2.265960434 \pm 7.986013290i$
2	2.258879819	1.989869132	-4.886076369	$-2.744979704 \pm 5.459259375i$
3	1.140887806	3.091516610	-2.853827876	$-2.485975489 \pm 5.783418042i$
4	0.893915449	3.393903081	-2.608053659	$-2.342566567 \pm 5.945917170i$
5	1.752537525	-2.000953101	-7.982680274	$5.575539147 \pm 5.799303852i$
6	1.401610005	-8.659556236	-0.795208976	$-0.118995944 \pm 3.110982262i$
7	2.350339665	-13.209338580	-0.467653580	$-0.075503592 \pm 7.402547429i$

Table 7.1: Nontrivial eigenvalues governing linearized stability of some circular motions reported earlier in table 6.1. In no. 5 the instability is oscillatory. 6 and 7 are stable.

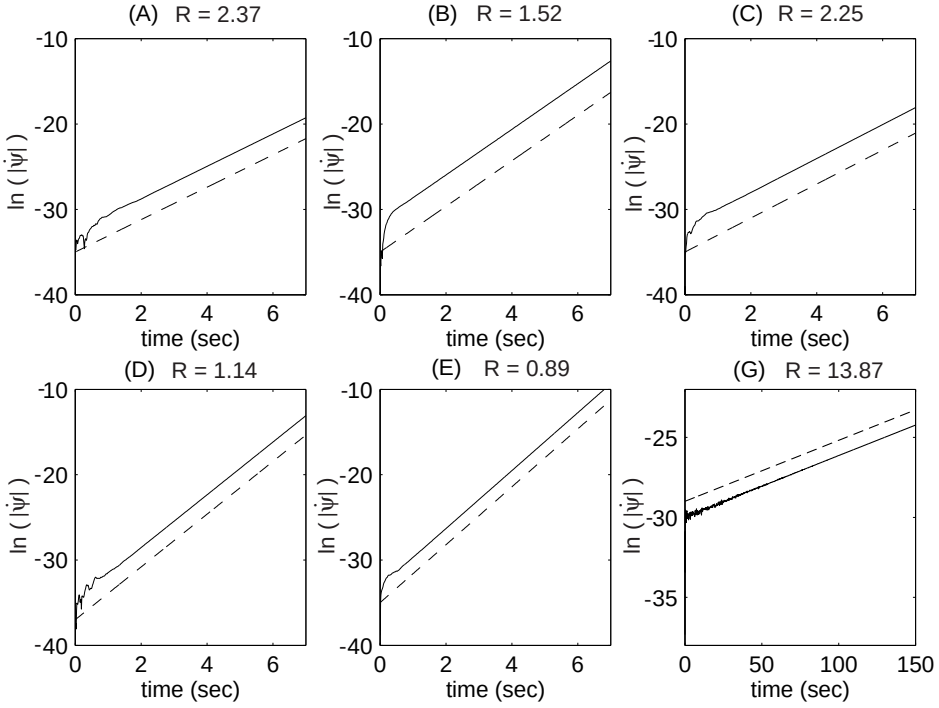

Figure 7.2: Plots of time vs. natural logarithm of $\dot{\psi}$ from numerical simulation of near-circular motions starting with six initial conditions, four of which are in table 6.1. $\dot{\psi}$ has exponential growth. The growth rate matches the largest positive eigenvalue from the stability analysis represented by dashed lines in each plot. These results provide support for the stability analysis.

7.2.2 Equation counting for stability analysis

Our discussion of equation counting for stability analysis of circular motions points to a potential procedural trap. One might be tempted to use the $\lambda_2 = 0$ equation and eliminate λ_2 from the list of unknowns, concluding that there were in fact 11 equations in 11 unknowns; and then seeking a unique solution. But a unique solution does not exist; the 11 (long and nonlinear) equations are not independent; and on discovering this a choice would have to be made about which equation to drop in one's search for a one-parameter family of solutions. The whole issue is further clouded by small roundoff errors in numerical evaluation of various quantities, leaving spurious and numerically small terms that would make the equations *seem* independent. In this light, our procedure seems numerically robust, practically useful, and conceptually manageable if not simple.

7.2.3 Ten zero eigenvalues for circular motions

There are 10 zero eigenvalues obtained in the stability analysis of circular motions.

7.2.3.1 Numerics

Some of these 10 eigenvalues are zero only to about a third of the decimal places we work with, say 5 out of 15. The multiplicity of zero eigenvalues seems structurally unstable. The nonzero eigenvalues remain less sensitive, accurate to 12 or more places of decimals.

The sensitivity of eigenvalues of matrices to small perturbations is well known, but an example is provided here. Consider the matrix

$$\begin{bmatrix} 1 & 0 & 1 \\ 0 & 0 & 1 \\ 0 & 0 & 0 \end{bmatrix}.$$

By inspection, its eigenvalues are $(1, 0, 0)$. Now let $\epsilon = 10^{-10}$, say. Perturb the above matrix by changing each zero element to ϵ. The eigenvalues become, essentially, $1 + \epsilon$ and

$\pm\sqrt{\epsilon}$. It is easy to find matrices where some eigenvalues shift by $\mathcal{O}\left(\epsilon^{1/3}\right)$, or even more, while others shift by much smaller amounts.

One way to view such sensitivity is to directly look at the roots of polynomials. Consider $\lambda^4 = 0$, with $\lambda = (0, 0, 0, 0)$. Now consider the perturbed equation

$$\lambda^4 = \epsilon,$$

for which

$$\lambda = \pm\,\epsilon^{1/4}, \pm\, i\epsilon^{1/4}.$$

Thus, the 4 roots at zero split and move sensitively for small ϵ. Finally, note that $\lambda^4 = 0$ is the characteristic equation for the linear differential equation

$$\frac{d^4y}{dx^4} = 0,$$

which when written in first order form gives rise to a coefficient matrix with 4 zero eigenvalues but only one eigenvector, i.e., with a single 4×4 Jordan block.

7.2.3.2 Counting

The 10 zero eigenvalues may be accounted for as follows. 5 come from differentiation of the 5 velocity constraint equations used. 3 come from individual infinitesimal changes in β_r, β_f and ϕ (the last is physically unrealizable, where the front wheel remains slightly above or below ground). One more comes from starting the bicycle slightly ahead but on the same circle. And a final one comes from motion on a slightly bigger or smaller circle.

7.2.4 Stability analysis of circular motions from finite differences

For quick numerical estimation of eigenvalues governing stability of circular motions, we use a 5-dimensional state vector

$$\eta = \{\psi, \psi_f, \dot{\psi}, \dot{\psi}_f, \dot{\beta}_r\}^T.$$

This shorter list is along the lines adopted by Lennartsson [14].

Given a state vector, ϕ is determined from front wheel contact as always; since three angular rates are known, the remaining rates are found from the velocity constraint equations; and all ignorable coordinate values are set to zero. This gives a complete state vector, suitable for our Newton-Euler equations. On evaluating the second derivatives thereby, $\dot{\eta}$ is picked out.

For points corresponding to a circular motion, $\dot{\eta} = 0$. By individually incrementing the 5 states one by one, we can estimate corresponding columns of a coefficient matrix J, such that the linearized dynamics is given by

$$\dot{\eta} = J\eta.$$

The eigenvalues of J govern stability of the circular motion of interest. One eigenvalue is known to be zero because of energy conservation, and serves as a partial check on accuracy for the numerical estimates. More accurate eigenvalues can be obtained using central differences instead of forward differences, but the latter suffice here.

Chapter 8

A Study of Other Bicycles With and Without Symmetrical Forks

8.1 Introduction

In this chapter, we study hands-free circular motions of some other bicycles. The parameters for these bicycles have been obtained by changing some of the same for the benchmark bicycle, which has been our subject of study so far. In the process we study in some detail the effect of handlebar asymmetry and the removal of the same on the circular motions of these bicycles. **(1)** We first start with a bicycle where we reduce the handlebar asymmetry existing in the benchmark bicycle by (i) improving the alignment between the fork axis and an eigenvector of the moment of inertia matrix of the front fork assembly and (ii) making the points H and Q (see figures 2.1 and 8.1) lie closer to the fork axis. In what follows, we refer to this bicycle as Case (1), and also NSB (for "nearly symmetric bicycle"). **(2)** Then we study a perfectly symmetric bicycle where H and Q lie exactly on the fork axis and an eigenvector points along the fork axis. In what follows we refer to this bicycle as Case (2) and also PSB (for "perfectly symmetric bicycle"). **(3)** After this we study another bicycle where we reduce the mass of the rear frame and increase the fork angle significantly. In what follows we refer to this bicycle as Case (3) and also DB (for "different bicycle"). **(4)** Next we symmetrize this bicycle (DB), and call it Case (4) and

SDB (for "symmetrized different bicycle"). **(5)** Finally, we study yet another bicycle with parameters which represent a motorcycle more closely, and refer to it as Case (5) or the "motorcycle".

We study the circular motions for all these cases, and their stabilities as well.

8.2 Symmetrization of the Benchmark Bicycle: Cases (1) and (2)

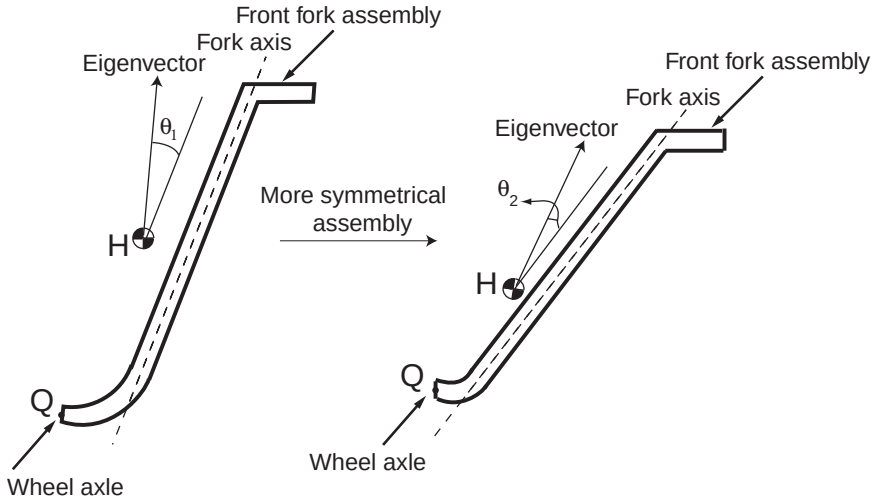

Figure 8.1: Schematic showing reduction of asymmetry in the front fork. Left: Less symmetric assembly. Right: More symmetric assembly. $\theta_2 < \theta_1$. Also H and Q are closer to the fork axis (the fork angle is increased slightly and trail is held constant). See text for details.

In this section, we study what happens if the front fork assembly of the benchmark bicycle is made progressively more symmetrical about the fork axis, with the limiting case being one where a π rotation of the handlebar gives exactly the same bicycle as before. We proceed as follows.

(a) First of all, we change the moment of inertia matrix of the front fork $I_{cm,ff}$ in its reference configuration in such a way that its eigenvalues remain the same, but now the smallest of the angles between the eigenvectors and the fork axis is made 1/4 of its original value. See figure 8.1.

(b) Also the perpendicular distance of the front wheel center Q from the fork axis is made 1/4 of the original value.

(c) Finally, the perpendicular distance of the center of mass H of the front assembly, from the fork axis, is made 1/4 of the original value.

Note that apart from changing some of the entries of $I_{cm,ff,ref}$, these changes will alter the location of H. We choose not to change the location of Q. To accomplish this, we change the fork angle, keeping the trail constant. All subsequent analyses are done keeping the trail constant and changing the fork angle.[1] See tables A.3 and A.4 in appendix A for actual parameter values used.

8.2.1 Circular motions

On examining the circular motions of the benchmark bicycle, the bicycle of Case (1) (NSB), and the bicycle of Case (2) (PSB) (see figure 8.2, top, middle, and bottom, respectively), we note some interesting qualitative facts. As the bicycle fork is made less and less asymmetrical, points B and C approach each other and merge in the limit when handlebar reversal has exactly zero dynamic consequence. Cusp-like points J and D both approach each other as well as, in a pair, approach a configuration of zero lean and $\pi/2$ steer, eventually merging with these limiting axes at a point that is fortuitously close, but *not identical* to, the coincident points G and H. The infinite-speed limit of K approaches zero lean and steer $\pi/2$; and so does a significant portion of the curve that terminated at K. Similarly, the zero-speed limit of A also approaches zero lean and steer $\pi/2$; and so does a significant portion of the curve that terminated at A.

The two finally remaining circular motion families, as well as a new one that has appeared, may therefore be described as follows:

[1] Alternatively, we could have kept the fork angle constant and altered the trail of the bicycle.

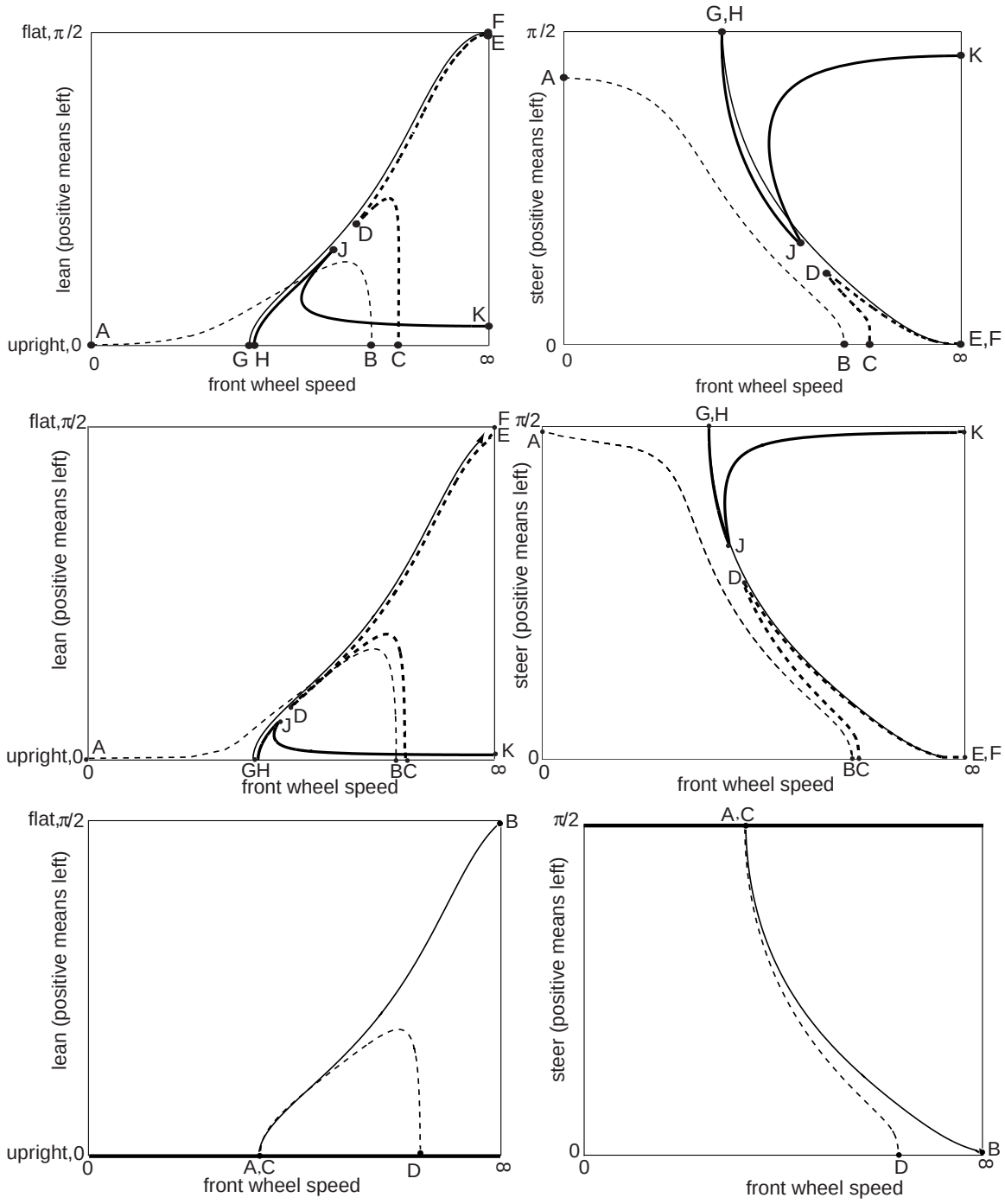

Figure 8.2: Circular motion families. Top: benchmark bicycle (schematic; left shows lean; right shows steer). The top two figures are reproduced from chapter 6; see discussion there for further details. Middle: partially symmetrized fork, as in Case (1); all other details are identical with top two figures. The continuation of the curve on to point F is indicated schematically with an arrowhead in the lean plot, although our continuation was terminated somewhat earlier. Bottom: fully symmetrical bicycle. The four solution family curves have now merged into two, with one new family of pivoting motions at all speeds. The points A and C, though coincidentally close, are distinct. See text for further details.

(i) There is a family that involves bifurcation from straight motion. Taking the bifurcating branch that involves leaning left, say, we find decreasing radius and increasing lean upto some point; thereafter the lean decreases again and the bicycle becomes upright with steer equal to $\pi/2$ to the left. When leftwards steer increases beyond $\pi/2$, the motion turns into a backward-moving version of another circular motion with rightwards-steer less than $\pi/2$; and following that branch with the rightwards-steer interpretation, we again reach the bifurcation point off straight motion, thus completing a loop.

(ii) There is another family where the bicycle may be viewed as starting with leftwards lean almost $\pi/2$ (i.e., almost flat), going around infinitely fast. From that limit, the bike may be viewed as rising up, with decreasing lean, eventually reaching a state of zero lean with steer exactly equal to $\pi/2$. Thereafter, following a symmetrical branch as in case (i) above, the circular motion family ends with the bicycle again nearly flat, going around infinitely fast, but now leaning to the right.

(iii) Now, at all speeds, there are circular motions where the rear contact point is stationary, lean is zero, steer is $\pi/2$, and the bicycle exhibits a pivoting motion about the rear contact point. Recall that an approximation to such motions played a key role in our discussion of the benchmark bicycle; here, such motions occur exactly, and at all speeds.

8.2.2 Stability of circular motions

All of the circular motions of the NSB with forward handlebar turn out to be unstable. Among the reversed-handlebar motions, all are found to be unstable. Recall that for the benchmark bicycle, small sections of stability were found near D and J as shown in figure 7.1. Also, all circular motions for the PSB turn out to be unstable.

8.3 Qualitatively Different Families for Cases (3) and (4)

The possible solution families for different bicycle parameter set choices can be quite different from those observed above for the benchmark, and its related bicycles (NSB and PSB, Cases (1) and (2) respectively).

To briefly explore the possibilities, and also to demonstrate that stability of circular motions is actually possible over a large range of motions, we now consider a different bicycle which has handlebar asymmetry. For this bicycle, which we call DB, we increased the fork angle to $\pi/7$ as opposed to $\pi/10$ for the benchmark bicycle and decreased the mass of the rear frame to 70 kg as opposed to 85 kg for the benchmark bicycle. For a full list of the parameters, see tables A.7 and A.8 in appendix A. This bicycle yields qualitatively new families of circular motions.

The lean and steer plots are shown side by side, separately for all four families for better visibility, in figure 8.3. In all the plots in figure 8.3, as before, lean is defined as $\psi - \pi/2$, positive when the bicycle leans left and shown here from 0 (upright) to $\pi/2$ (flat on the ground). Also, steer is plotted from 0 (straight handlebar) to $\pi/2$ (perpendicular leftwards) in figure 8.3. Note that for some of the families $\dot{\beta}_f r_2 < 0$, and $-\dot{\beta}_f r_2$ is plotted instead, because motions are reversible. For the families represented by curves DE and HIJ in figure 8.3, $\dot{\beta}_f r_2 < 0$ corresponds to the bicycle moving forward with a reversed handlebar (i.e. turned beyond $\pi/2$). For these two curves, π has been added to the steer, as also done earlier for the benchmark bicycle.

8.3.1 Circular motions

We now describe the four circular motion families.

One handlebar-forward family connects the points A, B and C shown in figure 8.3 (top row). The bicycle first starts from a flat-and-fast motion at A with lean from vertical nearly equal to $\pi/2$ and steer close to 0; lean and speed decrease, while steer increases up to

point B where a maximum steer angle of about $\pi/5$ is reached. Thereafter, steer decreases towards 0 while lean and speed increase until the bicycle again approaches a flat-and-fast limit depicted by point C. In our numerics, A and C show termination of our continuation scheme; in reality, the solution family reaches the limiting motion although it is numerically difficult to find it. There is no similar solution family for the benchmark bicycle.

A second circular motion family starts from the HF flat-and-fast limit D (see figure, second row). Note that the path radii of the rear wheel center at A and C differ from each other as well as from that at D. Velocity and lean initially decrease while the steer increases; beyond a turning point, the bicycle is nearly (but not quite) upright, and steer is nearly (but not quite) $\pi/2$, as speed increases towards infinity, producing a pivoting motion in the limit E. This point E corresponds to the infinite-speed pivoting motion K of the benchmark bicycle (see figure 8.2); however, for the benchmark bicycle the corresponding solution family curve had turned around and terminated at a finite-speed pivoting motion, while here the solution terminates at a *third* flat-and-fast limit D.

A third family starts at the handlebar-forward (HF) bifurcation from straight motion, shown as point F (see figure, third row). The circular motion family starting there has steadily increasing speed, and ends in a *fourth* flat-and-fast limit depicted in the figure as G. An interesting feature of this family is that the steer remains small throughout; this is a high-speed, leaning turn, similar to a corresponding family in the "motorcycle" of Case (5) below, and unlike any family of the benchmark bicycle.

The fourth and final family (see figure, bottom row) starts from handlebar-reversed (HR) bifurcation from straight motion (point J), shows increasing lean and speed up to a turning point (point I), and eventually ends in static equilibrium (point H) with lean exactly zero and steer very close to $\pi/2$. Though not identical in shape, this family is qualitatively similar to solution family AB of the benchmark bicycle, shown in figure 8.2.

All four lean and steer plots are shown together in figures 8.4 and 8.5 respectively.

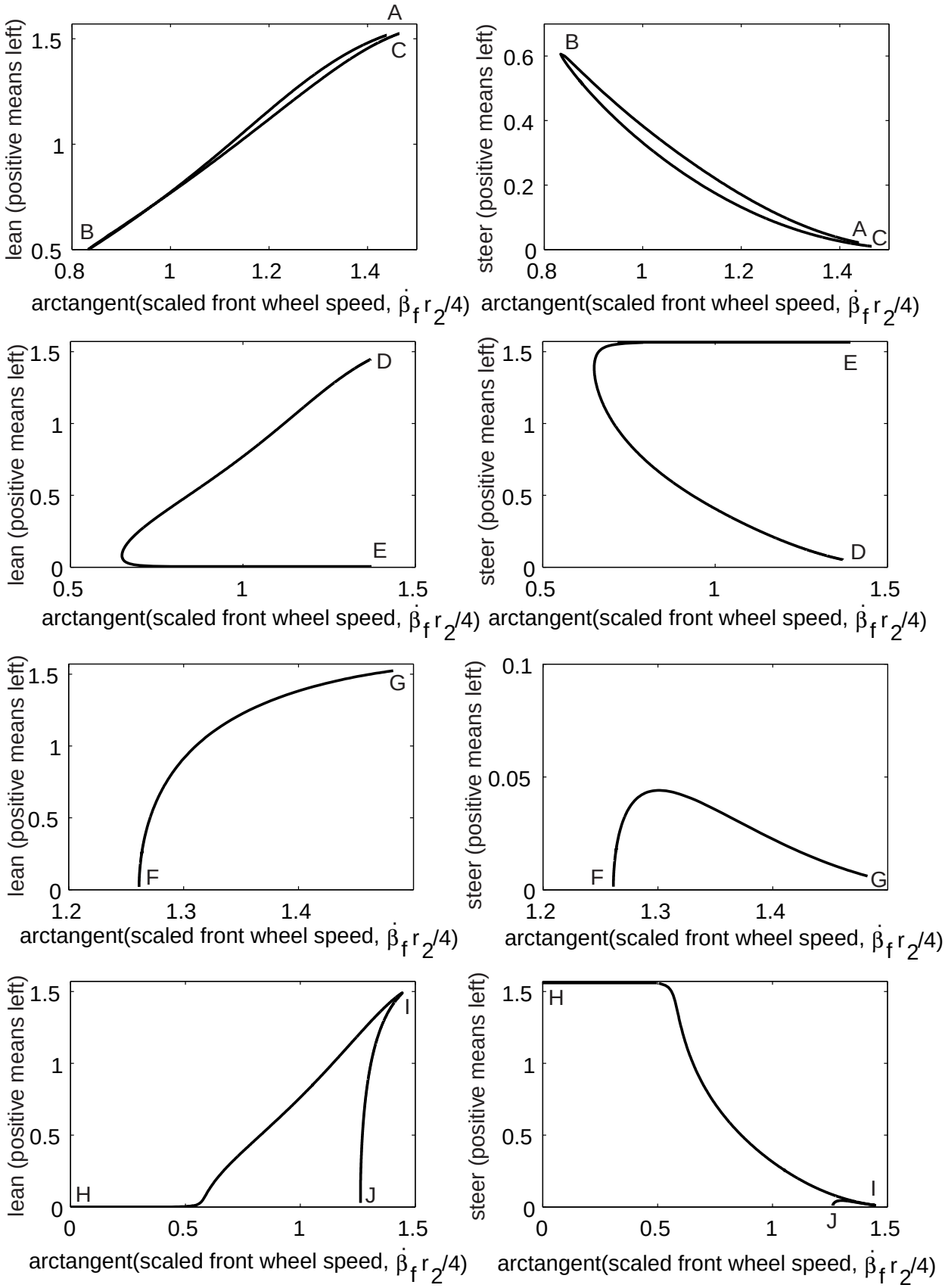

Figure 8.3: Circular motion families for the DB.

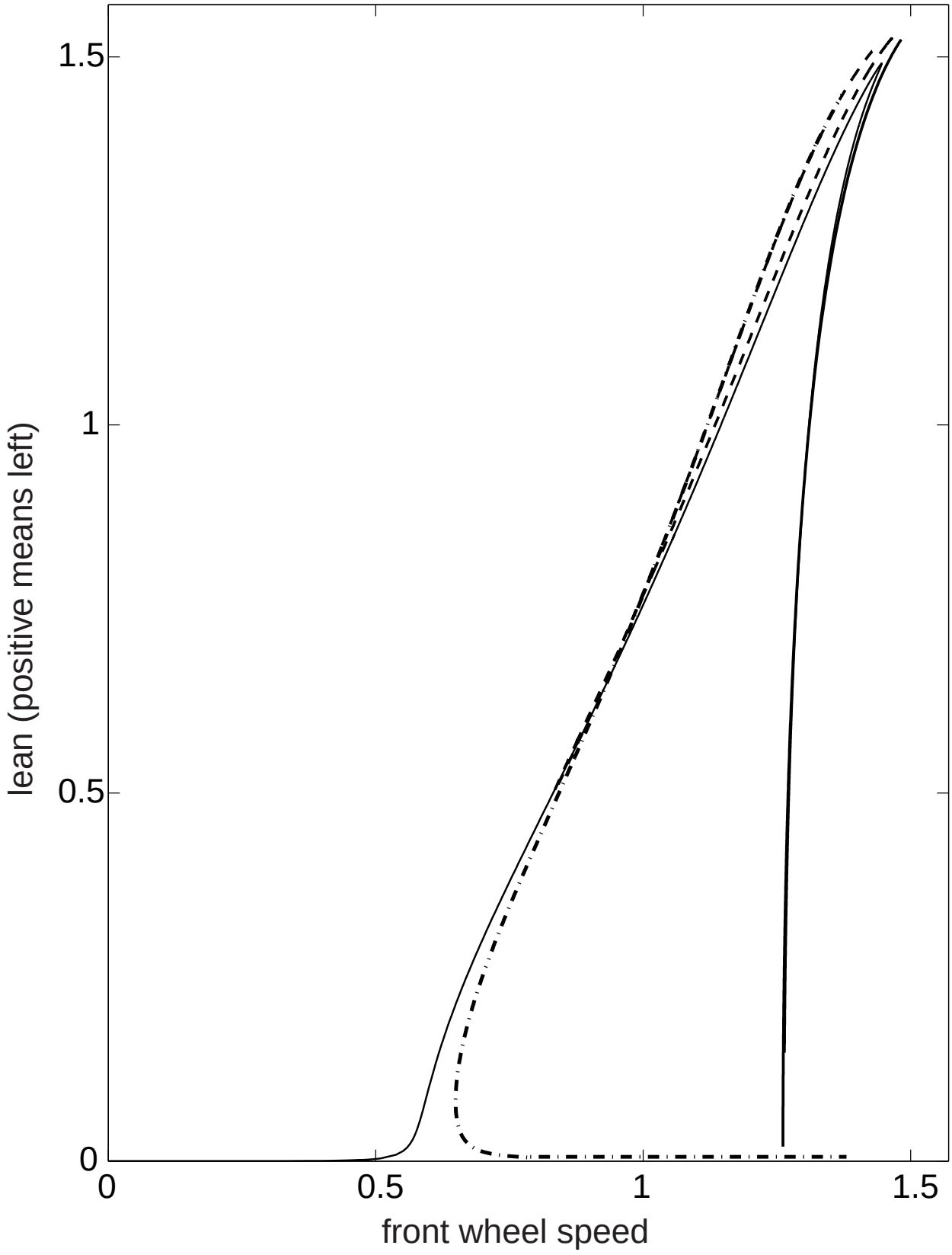

Figure 8.4: Circular motion families for the DB. Lean.

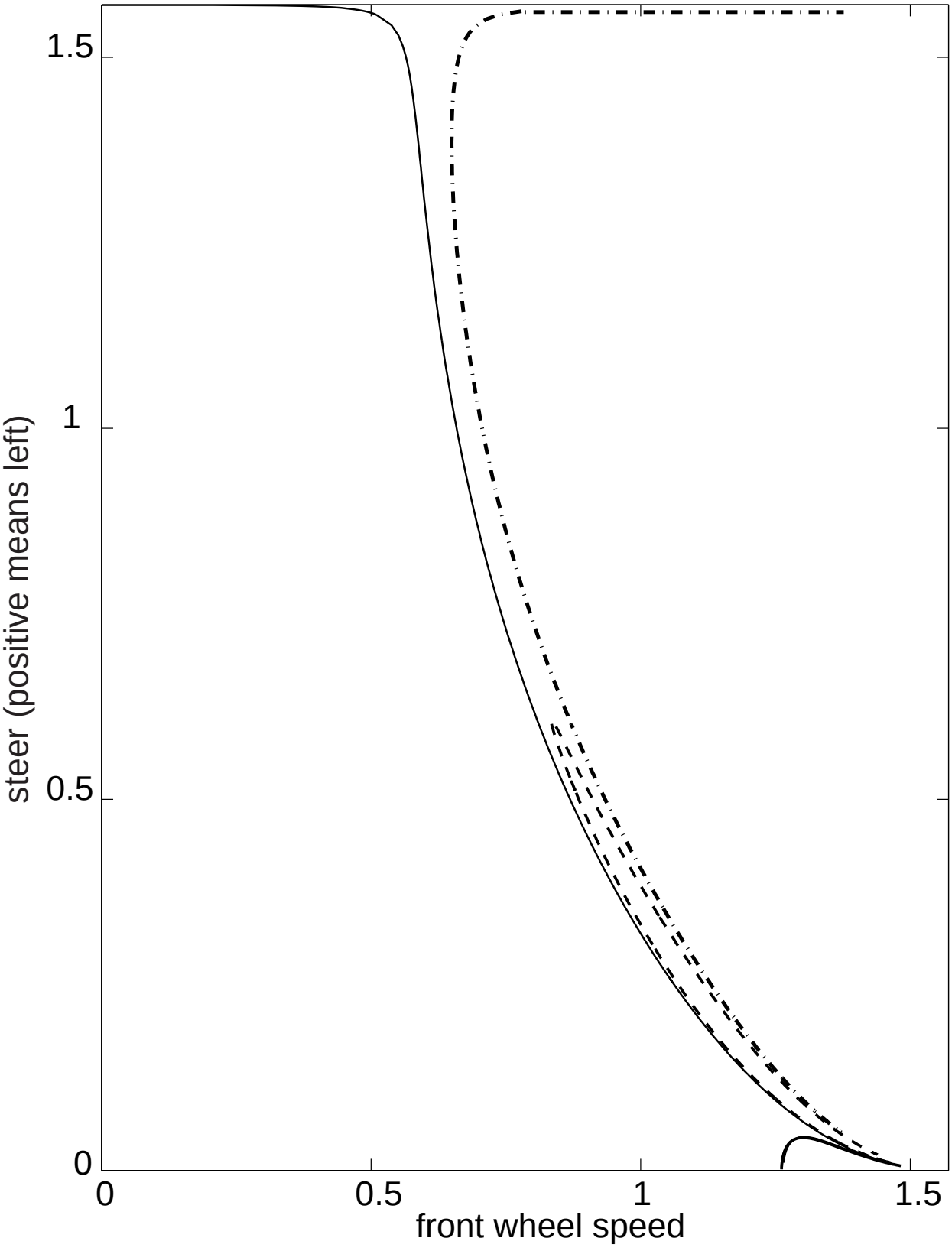

Figure 8.5: Circular motion families for the DB. Steer.

8.3.2 Stability of circular motions of DB

We now study the stability of the four circular motion families. For the family represented by curve ABC in figure 8.3, there is a very small section near point B with stable circular motions. For the family represented by HIJ, the entire portion IJ is stable. All points computed on the curve FG are stable, although we have no analytical extrapolation to the infinite speed limit and expect that stability may be lost at some finite speed. There are no stable points on the curve DE.

It is interesting to note that the circular motions of this bicycle (DB) differ from those of the benchmark in a few key ways. First of all, there are four as opposed to two flat-and-fast limiting motions. Secondly, the finite-speed pivoting motion with zero lean is now missing. Finally, large sections of two solution families are stable.

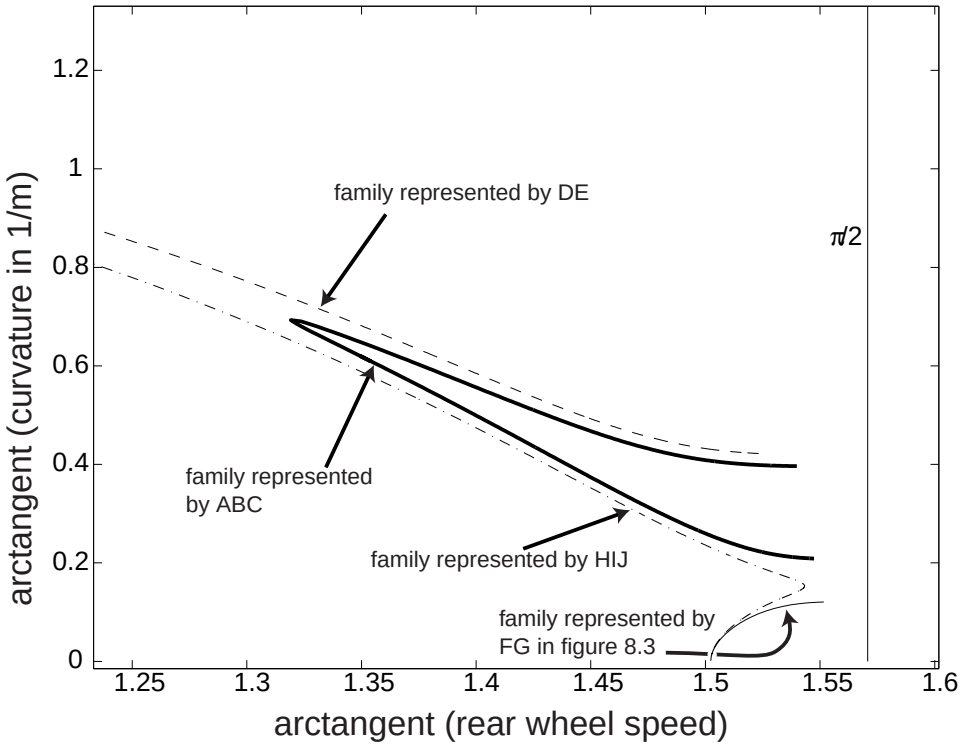

Figure 8.6: Two right curving circular motion families for the DB.

The distinction between the four flat-and-fast limits may be seen in figure 8.6 where curvature $1/R$ (R is the radius of the path traversed by the rear wheel centre) is plotted, using an arctangent transformation, against speed $v = r_1\dot{\beta}_r$ which is also plotted using the arctangent as before. As speed goes to infinity, it is clear that there are four different radii.

We now move on to Case (4), where we replace the front fork assembly of bicycle DB with a perfectly symmetric one, so that there remains no handlebar asymmetry. We call this the "symmetrized different bicycle" (SDB). We now study its circular motions. The schematic is shown in figure 8.7.

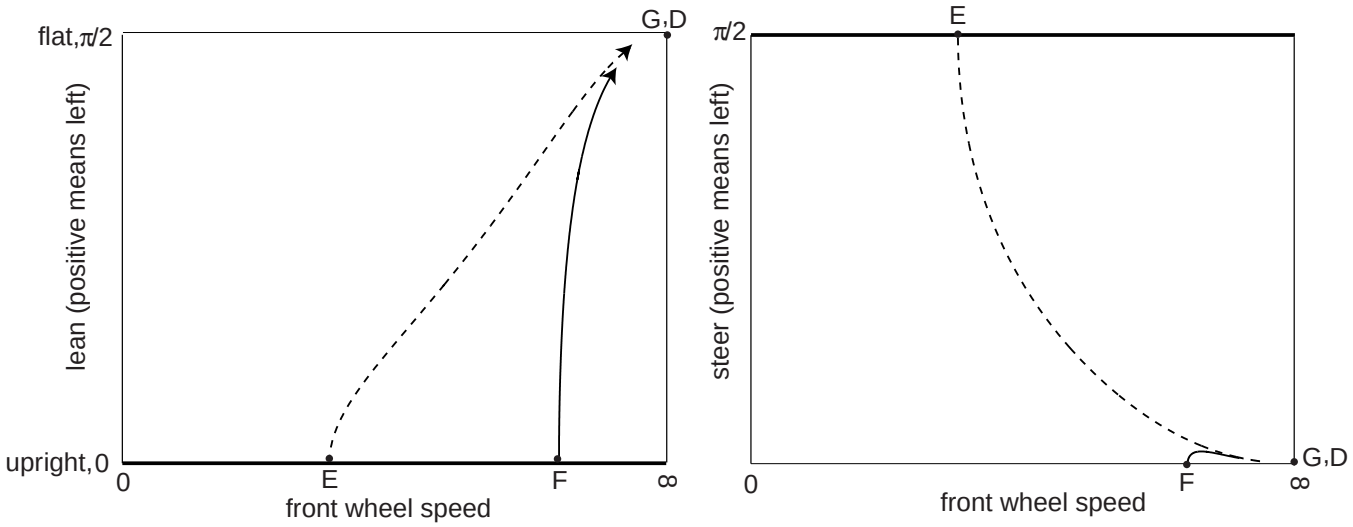

Figure 8.7: Circular motion families for the SDB. Left: lean. Right: steer. The continuation of the respective curves on to points D and G is indicated schematically with two arrowheads in the lean plot, although our numerics were terminated somewhat earlier.

We get three circular motion families for this bicycle. The circular motion family represented by curve ABC in figure 8.3 apparently disappears, presumably due to merging of the two endpoints, which are flat-and-fast limits (we found no such family, in any case). The portion IJ of the circular motion family HIJ in figure 8.3 has merged with FG in figure 8.7. Also the diagonal part of the curve HI is now coincident with a corresponding portion of curve DE in the figure, and the horizontal part has merged with the horizontal axis, because there are now pivoting solutions at all speeds (the third family), with zero lean

and steer $\pi/2$.

As might be anticipated, the entire family represented by FG is stable. There are no stable points on the curve DE.

8.4 Case (5): Parameters Closer to a Motorcycle

Finally, we consider parameters which represent a light motorcycle[2]. The wheel base is larger; the masses of the wheels are larger; the mass of the rear frame is larger; and the moment of inertia matrices for the wheels and the rear frame are closer to those of a motorcycle. For actual parameter values, see tables A.10 and A.11 in appendix A. The dynamics of the engine was not included in our analysis, though its mass may be considered to be included with the rear frame. Neither rotation of the swing arm nor width or deformation effects of tyres, though they are significant for actual motorcycles, were included in our idealized bicycle-motivated model. For ease of identification, however, we refer to this model as a motorcycle.

We now describe the circular motion families for the motorcycle. See figure 8.8.

The handlebar-forward (HF) family AB is qualitatively similar to a corresponding family for the benchmark bicycle, starting from bifurcation from straight motion at one end, and ending at static equilibrium with exactly zero lean and steer almost $\pi/2$.

The family CD also has a clear correspondence with the benchmark bicycle results, starting from the HF flat and fast limit D, and ending with the rear frame upright at pivoting motion C.

The handlebar-reversed (HR) bifurcation from straight motion is shown at point E. The circular motion family starting there has steadily increasing speed, and ends in a flat-and-fast limit depicted in the figure as D (note that in this figure, for clarity of depiction, two different flat-and-fast limits are depicted using a single label, D). The continuation of the curve on to point D is indicated schematically with an arrowhead in the lean plot,

[2]This parameter set was provided by K.V.M. Raju of TVS Motor Company.

although our numerics were terminated somewhat earlier. An interesting feature of this family is that the steer remains small throughout; this is a high-speed, leaning turn, similar to a corresponding family in the "different bicycle" of Case (3) above, and unlike any family of the benchmark bicycle.

The fourth and final circular motion family CGF is qualitatively similar to a corresponding family of the benchmark bicycle, starting at finite speed pivoting (zero lean) at C, and ending at infinite-speed pivoting (small lean) at F.

All points on the curve DE in figure 8.8 are stable.

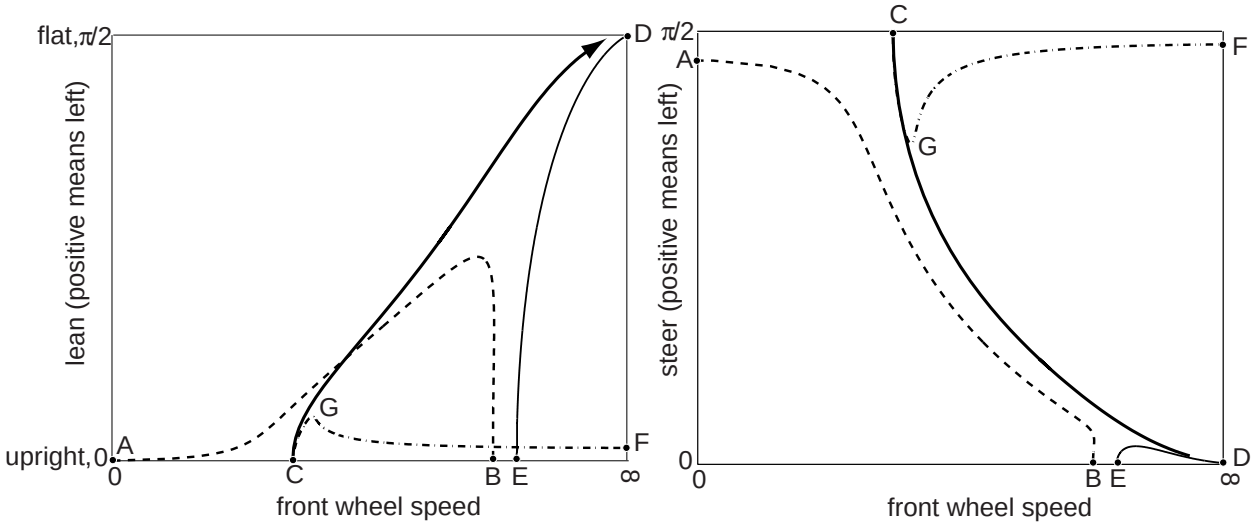

Figure 8.8: Circular motion families for the motorcycle. Left: lean. Right: steer. As was the case for the benchmark bicycle, here there are actually two points at C, but for simplicity we have used only one label. The point D represents flat-and-fast solutions, of which there are two different ones (as also for the benchmark bicycle); however, for clarity in the diagram, only one label is used. Finally, as for the benchmark, two families are shown with π added to the steer angle: these are DE and CGF.

Chapter 9

Qualitative Comparison With Prior Experiments

Several observations from experiments with bicycles are reported in an unpublished document (dated 1987) available at [24]. It is interesting to see how some of the results obtained in this thesis are in fact consistent with the experimental observations therein. For example, at the bottom of the first page in that document, James Papadopoulos describes how the handlebar torque changes magnitude and sign with varying speed along a curve of given radius. These observations seem directly related to the discussion in the last paragraph of subsection 6.2.5 of this thesis.

Consider again figure 8.7 of this thesis and the circular motion family represented by curve FG, which is stable. A bicycle travelling in a circle corresponding to some point on the curve FG will be stable. If there is some small dissipation, the bicycle will slow down and follow a nearly circular path as its motion slowly traverses curve FG towards F. When the point F is reached, the bicycle will become vertical and continue to move in a straight path. In this light, it is interesting to see the last page of [24], which describes experiments by Scott Hand. In particular, item 5 there seems to describe just such a sequence of motions.

Chapter 10

Conclusions and Future Work

In this thesis we have made a study of the dynamics and stability of an idealized bicycle. This thesis presents, for the first time, multiply cross-verified (benchmark) numerical results for certain bicycle parameter values that can be used with confidence by future researchers in bicycle dynamics as well as people interested in examining the accuracy of general purpose multibody dynamics codes.

The equations of motion for the bicycle have been derived in two different ways, first by using a Lagrangian formulation and then followed by a Newton-Euler formulation. We have demonstrated the equivalence of the two sets of equations. Lagrange's equations were subsequently linearized and the corresponding eigenvalue problem studied. The stability eigenvalues have been plotted as functions of the forward speed of the bicycle. In the process several eigenmodes of instability like weave and capsize have been identified and the speed ranges in which they are dominant have been found.

The main new findings in this thesis are in the area of hands-free circular motions of a benchmark bicycle and some other bicycles. Three different families of circular motions have been shown to exist for the benchmark bicycle. (i) A handlebar-forward family starts from the capsize bifurcation off straight-line motion and ends in an unstable static equilibrium, with the rear frame perfectly upright and the front wheel steered almost perpendicular to the symmetry axis of the frame. (ii) A handlebar-reversed family starts again from the capsize bifurcation and ends with the front wheel steered straight and the bicycle spins infinitely fast in small circles lying flat in the ground plane. This flat spinning motion

is possible only because of the absence of slip. (iii) Lastly, there is a family which joins a similar flat spinning motion with handlebar forward to a handlebar reversed limit. In doing so, the bicycle circles in dynamic balance at infinite speed, again with the frame being nearly (but not exactly) upright in this case and the front wheel almost perpendicular to it. This transition from handlebar forward to handlebar reversed motion takes place due to a pivoting motion occurring at a moderate speed with the rear wheel not quite rotating and the front wheel rotating appreciably and the frame virtually upright.

The effect of handlebar asymmetry has been examined in subsequent studies on other bicycles. Here we have reduced the handlebar asymmetry in the benchmark bicycle and then studied the circular motions of this new bicycle (NSB). (i) As the bicycle fork is made less and less asymmetrical, the capsize bifurcation points off straight motion for the HR and HF cases approach each other and merge in the limit when handlebar reversal has exactly zero dynamic consequence. (ii) The cusp-like points both approach each other as well as, in a pair, approach a configuration of zero lean and $\pi/2$ steer, eventually merging with these limiting axes at a point that is fortuitously close, but *not identical* to, the coincident points G and H in figure 6.1. (iii) The infinite-speed limit of K in figure 6.1 approaches zero lean and steer $\pi/2$; and so does a significant portion of the curve that terminated at K. (iv) Similarly, the zero-speed limit of A also approaches zero lean and steer $\pi/2$; and so does a significant portion of the curve that terminated at A.

Further, we have taken a bicycle (PSB) with a fully symmetric front assembly and expectedly found the absence of those families which existed due to the handlebar asymmetry. However, it leads to the appearance of a new family. (i) The family that involved bifurcation from straight motion for the benchmark bicycle is preserved here along with a family that starts from a flat-and-fast limit with the bicycle leaning leftwards and then rising up with decreasing lean and then achieving a state of zero lean with steer exactly equal to $\pi/2$. Thereafter, following a symmetrical branch, the family ends with the bicycle again nearly flat, going around infinitely fast, but now leaning to the right. (ii) Now, at all speeds, there are circular motions where the rear contact point is stationary, lean is zero, steer is $\pi/2$, and the bicycle exhibits a pivoting motion about the rear contact point. This was not present in the benchmark bicycle and its nearly symmetrical variant.

As a further exploration, we have considered another bicycle (DB), where we have reduced the mass of the rear frame and increased the fork angle significantly. This bicycle

yields new families of circular motions which are absent in the benchmark bicycle and its more symmetrical variants. (i) In one new family the bicycle first starts from a flat-and-fast motion with lean from vertical nearly equal to $\pi/2$ and steer close to 0; lean and speed decrease, while steer increases up to some maximum value. Thereafter, steer decreases towards 0 while lean and speed increase until the bicycle again approaches a flat-and-fast limit. (ii) In yet another family, the bicycle starts from a HF flat-and-fast limit. Velocity and lean initially decrease while the steer increases; beyond a turning point, the bicycle is nearly (but not quite) upright, and steer is nearly (but not quite) $\pi/2$, as speed increases towards infinity, producing a pivoting motion. This corresponds to the infinite-speed pivoting motion of the benchmark bicycle. However the difference to be noted here is that, for the benchmark bicycle, the corresponding solution family curve had turned around and terminated at a finite-speed pivoting motion, while here the solution terminates at a flat-and-fast limit. (iii) Another family starts at the handlebar-forward (HF) bifurcation from straight motion. The circular motion family starting there has steadily increasing speed, and ends in a *fourth* flat-and-fast limit. An interesting feature of this family is that the steer remains small throughout; this is a high-speed, leaning turn, and unlike any family of the benchmark bicycle. (iv) The fourth and final family starts from handlebar-reversed (HR) bifurcation from straight motion, shows increasing lean and speed up to a turning point and eventually ends in static equilibrium with lean exactly zero and steer very close to $\pi/2$. Though not identical in shape, this family is qualitatively similar to a solution family of the benchmark bicycle.

It is interesting to note that the circular motions of this bicycle (DB) differ from those of the benchmark in a few key ways. First of all, there are four as opposed to two flat-and-fast limiting motions. Secondly, the finite-speed pivoting motion with zero lean is now missing.

Then we have studied the symmetrized version of the DB. (i) Symmetrization of this bicycle (SDB) leads to the apparent disappearance of the solution family which started and terminated at flat-and-fast limits, presumably due to merging of the two endpoints. (ii) We also find that the portion IJ of the circular motion family HIJ in figure 8.3 has merged with FG in figure 8.7. (iii) Also the diagonal part of the curve HI is now coincident with a corresponding portion of curve DE in the figure. The horizontal part now merges with the horizontal axis giving rise to pivoting solutions at all speeds with zero lean and steer $\pi/2$ similar to the symmetrized version of the benchmark bicycle (PSB).

Finally we have considered parameters which represent a light motorcycle and studied its circular motions. (i) There are four circular motion families, three of which are qualitatively similar to the benchmark bicycle and one more family where the steer remains small throughout which is a high-speed leaning turn, that was also observed for the DB.

Finally, we have made a stability analysis of all these circular motion families.

The present work has explored in detail the dynamics and stability of different idealized bicycles. Possible extensions of the present work include the following:

(1) Further academic studies: Starting with the benchmark bicycle and all its variants that have been studied in chapter 8, there is still room for further work on the circular motions of bicycles. Given a bicycle with some meaningful design parameters, how many circular motions will exist for it and what are the starting and terminating points for those circular motions? More work can be carried out along these lines where these questions can be effectively addressed.

(2) More realistic models: Similar work can be performed on, eg, motorcycles with thick toroidal tyres, flexible frames and suspensions.

(3) Insights into handling of motorcycles: This work can also be a starting point for further work on motorcycle ride and handling. Starting with our work on the "light motorcycle", where we have found a circular motion family where the steer remains sufficiently low throughout, insights may be sought into the handling properties of a real motorcycle, where the rider leans into and out of high-speed turns at low steer angles.

Appendix A

Geometrical and Other Parameters for All Bicycles Studied in the Thesis

The following tables list the parameter values for all the bicycles that we have studied in this thesis. We start with the benchmark bicycle and then provide parameters of other bicycles that we studied in chapter 8.

Vectors joining the CG's of the rigid bodies in the reference configuration
$r_{G/P,ref} = (0.3, -0.6, 0)^T$
$r_{S/G,ref} = (0.57812215828725118741, 0.21713021929669624976, 0)^T$
$r_{H/S,ref} = (0.02187784171274881259, -0.01713021929669624976, 0)^T$
$r_{Q/S,ref} = (0.14187784171274881259, 0.33286978070330375024, 0)^T$
$r_{P/S,ref} = (-0.87812215828725118741, 0.38286978070330375024, 0)^T$

Table A.1: Vectors connecting the CG's of the rigid bodies in the reference configuration for the benchmark bicycle.

Parameter	Symbol	Value
Wheel Base	wb	1.02 m
Trail	t	0.08 m
Fork angle (with vertical)	μ	$\pi/10$ rad
Gravity	g	9.81 m/s^2
Forward speed	v	variable m/s
Rear Wheel		
Radius	r_1	0.3 m
Mass	m_{rw}	2 kg
Mass moments of inertia	(I_{xx}, I_{yy}, I_{zz})	$(0.0603, 0.0603, 0.12)$ kgm^2
Rear Frame		
Mass	m_{rf}	85 kg
Mass moments of inertia	$\begin{bmatrix} I_{xx} & I_{xy} & 0 \\ I_{xy} & I_{yy} & 0 \\ 0 & 0 & I_{zz} \end{bmatrix}$	$\begin{bmatrix} 9.2 & 2.4 & 0 \\ 2.4 & 2.8 & 0 \\ 0 & 0 & 11 \end{bmatrix}$ kgm^2
Front Frame		
Mass	m_{ff}	4 kg
Mass moments of inertia	$\begin{bmatrix} I_{xx} & I_{xy} & 0 \\ I_{xy} & I_{yy} & 0 \\ 0 & 0 & I_{zz} \end{bmatrix}$	$\begin{bmatrix} 0.05892 & -0.00756 & 0 \\ -0.00756 & 0.00708 & 0 \\ 0 & 0 & 0.06 \end{bmatrix}$ kgm^2
Front Wheel		
Radius	r_2	0.35 m
Mass	m_{fw}	3 kg
Mass moments of inertia	(I_{xx}, I_{yy}, I_{zz})	$(0.1405, 0.1405, 0.28)$ kgm^2

Table A.2: Parameters for the benchmark bicycle.

Parameter	Symbol	Value
Wheel Base	wb	1.02 m
Trail	t	0.08 m
Fork angle (with vertical)	μ	0.34704 rad
Gravity	g	9.81 m/s^2
Forward speed	v	variable m/s
Rear Wheel		
Radius	r_1	0.3 m
Mass	m_{rw}	2 kg
Mass moments of inertia	(I_{xx}, I_{yy}, I_{zz})	$(0.0603, 0.0603, 0.12)$ kgm^2
Rear Frame		
Mass	m_{rf}	85 kg
Mass moments of inertia	$\begin{bmatrix} I_{xx} & I_{xy} & 0 \\ I_{xy} & I_{yy} & 0 \\ 0 & 0 & I_{zz} \end{bmatrix}$	$\begin{bmatrix} 9.2 & 2.4 & 0 \\ 2.4 & 2.8 & 0 \\ 0 & 0 & 11 \end{bmatrix}$ kgm^2
Front Frame		
Mass	m_{ff}	4 kg
Mass moments of inertia	$\begin{bmatrix} I_{xx} & I_{xy} & 0 \\ I_{xy} & I_{yy} & 0 \\ 0 & 0 & I_{zz} \end{bmatrix}$	$\begin{bmatrix} 0.05741 & -0.01154 & 0 \\ -0.01154 & 0.00856 & 0 \\ 0 & 0 & 0.06 \end{bmatrix}$ kgm^2
Front Wheel		
Radius	r_2	0.35 m
Mass	m_{fw}	3 kg
Mass moments of inertia	(I_{xx}, I_{yy}, I_{zz})	$(0.1405, 0.1405, 0.28)$ kgm^2

Table A.3: Parameters for the NSB.

Vectors joining the CG's of the rigid bodies in the reference configuration
$r_{G/P,ref} = (0.3, -0.6, 0)^T$
$r_{S/G,ref} = (0.62614209928213866262, 0.21062627651044751731, 0)^T$
$r_{H/S,ref} = (0.00129500119047299141, -0.017130219296696249 76, 0)^T$
$r_{Q/S,ref} = (0.11658642145161090198, 0.33286978070330375024, 0)^T$
$r_{P/S,ref} = (-0.90341357854838909802, 0.38286978070330375024, 0)^T$

Table A.4: Vectors connecting the CG's of the rigid bodies in the reference configuration for the NSB.

Vectors joining the CG's of the rigid bodies in the reference configuration
$r_{G/P,ref} = (0.3, -0.6, 0)^T$
$r_{S/G,ref} = (0.61184405196876840155, 0.21713021929669624976, 0)^T$
$r_{H/S,ref} = (-0.00404954616169160944, -0.01062627651044751731, 0)^T$
$r_{Q/S,ref} = (0.09385790071786133738, 0.33937372348955248269, 0)^T$
$r_{P/S,ref} = (-0.92614209928213866262, 0.38937372348955248269, 0)^T$

Table A.5: Vectors connecting the CG's of the rigid bodies in the reference configuration for the PSB.

Front Frame								
Mass moments of inertia	I_{xx}	I_{xy}	0		0.05484	−0.01587	0	kgm^2
	I_{xy}	I_{yy}	0		−0.01587	0.01116	0	
	0	0	I_{zz}		0	0	0.06	

Table A.6: Parameters for the PSB which are different from those shown in table A.3. The other values not shown are to be taken same with the ones in table A.3.

Parameter	Symbol	Value
Wheel Base	wb	1.02 m
Trail	t	0.08 m
Fork angle (with vertical)	μ	$\pi/7$ rad
Gravity	g	9.81 m/s^2
Forward speed	v	variable m/s
Rear Wheel		
Radius	r_1	0.3 m
Mass	m_{rw}	2 kg
Mass moments of inertia	(I_{xx}, I_{yy}, I_{zz})	$(0.0603, 0.0603, 0.12)$ kgm^2
Rear Frame		
Mass	m_{rf}	70 kg
Mass moments of inertia	$\begin{bmatrix} I_{xx} & I_{xy} & 0 \\ I_{xy} & I_{yy} & 0 \\ 0 & 0 & I_{zz} \end{bmatrix}$	$\begin{bmatrix} 9.2 & 2.4 & 0 \\ 2.4 & 2.8 & 0 \\ 0 & 0 & 11 \end{bmatrix}$ kgm^2
Front Frame		
Mass	m_{ff}	4 kg
Mass moments of inertia	$\begin{bmatrix} I_{xx} & I_{xy} & 0 \\ I_{xy} & I_{yy} & 0 \\ 0 & 0 & I_{zz} \end{bmatrix}$	$\begin{bmatrix} 0.05892 & -0.00756 & 0 \\ -0.00756 & 0.00708 & 0 \\ 0 & 0 & 0.06 \end{bmatrix}$ kgm^2
Front Wheel		
Radius	r_2	0.35 m
Mass	m_{fw}	2 kg
Mass moments of inertia	(I_{xx}, I_{yy}, I_{zz})	$(0.1405, 0.1405, 0.28)$ kgm^2

Table A.7: Parameters for the DB.

Vectors joining the CG's of the rigid bodies in the reference configuration
$r_{G/P,ref} = (0.3, -0.6, 0)^T$
$r_{S/G,ref} = (0.55512417913532791422, 0.20763183019708073203, 0)^T$
$r_{H/S,ref} = (0.00650825608676337181, 0.01351453301853628689, 0)^T$
$r_{Q/S,ref} = (0.16487582086467208578, 0.34236816980291926797, 0)^T$
$r_{P/S,ref} = (-0.85512417913532791422, 0.39236816980291926797, 0)^T$

Table A.8: Vectors connecting the CG's of the rigid bodies in the reference configuration for the DB whose parameters are listed in table A.7

.

Front Frame							
Mass moments of inertia	$\begin{bmatrix} I_{xx} & I_{xy} & 0 \\ I_{xy} & I_{yy} & 0 \\ 0 & 0 & I_{zz} \end{bmatrix}$		$\begin{bmatrix} 0.04983 & -0.02111 & 0 \\ -0.02111 & 0.01617 & 0 \\ 0 & 0 & 0.06 \end{bmatrix}$				kgm^2

Table A.9: Parameters for the SDB which are different from those shown in table A.7. The other values not shown are to be taken same with the ones in table A.7.

Vectors joining the CG's of the rigid bodies in the reference configuration
$\underline{r}_{G/P,ref} = (0.22, -0.15, 0)^T$
$\underline{r}_{S/G,ref} = ((0.8964101542246793460, -0.17815515637003622024, 0)^T$
$\underline{r}_{H/S,ref} = (-0.0164101542246793460, -0.07184484362996377976, 0)^T$
$\underline{r}_{Q/S,ref} = (0.1335898457753206540, 0.27815515637003622024, 0)^T$
$\underline{r}_{P/S,ref} = (-1.1164101542246793460, 0.32815515637003622024, 0)^T$

Table A.10: Table of vectors connecting the CG's of the rigid bodies in the reference configuration for the motorcycle.

Parameter	Symbol	Value
Wheel Base	wb	1.25 m
Trail	t	0.10 m
Fork angle (with vertical)	μ	0.38397 rad
Gravity	g	9.81m/s^2
Forward speed	v	variable m/s
Rear Wheel		
Radius	r_1	0.25 m
Mass	m_{rw}	10 kg
Mass moments of inertia	(I_{xx}, I_{yy}, I_{zz})	$(0.19, 0.19, 0.378)$ kgm^2
Rear Frame		
Mass	m_{rf}	130 kg
Mass moments of inertia	$\begin{bmatrix} I_{xx} & I_{xy} & 0 \\ I_{xy} & I_{yy} & 0 \\ 0 & 0 & I_{zz} \end{bmatrix}$	$\begin{bmatrix} 11.5 & 7 & 0 \\ 7 & 8 & 0 \\ 0 & 0 & 15.2 \end{bmatrix}$ kgm^2
Front Frame		
Mass	m_{ff}	14 kg
Mass moments of inertia	$\begin{bmatrix} I_{xx} & I_{xy} & 0 \\ I_{xy} & I_{yy} & 0 \\ 0 & 0 & I_{zz} \end{bmatrix}$	$\begin{bmatrix} 1 & -0.35 & 0 \\ -0.35 & 0.30 & 0 \\ 0 & 0 & 1.20 \end{bmatrix}$ kgm^2
Front Wheel		
Radius	r_2	0.30 m
Mass	m_{fw}	8 kg
Mass moments of inertia	(I_{xx}, I_{yy}, I_{zz})	$(0.170, 0.170, 0.339)$ kgm^2

Table A.11: Parameters for the motorcycle.

Appendix B

Maple Code for Lagrange's Equations of Motion

Here we provide the Maple worksheet by which we generate the fully nonlinear equations of motion for the benchmark bicycle. For any other bicycle, the procedure will be the same. One needs to change the parameter values only.

```
> restart: with(linalg):with(LinearAlgebra):


> skew:= proc(a,b,c) return( matrix([ [0,-c,b],[c,0,-a],[-b,a,0] ]) ) end:
> Id:=array(identity,1..3,1..3): eval(Id):
> e1:=transpose(matrix([[1,0,0]])):e2:=transpose(matrix([[0,1,0]])):
> e3:=transpose(matrix([[0,0,1]])):
> scalarmult:= proc(sc, M)
  RETURN( multiply( matrix([[sc,0,0],[0,sc,0],[0,0,sc]]),M)) end:

Comment: The procedure below calculates the rotation matrix.

> rot_mat:= proc(unit_vector,angle) local S_temp;S_temp:=skew(unit_vector[1,1]
,unit_vector[2,1],unit_vector[3,1]);
```

```
> return evalm( scalarmult(cos(angle),Id)+
  scalarmult( 1-cos(angle), multiply(unit_vector,transpose(unit_vector
 )))+ scalarmult(sin(angle),S_temp)) end:
> R1:=rot_mat(e3,theta(t)): R2:=rot_mat( multiply(R1,e1), psi(t)):
> R3:= rot_mat( multiply(multiply(R2,R1),e3), phi(t)):
> R_final:=multiply(R3, multiply(R2, R1)): eval(R_final):
> matrix_simplify:= proc(any_matrix_input) local any_matrix, t1, t2;
  any_matrix:=matrix(3,3);
> for t1 from 1 to 3 do for t2 from 1 to 3 do
  any_matrix[t1,t2]:=simplify(any_matrix_input[t1,t2]);
> od; od; return(eval(any_matrix)) end:

Comment: This part computes the rotational  kinetic energy of the entire bicycle.

> A_temp:=matrix_simplify(R_final): eval(R_final):
> R_rf:=eval(A_temp):
> Icmrf:=matrix([[Ixxrf,Ixyrf,0],[Ixyrf,Iyyrf,0],[0,0,Izzrf]]):
> Icmff:=matrix([[Ixxff,Ixyff,0],[Ixyff,Iyyff,0],[0,0,Izzff]]):
> Icmrw:=matrix([[Ixxrw,0,0],[0,Iyyrw,0],[0,0,Izzrw]]):
> Icmfw:=matrix([[Ixxfw,0,0],[0,Iyyfw,0],[0,0,Izzfw]]):
> R_rw:=simplify(evalm(rot_mat((multiply(R_rf,e3),betar(t))) &* R_rf)):
> n_f:=transpose(matrix([[-sin(mu),-cos(mu),0]])):
> R_ff:=simplify(evalm(rot_mat((multiply(R_rf,n_f),psif(t))) &* R_rf)):
> R_fw:=simplify(evalm(rot_mat((multiply(R_ff,e3),betaf(t))) &* R_ff)):
> KER:=proc(R,MI) local temp1,temp2,temp3,temp4,temp5;temp2:=map(diff,R,t):
> temp1:=multiply(temp2,transpose(R)):
> temp3:=transpose(matrix([[temp1[3,2],temp1[1,3],temp1[2,1]]])) :
> temp4:=multiply(R,multiply(MI,transpose(R))):
> temp5:=1/2*(evalm(transpose(temp3)&*evalm(temp4&*temp3)  )[1,1]): end:
> T1:=KER(R_rf,Icmrf)+KE(R_ff,Icmff)+KE(R_rw,Icmrw)+KE(R_fw,Icmfw):

Comment: This part computes the translational  kinetic energy of the entire
bicycle.
> r_P:=array(1..3):r_P[1]:=x(t):r_P[2]:=y(t):r_P[3]:=z(t):r_GP_ref:=array(1..3):
> r_GP_ref[1]:=gx:r_GP_ref[2]:=gy:r_GP_ref[3]:=0:r_SP_ref:=array(1..3):
```

```
> r_SP_ref[1]:=sx:r_SP_ref[2]:=sy:r_SP_ref[3]:=0:
> r_SH_ref:=array(1..3):r_SH_ref[1]:=gfx:r_SH_ref[2]:=gfy:r_SH_ref[3]:=0:
> r_QS_ref:=array(1..3): r_QS_ref[1]:=qx:r_QS_ref[2]:=qy:
> r_QS_ref[3]:=0:empty:=array(1..3):
> empty[1]:=0:empty[2]:=0:empty[3]:=0:R11:=Matrix(3):
> KET:=proc(R,R11,arr1,arr2,arr3,m) local temp1,temp2,temp3,temp4;
> temp1:=evalm(arr1+evalm(R &*arr2)):
> temp2:=evalm(temp1-evalm(R11 &*arr3)): temp3:=map(diff,temp2,t);
> temp4:=(1/2)*m*(temp3[1]^2+temp3[2]^2+temp3[3]^2); end:
> T2:=KET(R_rf,R11,r_P,r_GP_ref,empty,mr)+KET(R_rf,R_ff,r_P,r_SP_ref,r_SH_ref,mf)
 +KET(R_ff,R11,evalm(r_P+evalm(R_rf &*r_SP_ref)),r_QS_ref,empty,mfw)
 +(1/2)*mrw*(diff(x(t),t)^2+diff(y(t),t)^2+diff(z(t),t)^2):
```

Comment: This part computes the potential energy of the entire bicycle.

```
> V:=mrw*g*r_P[3]+mr*g*evalm(r_P+evalm(R_rf &*r_GP_ref))[3]
    +mfw*g*evalm(evalm(r_P+evalm(R_rf &*r_SP_ref))+evalm(R_ff &*r_QS_ref))[3]
    +mf*g*evalm(evalm(r_P+evalm(R_rf &*r_SP_ref))-evalm(R_ff &*r_SH_ref))[3]:
```

Comment: Rear Wheel Constraints

```
> n_P_ref:=e3:n_P:=evalm(R_rw &*n_P_ref):
> n_P:=<n_P[1,1],n_P[2,1],n_P[3,1]>:
> e3:=<0,0,1>:
> lambdabar:=CrossProduct(n_P, e3):
> mag_lambdabar:=sqrt(lambdabar[1]^2+lambdabar[2]^2+lambdabar[3]^2):
> lambdabar:=<lambdabar[1]/mag_lambdabar,lambdabar[2]/mag_lambdabar,
  lambdabar[3]/mag_lambdabar>:
> r_PR:=(CrossProduct( lambdabar,n_P)):
> r_PR:=<r[1]*r_PR[1],r[1]*r_PR[2],r[1]*r_PR[3]>:Rdot_rw:=map(diff,R_rw,t):
> omegarw:=simplify(evalm(Rdot_rw &*transpose(R_rw))):
> omegarw:=<omegarw[3,2],omegarw[1,3],omegarw[2,1]>:
> tempr:=CrossProduct(omegarw, r_PR):
> constraint[1]:=diff(x(t),t)-simplify(tempr[1]):
> constraint[2]:=diff(y(t),t)-simplify(tempr[2]):
```

```
> constraint3:=diff(z(t),t)-simplify(tempr[3]):
> for k from 1 to 2 do constraint[k]:=simplify(subs(sqrt(1-cos(psi(t))^2)
  =sin(psi(t)),1/sqrt(1-cos(psi(t))^2)=1/sin(psi(t)),constraint[k]));end:

Comment: Front Wheel Constraints

> n_Q_ref:=e3:n_Q:=evalm(R_fw &*n_Q_ref):n_Q:=<n_Q[1],n_Q[2],n_Q[3]>:e3:=<0,0,1>:
> lambdabar1:=CrossProduct(n_Q, e3):
> mag_lambdabar1:=sqrt(lambdabar1[1]^2+lambdabar1[2]^2+lambdabar1[3]^2):
> lambdabar1:=<lambdabar1[1]/mag_lambdabar1,lambdabar1[2]/mag_lambdabar1
 ,lambdabar1[3]/mag_lambdabar1>:
> r_QF:=(CrossProduct( lambdabar1,n_Q)):
> r_QF:=<r[2]*r_QF[1],r[2]*r_QF[2],r[2]*r_QF[3]>:
> Rdot_fw:=map(diff,R_fw,t):omegafw:=simplify(evalm(Rdot_fw &*transpose(R_fw))):
> omegafw:=<omegafw[3,2],omegafw[1,3],omegafw[2,1]>:
> tempf:=CrossProduct(omegafw, r_QF):
> r_S:=evalm(r_P+evalm(R_rf &*r_SP_ref)):r_Q:=evalm(r_S+evalm(R_ff &*r_QS_ref)):
> v_Q:=simplify(map(diff,r_Q,t)):
> constraint[3]:=v_Q[1]-tempf[1]:constraint[4]:=v_Q[2]-tempf[2]:
> constraint[5]:=v_Q[3]-tempf[3]:
> constraint[5]:=subs(z(t)=r[1]*sin(psi(t)),constraint[5]):

Comment: Equations of Motion

> T:=T1+T2:L:=T-V:L:=subs(z(t)=r[1]*sin(psi(t)),L):
> const_part:=add(lambda[k]*constraint[k],k=1..5):
> ndof:=8: q[1]:=x(t): q[2]:=y(t): q[3]:=theta(t): q[4]:=psi(t): q[5]:=phi(t):
  q[6]:=psif(t): q[7]:=betar(t):q[8]:=betaf(t):
> for k from 1 to ndof do temp1:=subs(diff(q[k],t)=tempvar1,L):
  temp2:=subs(q[k]=tempvar2,temp1):
  temp3:=subs(tempvar1=diff(q[k],t),diff(temp1,tempvar1)):
  temp4:=subs(tempvar1=diff(q[k],t),tempvar2=q[k],diff(temp2,tempvar2)):
  eq[k]:=diff(temp3,t)-temp4: end do:
> for k from 1 to ndof do eq[k]:=eq[k]-coeff(const_part,diff(q[k],t)): end do:
> for k from 1 to 5 do eq[ndof+k]:=diff(constraint[k],t): end:
```

```
> for k from 1 to 13 do eq[k]:=evalf(subs(gx=0.3,gy=-0.6,sy=-0.38286978070330375024,
  sx=0.87812215828725118741,qx=0.14187784171274881259,qy=0.33286978070330375024,
  gfx=-0.02187784171274881259,gfy=0.01713021929669624976,r[2]=0.35,
  r[1]=0.3,g=9.81,mu=0.31415926535897932385,mrw=2,mrf=85,mfw=3,mff=4,Ixxrw=0.0603,
  Iyyrw=0.0603,Izzrw=0.12,Ixxrf=9.2,Iyyrf=2.8,Izzrf=11,Ixyrf=2.4,Ixxfw=0.1405,
  Iyyfw=0.1405,Izzfw=0.28,Ixxff=0.05892,Iyyff=0.00708,Izzff=0.06,
  Ixyff=-0.00756,eq[k])):end do:
```

Appendix C

Matlab Code for Newton-Euler Equations

Here we reproduce the Matlab code for simulating the Newton-Euler equations of motion.

C.1 Derivatives

The following Matlab m-file "N_E" gives the Newton-Euler implementation of the equations of motion. Given a state vector consisting of nine generalized coordinates and their nine time derivatives, the derivative of the state vector is returned. This m-file in turn calls two m-files called "rotmat" and "ssm" which are also given below.

function dq = N_E(t, q)

```
x=q(1);y=q(2);z=q(3);th=q(4);si=q(5);ph=q(6);sf=q(7);br=q(8);bf=q(9);
dx=q(10);dy=q(11);dz=q(12);dth=q(13);dsi=q(14);dph=q(15);dsf=q(16);
dbr=q(17);dbf=q(18);e3=[0;0;1];e2=[0;1;0];e1=[1;0;0];

% Rotation Matrices for the four rigid bodies.
```

```
ro1=rotmat(e3,th);ro2=rotmat(ro1*e1,si);r3=rotmat(ro2*ro1*e3,ph);rrf=ro3*ro2*ro1;
rrw=rotmat(rrf*e3,br)*rrf; nf_ref=[-sin(mu); -cos(mu); 0];
rff=rotmat(rrf*nf_ref,sf)*rrf;rfw=rotmat(rff*e3,bf)*rff;
Icmrf=rrf*Icmrfref*rrf';Icmrw=rrw*Icmrwref*rrw';Icmff=rff*Icmffref*rff';
Icmfw=rfw*Icmfwref*rfw';np=rrw*e3;nq=rfw*e3;
nf=rff*nf_ref;wrf=[e3 ro1*e1 ro2*ro1*e3]*[dth;dsi;dph];
wrw=wrf+dbr*np; wff=wrf+dsf*nf; wfw=wff+dbf*nq;

npdot=ssm(wrw)*np;
lambdar=-ssm(e3)*np/sqrt(np'*ssm(e3)'*ssm(e3)*np);
lambdardot=-ssm(e3)*npdot/sqrt(np'*ssm(e3)'*ssm(e3)*np)+...
ssm(e3)*np*(npdot'*ssm(e3)'*ssm(e3)*np)/(np'*ssm(e3)'*ssm(e3)*np)^(3/2);
nqdot=ssm(wfw)*nq;
lambdaf=-ssm(e3)*nq/sqrt(nq'*ssm(e3)'*ssm(e3)*nq);
lambdafdot=-ssm(e3)*nqdot/sqrt(nq'*ssm(e3)'*ssm(e3)*nq)+...
ssm(e3)*nq*(nqdot'*ssm(e3)'*ssm(e3)*nq)/(nq'*ssm(e3)'*ssm(e3)*nq)^(3/2);

Rgp=rrf*gp_ref;Rpg=-Rgp;Rsg=rrf*sg_ref;Rhs=rff*hs_ref;Rqs=rff*qs_ref;Rsq=-Rqs;
Rpr=cross(lambdar,np)*r1;Rrp=-Rpr;Rqf=cross(lambdaf,nq)*r2;Rfq=-Rqf;
Rps=rrf*ps_ref;Rsp=-Rps;Rgs=-Rsg;Rrq=Rrp+Rps+Rsq;Rpq=Rps+Rsq;Rgq=Rgs+Rsq;
Rhq=Rhs+Rsq;Rrg=Rrp+Rpg;Rfg=Rfq+Rqs+Rsg;Rhg=Rhs+Rsg;Rqg=Rqs+Rsg;Rqh=-Rhq;
Rrs=Rrp+rrf*ps_ref;

% Assembly of individual equations.

A=zeros(33,33);
A(1:3,1:3)=eye(3);A(1:3,13:15)=ssm(Rpr);A(4:6,10:12)=eye(3);A(4:6,22:24)=ssm(Rqf);
A(7:7,13:15)=-np'*Icmrw;A(7:7,25:27)=np'*ssm(Rrp);
A(8:8,1:3)=-nf'*ssm(Rps)*mrw;
A(8:8,4:6)=-nf'*ssm(Rgs)*mrf;A(8:8,13:15)=-nf'*Icmrw;
A(8:8,16:18)=-nf'*Icmrf;A(8:8,25:27)=nf'*ssm(Rrs);
A(9:9,28:30)=nq'*ssm(Rfq);A(9:9,22:24)=-nq'*Icmfw;A(10:12,1:3)=-mrw*eye(3);
A(10:12,4:6)=-mrf*eye(3); A(10:12,7:9)=-mff*eye(3);A(10:12,10:12)=-mfw*eye(3);
A(10:12,25:27)=eye(3); A(10:12,28:30)=eye(3);A(13:15,25:27)=ssm(Rrg);
```

```
A(13:15,28:30)=ssm(Rfg); A(13:15,1:3)=-ssm(Rpg)*mrw; A(13:15,13:15)=-Icmrw;
A(13:15,16:18)=-Icmrf;A(13:15,7:9)=-ssm(Rhg)*mff; A(13:15,19:21)=-Icmff;
A(13:15,10:12)=-ssm(Rqg)*mfw; A(13:15,22:24)=-Icmfw;A(16:18,1:3)=-eye(3);
A(16:18,4:6)=eye(3);A(16:18,16:18)=ssm(Rgp);
A(19:21,4:6)=-eye(3);A(19:21,7:9)=eye(3);
A(19:21,16:18)=ssm(Rsg);A(19:21,19:21)=ssm(Rhs);A(22:24,10:12)=eye(3);
A(22:24,7:9)=-eye(3);A(22:24,19:21)=ssm(Rqh);A(25:27,13:15)=eye(3);
A(25:27,16:18)=-eye(3);A(25:27,32:32)=-np;A(28:30,19:21)=eye(3);
A(28:30,16:18)=-eye(3);A(28:30,31:31)=-nf;A(31:33,22:24)=eye(3);
A(31:33,19:21)=-eye(3);A(31:33,33:33)=-nq;

B=zeros(33,1);
B(1:3)=r1*ssm(wrw)*(ssm(lambdardot)*np+ssm(lambdar)*npdot);
B(4:6)=r2*ssm(wfw)*(ssm(lambdafdot)*nq+ssm(lambdaf)*nqdot);
B(7)=np'*ssm(wrw)*Icmrw*wrw;
B(8)=nf'*ssm(Rps)*rw+ nf'*ssm(Rgs)*rf+nf'*ssm(wrf)*...
Icmrf*wrf+nf'*ssm(wrw)*Icmrw*wrw;
B(9)=nq'*ssm(wfw)*Icmfw*wfw;
B(10:12)=[0;0;(mrw+mrf+mff+mfw)*g];
B(13:15)=ssm(Rpg)*rw+ssm(Rhg)*ff+ssm(Rqg)*fw+ssm(wrw)*Icmrw*wrw+...
ssm(wrf)*Icmrf*wrf+ssm(wff)*Icmff*wff+ssm(wfw)*Icmfw*wfw;
B(16:18)=ssm(wrf)*ssm(wrf)*Rgp;
B(19:21)=ssm(wrf)*ssm(wrf)*Rsg+ssm(wff)*ssm(wff)*Rhs;
B(22:24)=ssm(wff)*ssm(wff)*Rqh;B(25:27)=dbr*ssm(wrw)*np;
B(28:30)=dsf*ssm(wff)*nf;B(31:33)=dbf*ssm(wfw)*nq;

d2z=A\B;
qq=ssm(ro1*e1*dsi+e3*dth)*ro2*ro1*e3*dph + ssm(e3*dth)*ro1*e1*dsi;
temp=[e3 ro1*e1 ro2*ro1*e3]\(d2z(16:18)-qq);
d2z=[d2z(1:3);temp;d2z(31:33)];
dq=[dx;dy;dz;dth;dsi;dph;dsf;dbr;dbf;d2z];
```

function rm = **rotmat**(**uv**, **angle**);

```
s=[0 -uv(3) uv(2);uv(3) 0 -uv(1);-uv(2) uv(1) 0];
rm=cos(angle)*eye(3)+(1-cos(angle))*uv*uv'+sin(angle)*s;
```

---

function s = **ssm**(**uv**);

```
s=[0 -uv(3) uv(2);uv(3) 0 -uv(1);-uv(2) uv(1) 0];
```

C.2 Initial Conditions

function r_F_z = **phi_initial**(**ph**);

```
% Do not touch this file.


global th si sif br bf
global e3 e2 e1 mu radr radf ps_ref qs_ref;
ro1=rotmat(e3,th);ro2=rotmat(ro1*e1,si);ro3=rotmat(ro2*ro1*e3,ph);
rrf=ro3*ro2*ro1;rrw=rotmat(rrf*e3,br)*rrf;
u_v_ff_ref=[-sin(mu);-cos(mu);0];
rff=rotmat(rrf*u_v_ff_ref,sif)*rrf;rfw=rotmat(rff*e3,bf)*rff;
nq=rfw*e3;lambdaf=cross(nq,e3)/norm(cross(nq,e3));
r_QF=radf*cross(lambdaf,nq);
temp1=rrf*ps_ref;temp2=-rff*qs_ref;
r_F_z=-(r_QF(3)-radr*sin(si)+temp1(3)+temp2(3));
```

---

function xicfull = **find_ics**(**xicpartial**);

```
global th si sif br bf radr;
th=0;
si=xicpartial(1);
sif=xicpartial(2);
br=0;
bf=0;

xicfull(1)=0;
xicfull(2)=0;
xicfull(3)=radr*sin(xicpartial(1));
xicfull(4)=0;
xicfull(5)=xicpartial(1);

phi_range_start=0;

Num=400;
zz=linspace(phi_range_start,2*pi+phi_range_start,Num);
zz1=zz;

for k=1:Num
    zz1(k)=phi_initial(zz(k));
end


zz1=sign(zz1(1:Num-1).*zz1(2:Num));
if sum(zz1<0)~=2
    disp('There is a problem in finding phi(0).')
    disp('It seems there is no phi(0) for which the front wheel will just
    touch the ground.')
    disp('This is most likely because your choice of psi(0) is too
    close to 0 or pi,')
    disp('and the choice of sif(0) (initial handle rotation) is
    too large; as a result,')
    disp('the bicycle front wheel is dipping below the ground for all phi(0).')
```

```
    disp('Please try other initial conditions.')
    disp('If you find other conditions under which no phi(0) solution exists,
    please email us!')
    xicfull=NaN;
else

[s1,s2]=sort(zz1);

temp2=newton('phi_initial',zz(s2(2)));

xicfull(6)=temp2;
xicfull(7)=xicpartial(2);
xicfull(8)=0;
xicfull(9)=0;
xicfull(10)=radr*cos(xicpartial(1))*xicpartial(3);
xicfull(11)=xicpartial(3);
xicfull(12)=xicpartial(4);
xicfull(13)=xicpartial(5);
xicfull=xicfull';
end
```

---

function partial_qdot = newprogram1(q);

```
global radr radf e3 e2 e1 mu ps_ref qs_ref
global gp_ref sg_ref hs_ref qs_ref ps_ref
x=q(1);y=q(2);th=q(3);si=q(4);ph=q(5);sif=q(6);br=q(7);bf=q(8);
dsi=q(9);dsif=q(10);dbr=q(11);

r1=rotmat(e3,th);r2=rotmat(r1*e1,si);r3=rotmat(r2*r1*e3,ph);rrf=r3*r2*r1;
rrw=rotmat(rrf*e3,br)*rrf; u_v_ff_ref=[-sin(mu); -cos(mu); 0];
rff=rotmat(rrf*u_v_ff_ref,sif)*rrf;rfw=rotmat(rff*e3,bf)*rff;

np=rrw*e3;nq=rfw*e3;
```

```
u_v_ff=rff*u_v_ff_ref;
lambdar=cross(np,e3)/norm(cross(np,e3));
lambdaf=cross(nq,e3)/norm(cross(nq,e3));
Rqs=rff*qs_ref;Rsq=-Rqs;
Rpr=cross(lambdar,np)*radr;Rrp=-Rpr;
Rqf=cross(lambdaf,nq)*radf;Rfq=-Rqf;
Rps=rrf*ps_ref;Rsp=-Rps;

A=[e3 r1*e1 r2*r1*e3];
Q=ssm(Rpr);Q1=ssm(Rqf);B=ssm(Rqs);C=ssm(Rps);D=(B-C)*A;

M=zeros(6,6);

M(1:3,1:3)=eye(3);
M(1:3,5:5)=Q*A(:,3);
M(1:3,4:4)=Q*A(:,1);

M(4:6,4:4)=-(-C*A(:,1)+B*A(:,1)-Q1*A(:,1));
M(4:6,5:5)=-(-C*A(:,3)+B*A(:,3)-Q1*A(:,3));
M(4:6,6:6)=Q1*nq;
M(4:6,1:3)=eye(3);

f=zeros(6,1);
f(1:3)=-Q*(A(:,2)*dsi+np*dbr);
f(4:6)=(-C*A(:,2)+B*A(:,2)-Q1*A(:,2))*dsi+B*u_v_ff*dsif-Q1*u_v_ff*dsif;

partial_qdot=M\f;
```

---

function dq = psv(t, q);

```
partial_qdot=newprogram1([q(1:2);q(4:9);q(11:13)]);

temp=N_E(1,[q(1:9);partial_qdot(1:4);q(11);partial_qdot(5);
```

```
q(12:13);partial_qdot(6)]);

temp([10,11,13,15,18])=[];
dq=temp;
```

---

function Yfull = final_run(t, Y);

```
% Do not touch this file.

augment=[];
for i=1:size(t)
    temp=Y(i,:);
    temp1=newprogram1([temp(1:2) temp(4:9) temp(11:13)]);
    temp1(3)=[];
    augment=[augment temp1];
end
augment=augment';
Yfull=[Y augment];
```

---

function [x, c] = newton(fun, x, showx);

```
n=length(x);
epsil=(1e-7*max(1,norm(x)));
pert=eye(n)*epsil;
iter=0;
nmax=60;
c=1;
ee=feval(fun,x);
while (norm(ee)*max(1,norm(x))>7e-11)*(iter<nmax)
iter=iter+1;
for k=1:n
D(:,k)=(feval(fun,x+pert(:,k))-ee)/epsil;
```

```
end
x=x-(D\ee);
if nargin == 3
disp(x)
end
ee=feval(fun,x);
end
%disp(iter), disp('iterations, that took')
if (iter == nmax)+(abs(x)==inf)
c=0;
disp('did not converge')
end
```

C.3 Instructions for Simulation

1. First create a file called "parameter_set.m" (not provided here) in Matlab, where all the parameter values of the bicycle are included. Then type `parameter_set` (that is one word, with an underscore symbol) at the Matlab command prompt. This will bring all the parameter values of the bicycle to the Matlab workspace. You can edit this file to change parameter values if you like. Note that parameter values for the benchmark bicycle and its variants are tabulated in appendix A.

2. Initial conditions. There is no harm in choosing zero initial conditions for x and y (initial horizontal coordinates of the center of the rear wheel), θ (heading), β_r (rear wheel rotation angle) and β_f (front wheel rotation angle). To incorporate these zero initial conditions and to further ensure consistency in the specified initial rates, you need to specify only 5 independent initial conditions in one vector as follows:

$$(\psi, \psi_f, \dot{\psi}, \dot{\psi}_f, \dot{\beta}_r)^T,$$

where ψ is the lean (where $\pi/2$ represents a vertical bicycle; values more than $\pi/2$ signify leaning to the left), ψ_f is the handle rotation (where 0 represents straight ahead, and positive values indicate a turn to the left), and $\dot{\beta}_r$ is the rear wheel rotation rate (representing forward speed). Let this restricted or partially specified vector of initial

conditions be Xic. For example, in Matlab, you can type

```
Xic=[1.5;0.1;0.1;-0.1;1];
```

3. Then type `Xicfull = find_ics(Xic)` to obtain the full set of initial conditions used by Matlab.

4. Choose the time instants at which you want the solution. For example, type

```
tspan=linspace(0,5,200);
```

.

5. Set the numerical integration accuracy. For example, type

```
options=odeset('RelTol',1e-8,'AbsTol',1e-8);
```

6. Now simulate. Type

```
[t,Y]=ode45('psv',tspan,Xicfull,options);
```

This will return a column matrix t (with, e.g., 200 points equally spaced between 0 and 5), and a matrix Y (with, corresponingly, 200 rows) with 13 columns.

7. Type

```
Yfull=final_run(t,Y);
```

to get all 18 quantities of interest, in the 18 columns of $Yfull$, in the sequence

$$(x, y, z, \theta, \psi, \phi, \psi_f, \beta_r, \beta_f, \dot{z}, \dot{\psi}, \dot{\psi}_f, \dot{\beta}_r, \dot{x}, \dot{y}, \dot{\theta}, \dot{\phi}, \dot{\beta}_f)^T.$$

8. Then, e.g., type `plot(t,Yfull(:,18))` to get a plot of $\dot{\beta}_f$ *vs.* time.

9. This completes one simulation. You can type `clear all` and begin again.

Appendix D

Linearized Stability Eigenvalues for the Benchmark Bicycle

In the following two pages, we list some eigenvalues governing the stability of straight motion for the benchmark bicycle. The eigenvalues have been tabulated for the forward speeds v ranging from 0 to 10 m/sec in steps of 1 m/sec. They have been obtained from linearized stability analysis. These values match exactly with those given in [17]. Fourteen digits are presented for benchmarking purposes.

v (m/s)	Real part of weave eigenvalue (1/s)	Imaginary part of weave eigenvalue (1/s)
0	–	–
1	3.52696170990070	0.80774027519930
2	2.68234517512745	1.68066296590675
3	1.70675605663975	2.31582447384325
4	0.41325331521125	3.07910818603206
5	−0.77534188219585	4.46486771378823
6	−1.52644486584142	5.87673060598709
7	−2.13875644258362	7.19525913329805
8	−2.69348683581097	8.46037971396931
9	−3.21675402252485	9.69377351531791
10	−3.72016840437287	10.90681139476287

Table D.1: Real and imaginary parts of the weave eigenvalues for different values of the forward speed as obtained from linearized stability analysis.

v (m/s)	Capsize eigenvalue (1/s)	Castering eigenvalue (1/s)
0	−3.13164324790656	−5.53094371765393
1	−3.13423125066578	−7.11008014637442
2	−3.07158645641514	−8.67387984831735
3	−2.63366137253667	−10.35101467245920
4	−1.42944427361326	−12.15861426576447
5	−0.32286642900409	−14.07838969279822
6	−0.00406690076970	−16.08537123098026
7	0.10268170574766	−18.15788466125262
8	0.14327879765713	−20.27940894394569
9	0.15790184030917	−22.43788559040858
10	0.16105338653172	−24.62459635017404

Table D.2: Capsize and caster eigenvalues for different values of the forward speed as obtained from linearized stability analysis.

References

[1] Aström, K. J., Klein, R. E., and Lennartsson, A., 2005, "Bicycle dynamics and control: adapted bicycle for education and research", *IEEE Control Systems Magazine*, **25**, pp. 26-47.

[2] Basu-Mandal, P., Chatterjee, A., and Papadopoulos J. M., 2007, "Hands-free circular motions of a benchmark bicycle", *Proceedings of the Royal Society A*, **463**, pp. 1983-2003.

[3] Collins, R. N., 1963, "A mathematical analysis of the stability of two-wheeled vehicles", Ph.D thesis, Department of Mechanical Engineering, University of Wisconsin.

[4] Cossalter, V., Doria, A., and Lot, R., 1999, "Steady turning of two-wheeled vehicles", *Vehicle System Dynamics*, **31**, pp. 157-181.

[5] Cossalter, V., and Lot, R., 2002, "A motorcycle multi-body model for real time simulations based on the natural coordinates approach", *Vehicle System Dynamics*, **37**, pp. 423-447.

[6] Fajans, J., 2000, "Steering in bicycles and motorcycles", *American Journal of Physics*, **68**(7), July, pp. 654-659.

[7] Franke, G., Suhr, W., and Rieß, F., 1990, "An advanced model of bicycle dynamics", *Eur. J. Physics*, **11**, pp. 116-121.

[8] Getz, N. H., and Marsden, J. E., 1995, "Control for an autonomous bicycle", In *IEEE Conference on Robotics and Automation*. 21-27 May, Nagoya, Japan.

[9] Hand, R. S., 1988, "Comparisons and stability analysis of linearized equations of motion for a basic bicycle model", M.S. thesis, Cornell University.

[10] Jones, D. E. H., 1970, "The stability of the bicycle", *Physics Today*, **23**(3), pp. 34-40.

[11] Kane, T. R., 1977, "Steady turning of single-track vehicles", *Society of Automotive Engineers*, Paper 770057, International Automotive Engineering Congress and Exposition, Detroit.

[12] Kane, T. R., 1968, *Dynamics*. New York: Holt, Rinehart and Winston.

[13] Le Hénaff, Y., 1987, "Dynamical stability of the bicycle", *European Journal of Physics*, **8**(3), pp. 207-210.

[14] Lennartsson, A., 1999, "Efficient multibody dynamics", Ph.D thesis, Royal Institute of Technology, Stockholm.

[15] Man, G. K., and Kane, T. R., 1979, "Steady turning of two-wheeled vehicles", *Society of Automotive Engineers*, Paper 790187. In *Proceedings of Dynamics of Wheeled Recreational Vehicles*, Detroit, February - March, pp. 55-75.

[16] Meijaard, J. P., and Popov, A. A., 2006, "Numerical continuation of solutions and bifurcation analysis in mutibody systems applied to motorcycle dynamics", *Nonlinear Dynamics*, **43**, pp. 97-116.

[17] Meijaard, J. P., Papadopoulos, J. M., Ruina, A., and Schwab, A. L., 2007, "Linearized dynamics equations for the balance and steer of a bicycle: a benchmark and review", *Proceedings of the Royal Society A*, **463**, pp. 1955-1982.

[18] Neĭmark, Ju. I., and Fufaev, N. A., 1972, "Dynamics of Nonholonomic Systems", Providence. RI: A.M.S. (Transl. from the Russian edition, Nauka, Moscow, 1967.)

[19] Psiaki, M. L., 1979, *Bicycle stability: A mathematical and numerical analysis*. Undergraduate thesis, Physics Department, Princeton University, NJ.

[20] Rankine, W. J. M., 1869, "On the dynamical principles of the motion of velocipedes", *The Engineer*, **28**, pp. 79, 129, 153, 175, **29** (1870), pp. 2.

[21] Roland, R. D., 1973, "Computer simulation of bicycle dynamics", In *Mechanics and sport* 4, ed J. L. Bleustein, American Society of Mechanical Engineers, New York.

[22] Sharp, R. S., 1971, "The stability and control of motorcycles", *The Journal of Mechanical Engineering Science*, **13**(5), pp. 316-329.

[23] Whipple, F. J. W., 1899, "The stability of the motion of a bicycle", *The Quarterly Journal of Pure and Applied Mathematics*, **30**, pp. 312-348.

[24] *http://ruina.tam.cornell.edu/research/topics/bicycle_mechanics/papers/bicycle_handling.pdf.*